Design and analysis of solid oxide electrolysis-based systems for synthetic liquid fuels production

Design and analysis of solid oxide electrolysis-based systems for synthetic liquid fuels production

MAHROKH SAMAVATI

Doctoral Thesis

Polytechnic University of Turin
Department of Energy
10129 Turin

KTH Royal Institute of Technology
Industrial Engineering and Management
Department of Energy Technology
Heat and Power Technology unit
SE-100 44 Stockholm,

This doctoral research has been carried out in the context of an agreement on joint doctoral research supervision between Politecnico di Torino − PoliTo, (Turin, Italy) and KTH Royal Institute of Technology, (Stockholm, Sweden). The research was partially funded by the European Commission through the SELECT+ (Environomical pathways for sustainable energy services) program, an Erasmus Mundus Joint Doctorate.

Printed by Universitetsservice US-AB Drottning Kristinas väg 53B SE-114 28 Stockholm Sweden.

ISBN 978-91-7729-807-6

TRITA-ITM-AVL 2018:17

Academic Dissertation which, with due permission of the KTH Royal Institute of Technology, is submitted for public defense on Tuesday the 8th June 2018, at 15:00 in Politecnico di Torino, Turin, Italy.

Abstract

During the past decades, considerable attention has been dedicated to renewable energy systems. This is due to the increased awareness regarding greenhouse gas emissions as well as limits of the future availability and reliability of conventional energy and power systems. Renewable energy can be considered as free, nearly infinite, and clean; however, such resources have their own drawbacks. Renewables face challenges in meeting instantaneous electricity demand and for utilization as transportation fuels. One of the main challenges of renewable energy sources like solar and wind is due to their variability, making them incapable of meeting the required energy demands at all the time. Therefore it is beneficial to add energy storage for handling supply and demand.

The current study is dedicated to the design and analysis of an integrated system for production of synthetic fuels as a way of renewable energy storage. The proposed system integrates solid oxide electrolysis, entrained gasification, and Fischer-Tropsch process. The main product of system is Fischer-Tropsch diesel which is produced from steam, CO_2, and different renewables, namely: lignocellulosic biomass, solar PV electricity, and wind electricity. This approach has the benefit of storing the excess electrical energy from renewables in the form of chemical energy of the hydrocarbon fuels for further usage during peak hours. Also, using these synthetic fuels results in an increase of the renewable energy share in the transportation system while utilizing existing distribution and conversion technologies.

The proposed system is analyzed from thermodynamic, economic, and environment perspectives. This study addresses several different research questions, from finding the optimum operating condition of precursor syngas producing subsystems to evaluating the theoretical potential of integrated systems in different locations.

Keywords: Solid oxide electrolyser, Entrained gasification, Fischer-Tropsch process, Thermodynamic analysis, Economy, Emission saving, Policy

Abstract

Negli ultimi decenni è stata dedicata una grande attenzione alle tecnologie che utilizzano fonti di energia rinnovabili. Ciò è dovuto alla maggiore consapevolezza riguardo alle emissioni di gas serra e ai limiti della disponibilità e affidabilità future dei sistemi basati su fonti fossili. L'energia rinnovabile può essere considerata come gratuita, semi-infinita e pulita; tuttavia, alcuni svantaggi devono essere tenuti in considerazione. La necessitá di adempiere ala domanda istantanea di elettricità e all'utilizzo come carburante per i trasporti rappresentano alcune delle piú importanti sfide che devono essere affrontate dalle fonti di energia rinnovabili. L'energia solare ed eolica, ad esempio, sono caratterizzate da una forte variabilità, che le rende incapaci di soddisfare istantaneamente la domanda di energia. Pertanto risulta fondamentale l'integrazione di un accumulo di energia per gestire il bilancio tra domanda e produzione. Il presente studio è dedicato alla progettazione e all'analisi di un sistema integrato per la produzione di combustibili sintetici come mezzo per l'accumulo di energia generata attraverso fonti rinnovabili. Il sistema proposto integra un elettrolizzatore ad ossidi solidi, un gassificatore a letto trascinato e la sintesi di Fischer-Tropsch. Il principale prodotto del sistema è il diesel di sintesi via Fischer-Tropsch, prodotto da vapore, CO2 e diverse risorse rinnovabili, ossia biomassa lignocellulosica ed elettricità generata da sistemi fotovoltaici ed eolici. Questo approccio presenta il vantaggio di accumulare, sotto forma di energia chimica dei combustibili idrocarburici, l'energia elettrica in eccesso proveniente dalle tecnologie a fonti rinnovabili, per un ulteriore utilizzo durante le ore di picco della domanda di energia. Inoltre, l'utilizzo di questi combustibili sintetici si traduce in un aumento della quota di energia da fonti rinnovabili nel sistema di trasporto. Nello stesso tempo vengono sfruttate tecnologie di distribuzione e conversione esistenti che presentano ancora buone efficienze operative. Il sistema proposto viene analizzato da diversi punti di vista, quali quello termodinamico, economico e ambientale. Questo studio include diversi aspetti della ricerca contemporanea, dalla ricerca della condizione operativa ottimale dei sottosistemi per produzione di syngas alla valutazione del potenziale teorico di sistemi integrati in diverse località.

Parole chiave: elettrolizzatore ad ossidi solidi, gassificatore a letto trascinato, la sintesi di Fischer-Tropsch, analisi termodinamica, economia, risparmio delle emissioni, politica

Sammanfattning

Under de senaste decennierna har förnybara energisystem fått stora uppmärksamheten. Anledningen härstämmar från ökade kunskaper om växthusgaser tillsammans med begränsningar i tillgängligheten och pålitligheten av konventionella energiresurser i framtiden. Förnybar energi kan betraktas som gratis, nästan obegränsad och ren; däremot har sådana resurser olika nackdelar. Utmaningar finns i förnybara energikällors förmåga att spontant bemöta elbehoven samt för användning som transportbränsle. En av de största utmaningar för solenergi och vindkraft gäller deras tidsvariation, som leder till svårigheter med anpassning mot energibehoven. Därför är det fördelaktigt att lägga till energilagring för att matcha tillförseln med efterfrågan.

Denna studie omfattar forskning omkring design och analys av ett integrerat system för framställning av syntesbränsle som ett sätt att möjliggöra energilagring. Det förslagna systemet integrerar fastoxid elektrolys, entrained-förgasning och Fischer-Tropsch processer. Systemets huvudprodukt är Fischer-Tropsch diesel-bränsle, som är framställt från ånga, CO2 och olika förnybara energikällor, nämligen lignocellulosisk biomassa, solelektricitet och vindkraft. Fördelen med detta koncept är möjligheten att kunna lagra överskottsel från förnybara energikällor i form av kolvätebränslens kemiska energi, som i sin tur kan utnyttjas när efterfrågan är hög. Användning av syntesbränslen utökar förnybar energis andel i tranportsektorn genom existerade distributions- och omvandlingstekniker.

Systemet är analyserat med hänsyn till termodynamiska, ekonomiska och miljömässiga perspektiv. Denna studie svarar på flera forskningsfrågor, från identifiering av optimala driftstillstånd för syntesbränslens upp- och nedströmsprocesser, till utvärdering av den teoretiska potentialen av integrerade system i olika geografiska områden.

Nyckelord: Fastoxidelektrolyser, Entrained förgasning, Fischer-Tropsch-processen, Termodynamisk analys, Ekonomi, Emissionsbesparing, Policy

Preface

An integration between solid oxide electrolysis (SOEC), entrained gasification (EG), and Fischer-Tropsch (FT) process and product upgrading technologies is suggested in this study. The main product of the system is FT diesel that is produced from precursor syngas that in turn is supplied from steam, carbon dioxide, and electricity inputs to SOEC and biomass to EG subsystem. Such a system not only increases share of renewables in the transportation system but also can play renewable energy storage role provided that required electricity for co-electrolysis is provided from one or more renewable resources.

This dissertation is organized into nine Chapters, ordered in such a way to present a logical picture of the proposed integrated system and technologies that are involved.

Chapter 1 provides a brief overview of the current issues in including renewables in existing transportation and electricity networks. Moreover, possible solutions to these issues and the role that the proposed integrated system can play are discussed in this Chapter. Objectives and methodology are also included.

Chapter 2 gives a historical background of each technology that is used in the integration. A brief overview of availability of each technology also can be found in this Chapter. Furthermore, the suggested schematic of each subsystem including all the typical and necessary equipment is provided.

Chapter 3 then continues with detail description of procedure that is used to model every individual component of system. Models that are used to estimate performance, energy and exergy efficiency, final production cost of FT diesel, possible GHG emission savings, and renewable potential of a given location are explained here.

Chapter 4 is dedicated to find the optimum operating condition of SOEC and EG subsystem to improve performance of system for production of certain amount of FT diesel.

Chapter 5 presents results of different possible integration approaches for the suggested technologies. In this Chapter two operation modes are suggested and their performance is compared to each other.

Chapter 6 continues with presenting the results that may help plant developers to find proper sizing of SOEC and EG subsystems. In other words, this Chapter presents result of system analysis from operational, economic, and environmental perspectives when different sizes of SOEC and EG are merged together.

Chapter 7 investigates implementation potential of the final detailed integration of the system based on the findings of previous Chapters. Four different cities in Europe are selected to study the impact that such integrations may have on the existing electricity, transportation, and heat networks.

No new idea can reach its full potential without proper and efficient initial support schemes. Hence, Chapter 8 gives a brief overview of available support policies that can be useful in promoting implementation of such systems. A few suggestions are provided for increasing the speed of development and integration of this system and similar systems in the current energy system. Since a thorough study of current political structure of every country is beyond the scope of this study, only available policies in Italy and Sweden are presented in this Chapter. The choice of country is in agreement with the location of cities that are used in the performed case study in the previous Chapter.

Finally, Chapter 9 provides a general conclusion based on findings of previous Chapters. Also, some suggestions to tackle the issues that may arise from implementation of this system are given and can be used as suggestions for future research.

Acknowledgements

I would like to express my gratitude to my supervisory team, Professor Massimo Santarelli, Professor Andrew Martin, and Dr. Vera Nemanova. I am especially grateful of my supervisor Professor Andrew Martin whose guidance, understanding, and support helped the progress of this project immensely. My especial thanks go to Dr. Yohannes Kiros for acting as my internal reviewer and his comments and suggestions. I would like also to express my gratitude to Anders Malmquist, Justin Chiu, and Vladimir Kutcherov for acting as members of the internal reviewing committee. I am also grateful of support and patience of the study director of PhD program (KTH) Professor Rahmatollah Khodabandeh and KTH postgraduate studies officer Ms. Gülten Baysal. Help of my dear friend, Ms. Monica Arnaudo, in translating the Italian abstract is highly appreciated.

My grateful thanks also go to Erasmus Mundus Joint Doctoral Programme SELECT+ that provided the necessary fund for this PhD topic. Support of Ms. Chamindie Senaratne, deputy program director of SELECT+, is gratefully acknowledged. Her kind support was greatly helpful to overcome usual and unusual challenges that occurred during my PhD. I also would like to acknowledge the EU projects DEMOSOFC, BRISK 2, and Pilots4U that provided funding for the final months of my PhD.

Great deals of appreciation go to my parents whose love and patience encourage me to be a better person. Especial thanks go to my dear father who always was a role model in my life and his untimely departure would always be a burden on my heart and soul. Also, especial thanks go to my wonderful mother who always believes in me and supports and encourages me in every step of my life. I also like to thank my dear sister, Mehrnoush Samavati, and my lovely brother, Soheil Samavati, who are always there through ups and downs of my life. I would like to thank my friends Sara Ghaem Sigarchian, Mazyar Karampour, and Yasaman Saffari, for being by my side through the darkest hours of my life.

At last but not least, I am grateful of my wonderful friends and colleagues, Saman Nimali Gunasekara, Jose Fiacro Castro Flores, Fumi Harahap, Maria Xylia, and Marta Gandiglio.

Publications

This Doctoral thesis is based on the scientific publications listed below.

I. Samavati, M., Santarelli, M., Martin, A., Nemanova, V., "Thermodynamic and economy analysis of solid oxide electrolyser system for syngas production". *Energy*, 2017, DOI: 10.1016/j.energy.2017.01.067

II. Samavati, M., Nemanova, V., Santarelli, M., Martin, A., "Energy and Exergy analysis of syngas production via Biomass Gasification", 24th European Biomass Conference and Exhibition, June 6-9, 2016, Amsterdam, The Netherlands, DOI: 10.5071/24thEUBCE2016-2CV.3.51

III. Samavati, M., Martin, A., Nemanova, V., Santarelli, M., "Integration of Solid Oxide Electrolyser, Entrained Gasification, and Fischer-Tropsch Process for Synthetic Diesel Production: Thermodynamic Analysis", *International Journal of Hydrogen Energy*, 2018, DOI: 10.1016/j.ijhydene.2018.01.138

IV. Samavati, M., Santarelli, M., Martin, A., Nemanova, V., "Production of Synthetic Fischer-Tropsch Diesel from renewables _ Thermoeconomic and Environmental Analysis", *Energy and Fuels*, 2017, DOI: 10.1021/acs.energyfuels.7b02465

V. Samavati, M., Martin, A., Santarelli, M., Nemanova, A., "Synthetic diesel production as a form of renewables electricity storage", *Energies*, DOI:10.3390/en11051223

In papers I-IV, first author was the main author, performed the literature review, developed the methodology, built the simulation model, performed the analysis, and interpretation of the results. The other authors acted as mentors and reviewers. In paper V, first author was the main author, performed the literature review, developed the methodology, built the simulation model, performed the analysis, and interpretation of the results. The second author was also involved in the development of paper methodology. The other authors acted as mentors and reviewers.

Nomenclature

Abbreviation

abs	Absolute pressure
ASR	Area specific resistance
ASU	Air separation unit
BCC	Base capacity of component
CCR	Capital charge rate
DH	District heating
ECC	Estimated capacity of component
EG	Entrained gasification
FT	Fischer-Tropsch process
GHG	Greenhouse gas emission
GTS	Gas turbine share
HTE	High temperature electrolyser
IC	Interest during construction of plant
LGHC	Light gaseous hydrocarbons
LHV	Lower heating value
LTE	Low temperature electrolyser
LTFT	Low temperature Fischer-Tropsch
MP	Medium pressure
OCV	Open circuit voltage
O&M	Operation and maintenance
PV	Photovoltaic
RES	Renewable energy systems
SOEC	Solid oxide electrolysis cells

TPC	Total plant cost
WGS	Water gas shift

Greek symbols

α	Relative mole fraction of methane
β	Biomass exergy constant
$\Psi_{biomass}$	Exergy content of biomass, MW
$\Psi_{F,sys}$	Exergetic fuel, MW
$\Psi_{P,sys}$	Exergetic product, MW
η_s	Energy efficiency of the system

Latin symbols

A	Heat exchange area, m^2
a	Wind shear exponent
b	Exergy content of stream, MW
b_{ph}	Physical exergy content of stream, MW
b_{ch}	Chemical exergy content of stream, MW
C_{ICP}	Annualized cost of installed capital of plant, $/year
$C_{O\&M}$	Annualized cost of operation and maintenance, $/year
C_U	Annualized cost of utilities, $/year
$C_{El.}$	Annualized cost of electricity, $/year
$C_{Feedstock}$	Annualized cost of feedstocks, $/year
C_{income}	Annualized income from selling the byproducts, $/year

C_p	Purchase cost of heat exchanger, $
C_B	Heat exchanger base cost, $
$C_{HX\text{-}Capital}$	Capital cost of heat exchanger, $
C_{base}	Base cost of each component, $
$C_{component}$	Capital cost of each component, $
E_s	Exergy efficiency of the system
E	Total emissions from the use of the renewable fuel, g_{CO2eq}/MJ
E_f	Emissions from the use of the fossil based fuel, g_{CO2eq}/MJ
e_{ec}	Emissions from the extraction or cultivation of raw materials, g_{CO2eq}/MJ
e_l	Annualized missions from carbon stock changes caused by land-use change, g_{CO2eq}/MJ
e_p	Emissions from processing, g_{CO2eq}/MJ
e_{td}	Emissions from transport and distribution, g_{CO2eq}/MJ
e_u	Emissions from the fuel in use, g_{CO2eq}/MJ
e_{sca}	Emission saving from soil carbon accumulation via improved agricultural management, g_{CO2eq}/MJ
e_{ccs}	Emission saving from carbon capture and geological storage, g_{CO2eq}/MJ
e_{ccr}	Emission saving from carbon capture and replacement, g_{CO2eq}/MJ
e_{ee}	Emission saving from excess electricity from co-generation, g_{CO2eq}/MJ
F	Faraday constant, 96485 J per volt. gram equivalent
F_P	Pressure factor of heat exchanger
F_M	Material factor of heat exchanger
$F_{O\&M}$	Operation and maintenance factor
G	Average global solar irradiance, W/m^2

G_{soc}	Irradiance at standard operating condition, W/m^2
G_{stc}	Irradiance at standard test condition, W/m^2
$\Delta G_{f,\,i}$	Gibbs free energy of formation, (i: water, CO_2), kJ/kmol
i	Current density, A/cm^2
I_F	Faradic current, A
K	Approximate effect of temperature on power, %/ ^oC
m	Mass flow rate, kg/s
n_{O2}	Production rate of oxygen, mol/s
P	Operating pressure of the electrolyser, bar
P_{std}	Pressure at the standard condition 1.013 bar
P_{PV}	Power output of PV cells, W
Q_{tot}	Total heat input to the system, MW
R	Universal gas constant, 8.31451 J/mol.K
S	Entropy, kJ/kg.K
T	Temperature, ^oC
T_c	Cell operating temperature, ^oC
T_{soc}	Cell temperature at standard operating condition, ^oC
T_{stc}	Cell temperature at standard test condition, ^oC
U_n	Wind speed at hour n, m/s
U_{ave}	Daily average wind speed, m/s
U_{max}	Daily maximum wind speed, m/s
U_z	Wind speed at the wind turbine hub height, m/s
U_{zr}	Wind speed at the reference height, m/s
V_N	Nernst Voltage, V
V_o	Operating cell voltage, V
V_{OC}	Open circuit voltage, V
V_{TN}	Thermo-neutral Voltage, V

$W_{el,tot}$	Total electrical power demand of system, MW
x	Cost scaling factor
y_i	Molar fraction of each component in flow stream
Z	Wind turbine hub height, m
Z_r	Reference height, m

Table of Contents

List of Figures

List of Tables

1 Introduction

During the past decades considerable attention has been dedicated to renewable energy systems (RES). This is due to the increased awareness regarding greenhouse gas (GHG) emissions as well as limits of the future availability and reliability of conventional energy and power systems. On one hand the energy sources that human societies are currently built on, fossil fuels, are finite. On the other hand there is a significant scientific consensus that anthropogenic activities cause rapid and severe climate change beyond the adaption potential of ecosystems [1]. In addition, national security concerns and significant increase of fossil fuel prices in the global energy markets direct the societies towards utilizing renewable energy resources.

Renewable energy originate from the solar radiation (e.g. solar, wind), movement and gravitation of the planets (e.g. tidal), and the stored heat in the earth (geothermal). Regardless of the renewable energy origins, they are considered as free, nearly infinite, and clean resources having very low impacts on the environment [2]. However, such resources have their own drawbacks. Renewables face challenges in meeting instantaneous electricity demand and for utilization as transportation fuels [3]. One of the main challenges of renewable energy sources like solar and wind is due to their variability, making them incapable of meeting the required energy demands at all times. For example, wind can be down for days or there is no sunlight during night. Conversely, there might be periods where power production from these sources exceeds demand. These issues can cause power flow imbalances through the energy supply system, making it less reliable. Therefore, it can be beneficial to store excess electricity for further usage. Hence to tackle the intermittent nature of renewable energy sources, different types of energy storage technologies have been proposed and applied. The following is a brief description of few common storage techniques that are suitable for mid-term and long-term energy storage [4–6]:

- *Pumped-Hydroelectric Energy Storage (PHES)*: This is the most mature and largest storage technique available so far. It requires two water reservoirs at different altitudes. During off-peak electrical demand, water is pumped from a lower reservoir to the higher reservoir to be stored until it is needed. However, its main drawback is due to specific geological requirements - the necessity of locating two large reservoirs with a sufficient amount of hydraulic head between them near the energy system.

- *Underground Pumped-Hydroelectric Energy Storage (UPHES)*: This system has the same operating principle as PHES system with one major difference that is the lower reservoir is located below the earth's surface while the upper reservoir is at the ground level. Since the lower reservoir can be obtained by drilling underground the geological dependence is not as high as PHES. However, this may lead to higher capital costs. Nevertheless, this technology is not commercially mature and there are very few, if any, UPHES facilities in operation.

- *Compressed Air Energy Storage (CAES)*: In this technology air is pre-compressed using off-peak electrical power and stored in large high pressure storage reservoirs. During peak hours, the compressed air is then released and partially mixed with gas and used in gas turbine cycle producing electricity. Like PHES, its main drawback is dependency on geographical location. It is difficult to locate sufficiently large underground reservoirs close enough to the specific application.

- *Battery Energy Storage (BES)*: BES operate similarly to conventional consumer-oriented batteries but in larger scales. The three most important large scale types of batteries are Lead-Acid, Nickel-Cadmium, and Sodium-Sulfur. BES is mostly suitable for small to medium energy storage applications. Also, disposal of the batteries maybe problematic due to the usage of toxic materials in their structure. Moreover, the battery life time is greatly affected by the rapid charge and discharge cycles as well as variations in environmental conditions.

- *Supercapacitor Energy Storage (SCES)*: Super-capacitors have the same operating principle as conventional capacitors, storing energy in an induced electrical field. However, they have a low energy storage density which not only makes them heavier and bulkier than batteries but also leads to higher capital cost in large scale applications.

- *Chemical Energy Storage (CES)*: Carbon and hydrogen content of biomass and municipal solid waste can be converted to form short and long chain hydrocarbons using processes such as Fisher-Tropsch.

Of these technologies CES allows for immediate conversion of renewable energy and is largely independent of geographical and geological situation or scale of the application. Uniquely, it offers a pathway for production of CO_2-neutral transportation fuels. The transportation sector contributes to about 14% of global CO2 emissions worldwide [7]. The majority of greenhouse gas emissions in this sector is the CO_2 produced in internal combustion engines from combustion of fossil-based fuels like gasoline and diesel. Renewable CO_2-neutral transportation fuels produced via CES technologies can therefore reduce the net CO_2 emissions of the road transportation system and reduce the dependency on fossil fuels. So far the proposed systems include gasification of biomass to produce the precursor syngas for further production of transportation fuels [8–15]. Several feedstocks can be considered for gasification process such as vegetable oils, sugar cane, and lignocellulosic biomass. The latter feedstock is favored since such second-generation biofuels do not compete with food production. However the available amount of lignocellulosic biomass is not sufficient to cover the transportation sector demands on its own. For example, considering 50% yield from biomass to biofuel, Sweden's annual potential for production of biofuels from lignocellulosic biomass is estimated to be in range of 25-30 TWh while the transport sector used around 32 TWh gasoline and 45 TWh diesel in 2013 [16].

As a solution to these issues, a second pathway can be included in the CES system for supplying the required syngas. For this purpose, electrolysis units can be used for production of pure hydrogen or syngas via electrolyzing of steam or mixture of steam/carbon dioxide. This approach has the benefit of storing the excess electrical energy from

renewables such as solar electricity in form of chemical energy of the hydrocarbon fuels for further usage during the peak hours. Also, using these synthetic fuels results in an increase of renewable energy share in transportation system. Electrolysis cells (also called electrolysers) have gained attraction because of their simplicity, performing the dissociation in a single step without need of any moving parts, and producing and releasing the products separately in the anode and cathode compartments of the cell [17]. Electrolysers are generally divided into two main categories based on the operating temperature: low temperature (50-80 ^{o}C) and high temperature (700-1000 ^{o}C). Low temperature electrolysers (LTE) can be used for hydrogen production, while high temperature electrolysers (HTE) have the ability to electrolyze steam and carbon dioxide simultaneously to produce synthetic gas (hydrogen and carbon monoxide). Such products can then be used directly in a conventional power plant or fuel cells to cover power demands [18,19]. Since gaseous hydrogen has a considerably lower energy density compared to liquid and even gaseous hydrocarbons, it is beneficial to convert the produced hydrogen or syngas into high value hydrocarbons and other products. In this case, there is no need for new infrastructure since these synthetic fuels are quite similar to fossil fuel counterparts, and they can be stored, transported and consumed using established technologies and infrastructure [18,20].

Another unique advantage that can be gained by including the co-electrolysis process as an extra syngas production pathway is the possibility of recycle and reuse of carbon dioxide. Figure 1 illustrates annual greenhouse gas emission by economy sector and by type of gases. As can be seen, carbon dioxide from two sectors – fossil-based transportation fuels and industry – accounts for around 65% of total global emissions for 2010. Reuse of carbon dioxide in a co-electrolysis process for production of synthetic hydrocarbon fuels can have a positive impact on mitigation of this part of GHG emission. Strictly speaking, implementation of such a system can be useful in reduction of GHG emission not only in electricity and heating sector by making integration of intermittent renewables to the existing energy system simpler, but also in transportation and industry sector by using the produced CO_2-neutral synthetic hydrocarbons in these sectors.

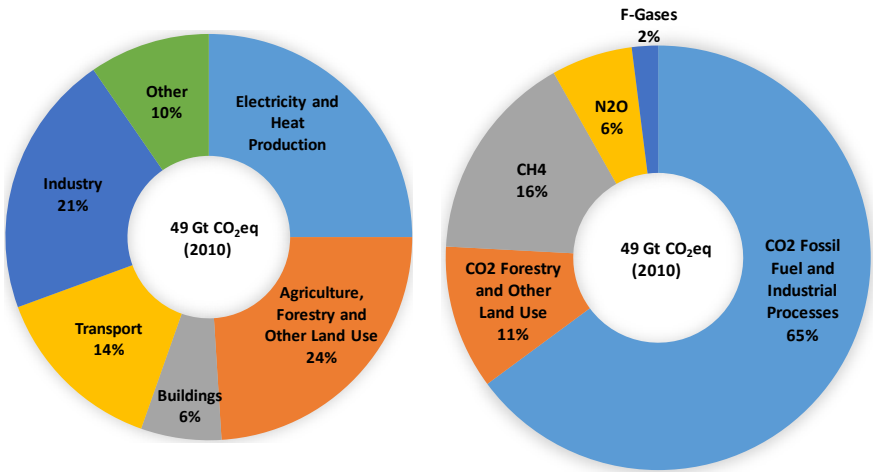

Figure 1- Annual global greenhouse gas emissions by A) economy sector, B) groups of gases [7]

Most published studies in this area consider production of Fischer-Tropsch (FT) liquid transportation fuels from biomass sources:

- Manganaro et al. [21] presented an energy balance on production chain of high quality liquid transportation fuel from harvesting of surplus biomass to production of FT diesel. They showed that the mass of produced FT diesel accounts for about 13% of initial biomass input, and recommended that use of produced char and non-condensable gases during gasification process for drying and pyrolysis of biomass would increase the system efficiency dramatically.

- Baliban et al. [22] introduced a process framework for the conversion of hardwood biomass to liquid transportation fuels. They studied 12 cases to determine the effect of key operating parameters on the overall system cost. The results showed that after reaching a certain price of hardwood biomass, the proposed refinery cannot economically compete with crude oil refineries.

- Niziolek et al. [23] used an optimization-based process synthesis framework to investigate production of liquid transportation fuel from coal and biomass in 24 case studies. Production of liquid transportation fuels from mixture of biomass and coal was found to be economically competitive with conventional fuels with GHG emission reductions of 30-50%.

- Trippe et al. [9] compared two different pathways of biomass-to-liquid, production of gasoline through dimethyl ether (DME) synthesis and production of gasoline and diesel via FT process. Their results showed that the production cost of biofuels is 76 to 93% higher than current market prices. However, these price differences can be lowered down to 7 to 18% when coal is replacing biomass as a feedstock.

- Kim et al. [15] focused on long-term operation of biomass-to-liquid through integration of gasification and FT process. The main goal was to produce syngas with high level of purity that satisfy the required condition in the FT reactor. The integrated system operated for 500 hr over several runs and their results proved the technical feasibility of such integrations.

- Leibbrandt et al. [14] predicted syngas composition from biomass at different operating conditions using a thermodynamic equilibrium model. System efficiencies as high as 51%, corresponding with maximum gasification efficiency of 75%, were determined. Inclusion of a shift reactor downstream of gasifier was shown to be more energy efficient than regulating steam to biomass ratio at the entrance of system.

- Buragohain et al. [13] used a non-stochimetric equilibrium model to estimate the optimized operating condition of gasification for production of FT fuels. An operating temperature of 800-1000 ^{o}C with air as oxidant instead of steam or steam/air mixture was suggested as the optimum operating condition.

- Swain et al. [10] performed a life cycle assessment on production of high-quality FT fuels from biomass resources. Findings showed that transportation sector emissions can be reduced by

28-69% by using FT fuels that are produced from straw, forest wood or short-rotation wood. Further improvements in the life cycle of first generation of biofuels are required to ensure desired GHG emission reductions.

In contrast to these investigations, there are only a handful of studies that consider integration between electrolysis and FT process. Becker et al. [24] proposed a theoretical model for integration of FT to a high temperature solid oxide co-electrolyser unit, and showed that it is possible to produce liquid hydrocarbon fuels with system efficiency as high as 54.8 % (HHV base). In a more recent study, Stempien et al. [25] used a thermodynamic model of a simplified integration between SOEC and FT systems and concluded that driving system compressors with the energy of recovery turbines will result in highest system efficiency (about 66%). Li et al. [26] suggested a route for synthetic fuel production via integration of electrochemical conversion of CO_2 and FT process. According to this study, the produced synthetic fuels cost would be in range of 3.80 to 9.20 $/gallon depending on the level of technology advancement. Chen et al. [27] performed a numerical study on SOEC-FT for methane production at pressures 1-5 bar. In this pressure range, they suggested optimal pressure of 3 bar where methane production would be at its peak value. However, the main focus of their study was the reactor and reactions and they did not consider other elements that are required for the system. Until now there is no available publication that considers the integration of the three key subsystems for biomass to syngas conversion, electrolysis, and syngas to liquid fuel conversion.

1.1 Objectives

The main objective of this investigation is to develop a pathway for synthetic hydrocarbon liquid fuel production from renewable sources. Such systems not only increase share of renewable energy in transportation section but also can be considered as solution for intermittent nature of renewables. Furthermore, these synthetic fuels are quite similar to the fossil based fuels and consequently can be stored, transported and utilized using the current technologies and infrastructure. Moreover, this integration increases production potential of advanced liquid hydrocarbon fuels and consequently decreases the gap between production rate and transportation demand in a specific location. In

general, including solid oxide electrolysis and entrained gasification technologies in the integration system 1) guarantees annual production of certain amount of FT fuels for transportation system, 2) increases capacity factor of integrated system, 3) increases nominal size of FT system, 4) provides a reliable source of carbon dioxide on site, and 5) allows recycle and reuse of carbon dioxide. At last but not least, such integrated systems have capability of operating at or near closed-loop operation.

This study is dedicated to a thorough analysis of a possible pathway for production of FT diesel from renewable energy sources. Such studies are useful in understanding of the technology from a system perspective, which is an essential step for development and deployment in future energy systems. In this context, an integrated system is proposed which consists of RES-fed solid oxide electrolyser (SOEC), entrained gasification (EG), and Fischer-Tropsch process (FT) and upgrading system. The main output of the system is FT diesel while the input is biomass, carbon dioxide, steam and (excess) electricity from renewable plants such as solar and wind. Naphtha, wax, light hydrocarbons, hydrogen, and heat which are produced during Fischer-Tropsch process and product upgrading are considered as byproducts of the integrated system. Figure 2 illustrates the simplified concept of integrated system as a control volume and its interaction with its environment.

Figure 2- Simplified schematic of integrated system concept

This study addresses the following research questions:

- What are the optimal system operating conditions?
- What are the possible ways to integrate the selected technologies?
- What is the optimal subsystem sizes?

- What is the possible synthetic liquid production rate for a certain location?

1.2 Methodology

A hypothetic-deductive method is chosen to meet the objective of this study. In other words, a theoretical model is developed based on the available data and its simulation results are verified by comparing them with the available experimental results in the literature. The system was modeled using ASPEN Plus software. To reduce complexity of system model, the system was divided into three subsystems:

- Solid oxide electrolyser subsystem
- Entrained gasification subsystem
- Fischer-Tropsch subsystem

These models include all the main components that can be found in real systems. Each model then was validated by comparison between achieved results and the available experimental results in published literature. Finally, the developed models were merged together and studied considering different criteria in an attempt to find the answer to the proposed research questions. More information on subsystem models and details regarding the approaches that are employed to investigate different aspects of proposed integrated system can be found in Chapter 3.

2 System Description

The simplified schematic of the integrated system is shown in Figure 3. Such integrated system can act as:

- a RES-electricity storage in form of chemical energy of liquid hydrocarbon fuels
- a pathway for production of CO_2-nuetral transportation fuels.

Although FT diesel is considered as the main product, other byproducts (produced during FT and upgrading process) such as naphtha and wax would be available. As can be seen in Figure 3, syngas is produced from either high temperature co-electrolysis or entrained gasification of biomass which consequently will results in increase of potential production of FT diesel from renewables. In addition, it allows the internal recovery of subsystems by-products. To exemplify, pure oxygen which is produced during co-electrolysis can be used as an oxidant agent in the gasification subsystem. Alternatively, the produced carbon dioxide in the gasification subsystem serves as a source of input to the SOEC subsystem. Hence, based on the chosen system operation scheme and its configuration, near closed-loop operation may be possible.

A brief introduction of history and background of each technology that is used in the integrated system is presented in this Chapter.

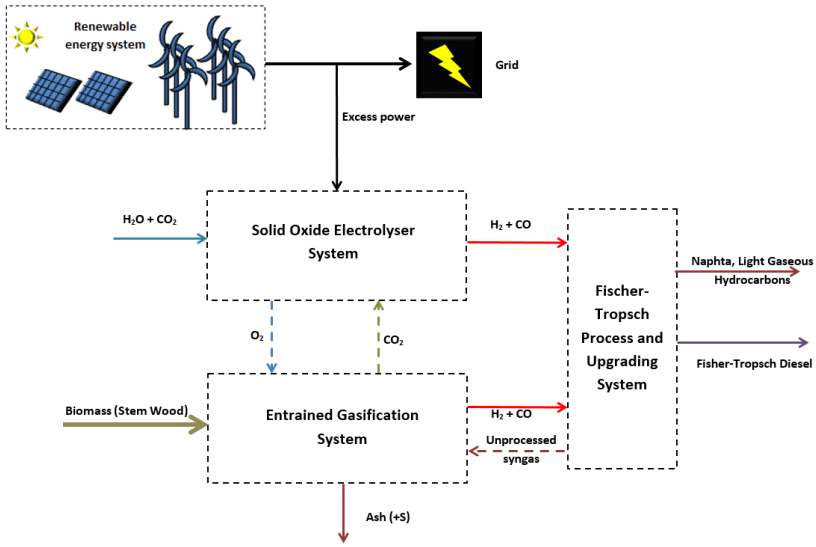

Figure 3- Integrated system schematic

2.1 Electrolyser

2.1.1 Background

An electrolyser is an electrochemical device in which an electrical current is passed through water and decomposes it into its structural elements, hydrogen and oxygen. The electrolyser consists of several electrolysis cells which in turn are made of two electrodes, cathode and anode, separated by the electrolyte layer. Hydrogen is formed in the cathode compartment while oxygen in anode electrode. There is no necessity for using downstream equipment to separate electrolysis products. Also, due to its simple concept they can be applied at a great range of scale.

References [28–30] provide an historical overview of electrolysis. The possibility of hydrogen production from water was first discovered by Nicholson and Carlisle in 1800. However, it was not until 1939 that the first large water electrolysis plant with a capacity of 10,000 Nm^3 H_2/h went into operation. Zdansky/Loza produced first pressurized industrial electrolyser in 1948. In 1966, General Electric introduced first solid

polymer electrolysis device which later has been developed by ABB (formerly Brown, Boveri Ltd) Switzerland between 1976 and 1989. On the other hand, the first solid oxide water electrolyser was developed in 1972. In 1978, the first advanced alkaline system started. To this date, optimization and development of different electrolysis technologies continues [28–30].

2.1.2 Classification of Electrolyser

Generally, electrolysers are named based on the type of electrolyte that they use and classified based on their operating temperature. Currently, only low temperature electrolysers are commercially developed which includes, alkaline and proton exchange membrane electrolyser. However, recently third option is introduced by using high temperature electrolysis via solid oxide electrolyser which is still under research and development. Operating principles and properties of each technology are as follows [28,29,31], with schematics and key data contained in Figure 4 and Table 1 respectively:

- *Alkaline electrolyser (AE)*: Water enters the cathode electrode where it is reduced to hydrogen and hydroxyl ions. Hydrogen ions escape the cathode surface, are recombined in gaseous form, and then exit the cathode. Simultaneously hydroxyl ions move toward the anode through electrolyte under the influence of an electrical field. In the anode compartment, hydroxyl ions react with each other to produce oxygen and water molecules. This technology is the most advanced type of electrolysis and is currently standard for large-scale applications. Since there is no necessity for noble catalysts in its structure, it is cheaper than other types of low temperature electrolysers. However, the produced gases have lower purity due to the crossover of gases. Also, they have limited ability to respond to fluctuations in electrical input which is an intrinsic character of renewable sources.

- *Proton exchange membrane electrolyser (PEM)*: this electrolyser uses a solid electrolyte with the ability to transport only positive ions through it, hence the name proton exchange membrane. Unlike AE, water enters anode compartment where is decomposed to hydrogen and oxygen ions. Positive hydrogen ions are transported toward cathode side via electrolyte

membrane where they form hydrogen gas. Since the electrolyte is almost impenetrable by negative oxygen ions, the produced hydrogen has a high purity. Also, PEM has fast response times to electrical input fluctuations and are able to operate from zero to 100% of their nominal power without any efficiency penalty. These characteristics make them an interesting option in case of renewable energy storage. However, PEM needs a metal-based catalyst (usually nickel) for its operation and therefore the water should be pure enough to prevent any catalyst degradation and poisoning. Another consequence of necessity to use catalyst is the higher cost of stack and the system.

- *Solid oxide electrolysis cells (SOEC)*: Due to high operating temperature of this type, steam is used in the cathode side, which decomposes to hydrogen and oxygen ions. The former recombines on the cathode side and leaves the electrolysis cell as gaseous hydrogen. The latter, on the other hand, moves towards anode electrode through solid oxide electrolyte to form oxygen gas. Steam dissociation requires less energy than water; i.e., the electricity demand of this technology is much lower than the other approaches (Table 1). It is the only available technology that has the possibility of internal methane and syngas production by co-electrolysis of steam and carbon dioxide. The produced syngas then can be converted to liquid fuels making them an attractive candidate for long term storage and distribution of renewable sources. SOEC also benefit from high achievable efficiencies. However, this technology is still at R&D stage and there are not enough information especially regarding their durability and cost.

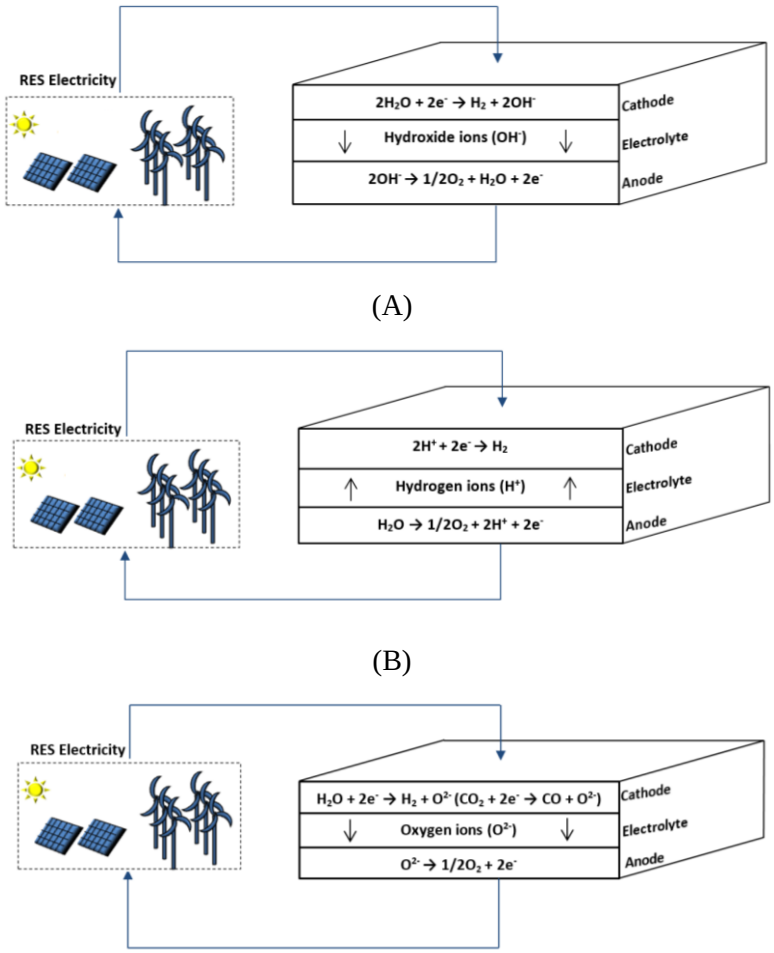

Figure 4- Diagram of operation principle of A) alkaline, B) proton exchange membrane, C) solid oxide electrolysers

Table 1- characteristics of different electrolysis technologies [31–33]

Specification	unit	Alkaline	PEM	SOEC
Cell temperature	^oC	60-80	50-80	800-1000
Outlet pressure	bar	32	30	8
Capacity range	Nm^3/h	1-1000	1-30	3
System price	€/Nm^3/h	7000-8500	15,000	4000
System electrical consumption at the beginning of lifetime	kWh/Nm^3	4.8-5.5	4.2-5.6	3.3
Power consumption increase due to cell degradation (@ 24x365 operation)	% per year	2-4	2-4	8
Cell/stack life time	h	<90,000	<20,000	<40,000
System life time	year	10	3	1

*2.1.3 Solid Oxide Electrolysis System**

Figure 5 shows a simplified schematic of the solid oxide electrolyser system for co-electrolysis. This system consists of all major components that would be present in the actual system, e.g. compressors, pumps, solid oxide electrolyser, heat exchangers, several mixers and a separator.

A water stream (stream 8) is first pressurized to the subsystem operating pressure (stream 9) before being mixed with the condensate stream (stream 19) from the condenser. The pressurized water (stream 10) then goes through a steam generator to produce pressurized steam (stream 11). This stream then enters cathode mixer where it is mixed with pressurized carbon dioxide (stream 7) and recycled syngas (stream 21). The latter is a requirement to preserve the reducing condition on the

* This section is based on the first, third, fourth, and fifth papers.

cathode electrode. The mixture (stream 12) is then heated (cathode heat exchanger) to reach the SOEC operating temperature before entering the cathode compartment (stream 13). In the electrolysis unit, the reactants mixture is converted to syngas (cathode) and oxygen (anode). At the cathode outlet, the produced syngas (stream 14) is separated into two streams. A fraction of syngas (stream 20) first goes through recycle compressor to compensate for the pressure loss in the components before being recycled back (stream 21) to the cathode inlet. The remaining syngas (stream 15) is cooled down in syngas heat exchanger I and the condenser, yielding a dry product gas. Water circulation pump and recirculating compressor are included to compensate for related pressure losses.

On the anode side, sweep air (stream 1) is pressurized in the air compressor and then is heated to reach the operating temperature of SOEC in the anode heat exchanger I. Stream 3 then enters anode compartment and is mixed with the produced oxygen before leaving the SOEC (stream 4). Afterward, anode exhaust gases (stream 4) are cooled down in anode heat exchanger II before being purged to the environment. Although it is possible to produce pure oxygen in the anode compartment by eliminating the sweep gas, there are technical issues associated with handling and storing high-temperature pure oxygen [34,35]. So, whenever internal recovery of oxygen inside the integrated system has not been considered, produced oxygen in the anode compartment will be diluted using sweep air.

The developed Aspen Plus flowsheet of SOEC subsystem can be found in Appendix I- Aspen Plus Flowsheets.

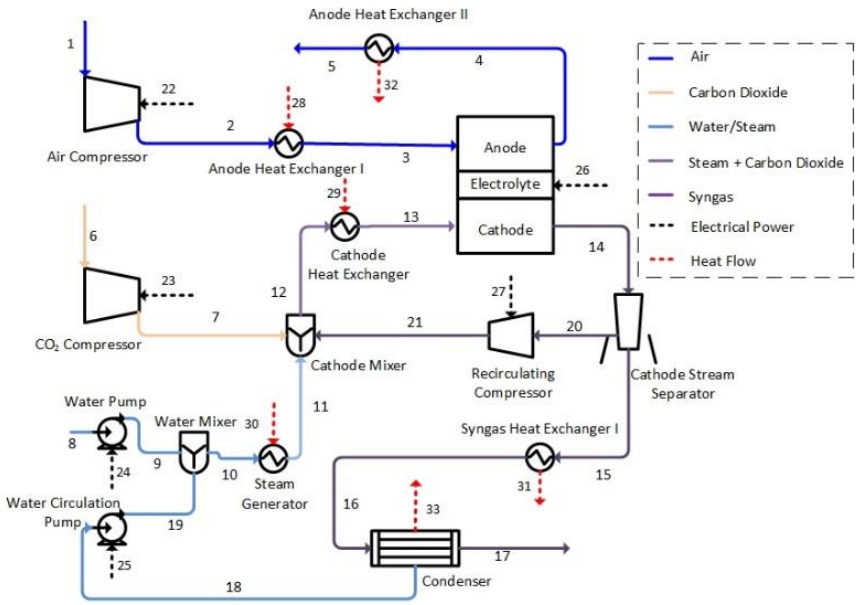

Figure 5- Schematic of Solid oxide Electrolyser system for co-electrolysis

Figure 6 illustrates the SOEC subsystem for the case of steam electrolysis. As can be seen, the major difference between SOEC subsystem for electrolysis and co-electrolysis is the elimination of the CO_2 compressor.

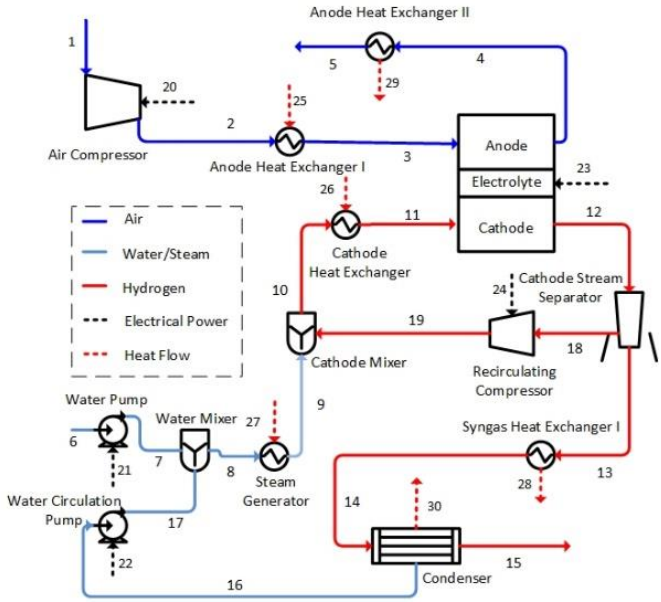

Figure 6- Schematic of Solid oxide Electrolyser system for electrolysis

2.2 Gasification

2.2.1 Background

Gasification is a chemical process that converts organic or fossil fuel based carbonaceous materials into mixture of light gases including hydrogen, carbon monoxide and carbon dioxide. Therefore, it can be considered as an upgrading process in which solid fuels transform to gaseous materials which are easier and more convenient to handle and use.

Jan Baptista Van Helmont first discovered the possibility of producing gaseous materials from heating wood or coal in 1609 [36]. However, early developments in gasification process date back to 1790s when a Scottish engineer, William Murdock, successfully commercialized coal gasification for the gas-lighting systems, which cost almost 75% less than oil lamps and candles [37]. Lighting was an accessory to the industrial revolution due to the possibility of extended work hours in factories.

However, the invention of the incandescent light bulb in the 1900s as well as exploitation of natural gas reduced usage of coal and biomass gasification technologies for lightning and heating. During the Second World War, interest in gasification process for production of synthetic fuels regained. However, end of war and the abundance of cheap oil from Middle East eliminated the necessity for production of synthetic fuels and chemicals and consequently reduced development rate of coal and biomass gasification technologies. Nevertheless, since the 1970s, after the oil embargo incidence which shocked the global economy, the gasification process regained interest especially in Western countries to reduce dependency on imported oil. Also, global warming and the efforts to move away from fossil fuel based chemicals and technologies pushed the development of gasification technologies forward [36–38]. Figure 7 shows historical worldwide growth of gasification capacity since 1970 [39].

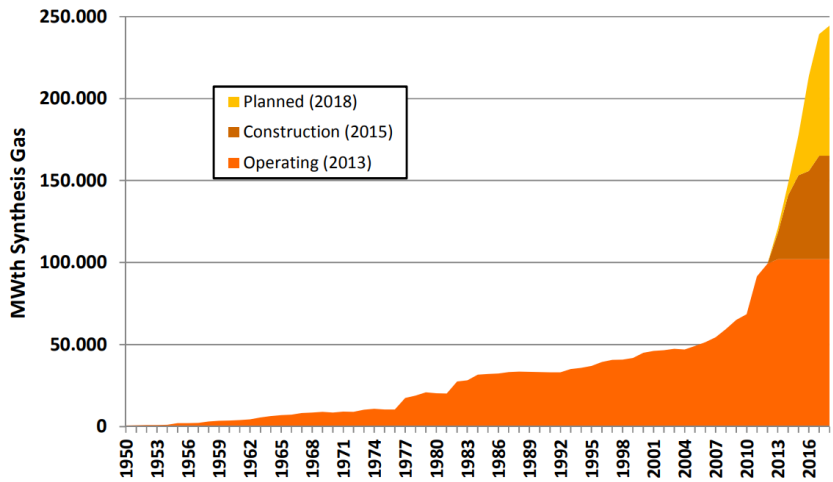

Figure 7- Cumulative Worldwide Gasification Capacity and Planned Growth by year [40]

2.2.2 Classification of Gasifiers

In general gasification technologies are classified either based on the type of oxidant flow, air blown or oxygen blown, or type of gasifier

reactor. The latter, however, is mostly used to identify the type of gasification system. Based on the reactor type gasification technologies are classified into three groups [41],

- *Moving Bed*: fuel particles enter gasifier at top and gasified while moving through reactor in a downward motion (Figure 8A). Ash and residue will be collected at the bottom of gasifier. On the other hand, oxidant flow enters from the bottom. Moving bed gasifiers are counter-current flow reactors: produced syngas leaves the reactor at top and therefore pre-heats fuel particles before entering gasification area. Hence, syngas temperature is lower than required temperature for complete carbon conversion. Residence time in these reactors is on the order of hours.

- *Fluidized Bed*: like moving bed reactors, fuel particles enter gasifier at the top of reactor while oxidant flow enters from bottom (Figure 8B). The provided oxidant flow rate should be enough to float fuel particles inside the reactor, so new fuel particles will be well mixed with partially and fully gasified particles. Hence temperature gradients throughout the reactor can be considered uniform. Generally a cyclone is required to be installed downstream to capture bigger particles entrained in the syngas which are recycled back to the reactor. Normally, the residence time is shorter than moving bed reactors.

- *Entrained Flow*: Figure 8C shows a generic diagram of entrained gasifier. Since both fuel particles and oxidant flow enter at the top of reactor and move toward bottom, this gasifier is considered a co-current flow reactor. These types of gasifiers operate at high temperatures and consequently residence time is in order of seconds. Also, due to very low residence time only very small fuel particles should be used to ensure complete carbon conversion. To achieve such high temperatures, entrained gasifiers use oxygen as oxidant rather than air.

Table 2 lists typical characteristic of different types of gasifiers.

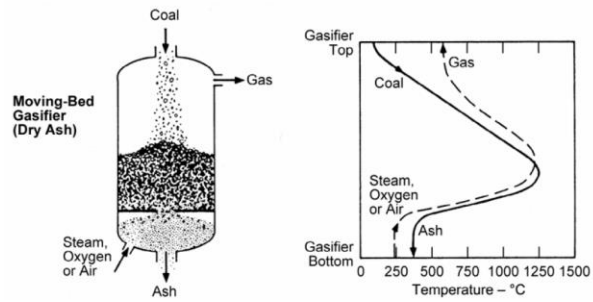

(A)

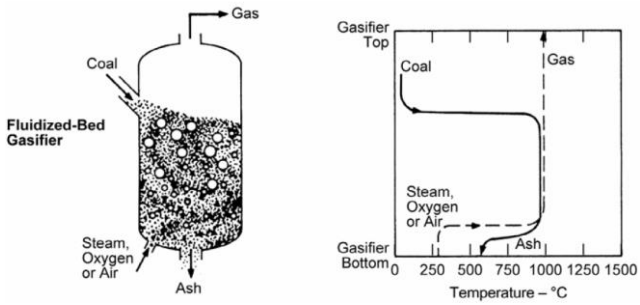

(B)

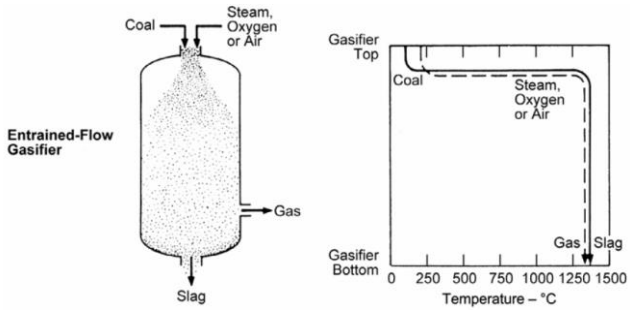

(C)

Figure 8- Diagram of generic A) moving bed, B) fluidized bed, C) entrained gasifier [41]

Table 2- Classification of gasification technologies [42,43]

Features	Moving bed	Fluidized bed	Entrained flow
Temperature (°C)	425-650	900-1050	1250-1600
Fuel particle size (mm)	5-80	<6	<0.1
Fuel feeding	Dry	Dry	Dry/Slurry
Oxidant demand	Low	Moderate	High
Tar	Yes	Some tar and particulates	None or negligible
H_2:CO	>2:1 to <1:1	<1:1	~1:2

*2.2.3 Entrained Gasification System**

The simplified schematic of the entrained gasification subsystem is illustrated in Figure 9.

As explained in the previous section, the residence time in entrained gasifier is low. Consequently to have high conversion rates, fuel particles should be minuscule (in µm range). Therefore the sizing unit, including granulators and hammer mills, is the first component of subsystem where the size of biomass particles (stream 1) are adjusted to the desired value. Both fuel particles (stream 2) and oxidant enter at the top of the gasifier and convert to syngas which leave the gasifier at the bottom. Syngas at the gasifier outlet (stream 3) has a high temperature (1000-1400 °C). Thus syngas and molten slag first goes through a water spray chamber and then into a water bath at the bottom of the gasifier to decrease syngas temperature within a safe range for downstream equipment. Slag is cooled down quickly and passes through the critical temperature range where the ash becomes dry and consequently can be removed easily from the bottom of water bath. The syngas output from quench system (stream 4) is saturated with water vapor, which is enough to drive water gas shift

* This section is based on the second, third, fourth, and fifth papers.

reaction to achieve the desired hydrogen percentage as well as hydrogen to carbon monoxide ratio [16]. This arrangement allows the cyclone-cleaned syngas stream (stream 5) to directly enter the shift reactor without adding extra steam to the stream. Afterwards, the hydrogen enriched syngas (stream 6) is cooled down to near-ambient temperature. Cold syngas in stream 7 then passes through the water knockout tank before entering the Selexol unit (stream 8) where the selective removal of hydrogen sulfide and bulk removal of carbon dioxide occurs. Finally, the clean syngas stream leaves the system (stream 10).

The developed Aspen Plus flowsheet of EG subsystem can be found in Appendix I- Aspen Plus Flowsheets.

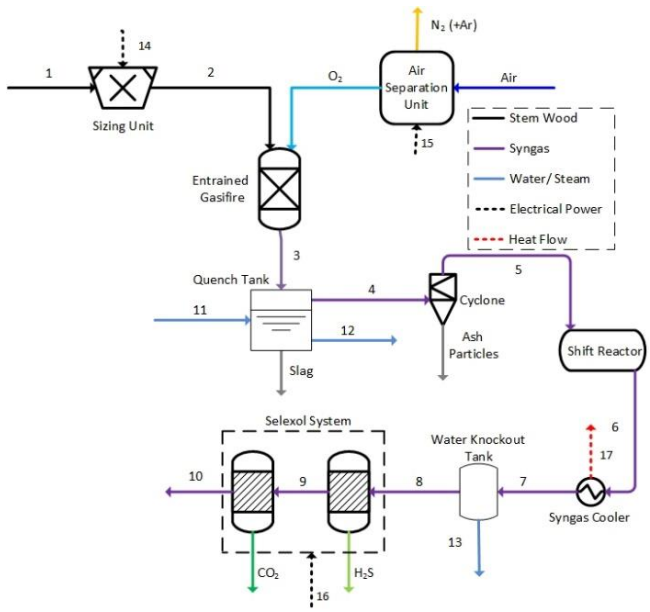

Figure 9- Schematic of Entrained Gasification System

The gasification subsystem depicted in Figure 9 is included in the integrated system wherever SOEC subsystem operates in co-electrolysis mode. Therefore, including water gas shift reactor to achieve the desired ratio of hydrogen to carbon is vital. However, in case of steam electrolysis, the required hydrogen to enrich the input syngas stream to FT reactor would be provided outside of EG subsystem. Consequently,

including water gas shift reactor would not be required. Arrangement of other components remains similar as described previously.

2.3 Fischer-Tropsch

2.3.1 Background

Fischer-Tropsch (FT) process has recently attracted much attention as an option for clean transport fuels, regardless of its near ninety-year history. FT process is a collection of chemical reactions that converts a gas mixture of carbon monoxide and hydrogen into liquid hydrocarbons. The development of FT technology has been described by Schulz [44] and Dry [45], and a brief summery is contained below.

It was first invented and developed by Franz Fischer and Hans Tropsch in 1925 in Germany. However, the fuel production was first started in 1935 at the Ruhrchemie Company and a total of nine coal-to-liquid plants were built in Germany and shut down in 1945. Although new processes have been developed after the Second World War, only marginal interest in FT synthesis with few scientifically interested research groups survived due to the vast usage of cheap oil. Nevertheless, it gained more interest in the late 1970s and early 1980s due to high oil prices as well as frightening forecasts regarding fading world oil reserves and oil boycotts by major oil producing countries. At any rate the actual interest in FT synthesis has grown recently due to the environmental demands to produce clean and environmental friendly fuels especially for the transportation sector. For example, in Japan and USA, FT synthesis is used to produce clean diesel via syngas from residual heavy oils as an outlet for this unfavorable materials. Also, there is a commercial FT synthesis plant on the basis of low price coal in South Africa which is primarily used for production of valuable olefins [44,45].

2.3.2 Fischer-Tropsch Process

Performance of the FT synthesis depends strongly on reaction temperature. Consequently, FT processes are categorized based on their operating temperature to low temperature Fischer-Tropsch (LTFT, 200-240 ^{o}C) and high temperature Fischer-Tropsch (HTFT, ~340 ^{o}C). Fixed bed reactors are generally suited for the former aiming at a high to average molecular weight of the products while fluidized bed and circulating-catalyst-reactors are used for high temperature synthesis to

produce low molecular weight olefinic hydrocarbons. Table 3 shows properties of each one of these processes .[44]

Table 3- Characteristics of different FT processes [44]

System	Temperature (ºC)	Pressure (bar)	Reactor Type	Products
High Temperature Fischer-Tropsch (HTFT)	~ 340	30-60	Fixed bed (generally)	Short chain linear alkenes/low molecular weight olefins
Low Temperature Fischer-Tropsch (LTFT)	200-240	30-60	Fluidized bed / circulating-catalyst	Diesel, Gasoline and wax production

The LTFT synthesis is ideally suited for the production of high-quality middle distillates (diesel and jet fuel) after hydrocracking process of the long chain waxes. In addition, the heavy product spectrum provides chemical industry with valuable compounds in the form of waxes and base oils. The by-product naphtha has a high-quality which can be used in naphtha steam crackers that produce mainly ethylene and some propylene [46]. On the contrary, the HTFT light product spectrum is best suited to the production of gasoline, but the high selectivity toward linear 1-olefins and oxygenates allows for the extraction of chemicals from the outcomes as well. Table 4 compares the composition of produced syncrude from FT technologies and crude oil.

Table 4- Composition of syncrude and crude oil (wt%)[47]

Fraction	HTFT	LTFT	Crude Oil
Paraffins	>10%	major product	major product
Naphthenes	<1%	>1%	major product
Olefins	major product	>10%	none
Aromatics	5-10%	<1%	major product
Oxygenates	5-15%	5-15%	<1%
Sulfur Components	none	none	0.1-5%
Nitrogen Components	none	none	<1%
Water	major by-product	major by-product	0-2%

Regardless of operating temperature, FT reactions require a catalyst to occur. Although iron and cobalt remain as only catalysts for industrial applications of FT process, nickel and ruthenium are also used mainly for production of high molecular weight hydrocarbons. The typical LTFT heavy product spectrum is mainly composed by waxes, which are liquid under reaction conditions. So, three phases would be present in the reactor: gas, liquid, and solid. Both cobalt and iron catalysts can be used in LTFT synthesis, although in the lower half of this temperature range, cobalt catalysts are typically more preferable [46]. On the other hand, the reactor conditions that characterized the HTFT synthesis process are such that products are only in the gas phase. At this operating temperature range using cobalt catalysts results in high production rate of methane and thus Fe-based catalysts prove to be the unique option for this application. Table 5 shows characteristics of each FT catalysts, while Table 6 lists and compares composition of syncrude from LTFT and HTFT based on the used catalyst in detail.

Table 5- FT different catalysts characteristics [44,46]

Catalyst	Characteristics
Cobalt	No water inhabitation Higher conversion per pass Selectivity strongly depend on the partial pressures of CO and H_2 (in order to avoid excessive methane formation) Widely is used for FT diesel production due to its high selectivity for wax production
Iron	Water inhabitation Lower conversion per pass Carbon accumulation on the catalyst Low methane selectivity even at higher operating temperature Favorable for rich CO syngas mixtures due to its water gas shift reaction activity Suitable for both high and low temperature applications
Nickel	High activity Suitable for low operating temperatures Selectivity changes to mainly methane at high temperatures Expensive
Ruthenium	The most active catalyst The lowest operating temperature (150 ^oC) Provides simplest catalytic system Selectivity changes to mainly methane at high temperatures Expensive Limited world resources

Table 6- Comparison of syncrude compositions in different FT technologies (%) [48]

Compounds		**Fe-LTFT**	**Co-LTFT**	**Fe-HTFT**
Gaseous hydrocarbons	Methane	4.3	5.6	12.7
	Ethane	1.0	0.1	5.6
	Ethene	1.0	1.0	4.5
	Propane	3.5	2.0	11.5
	Propene	0.9	0.9	1.6
	Butanes	2.5	1.4	9.7
	Butenes	0.8	0.8	1.4
Naphtha C_5-C_{10}	Alkanes	7.7	7.8	25.8
	Alkenes	3.3	12.0	4.3
	Aromatics	0	0	1.7
	Oxygenate	1.4	0.2	1.6
Distillate (C_{11}-C_{22})	Alkanes	5.7	1.1	4.8
	Alkenes	13.5	20.8	0.9
	Aromatics	0	0	0.8
	Oxygenate	0.3	0	0.5

Table 6- Comparison of syncrude compositions in different FT technologies (%) [48] *(continued)*

Compounds		Fe-LTFT	Co-LTFT	Fe-HTFT
Residue/Wax fraction	Alkanes	0.7	0	1.6
	Alkenes	49.2	44.6	0.4
	Aromatics	0	0	0.7
	Oxygenate	0	0	0.2
Aqueous products	Alcohols	3.9	1.5	4.5
	Aldehydes and ketones	0	0	3.9
	Carboxylic acids	0.3	0.2	1.3

Industrial FT technology is proven to be stable and economically sustainable when its production capacity approximates to at least 50,000 tonne per year [48]. Hence the normal trend is to increase the plant capacity. Nonetheless, the capital cost and risk associated with such large scale plants cannot be neglected. Also, such plants cannot be used in regards of limited capacity feedstock such as biomass. Therefore, it is anticipated that in the near future small to medium scale FT plants will be developed and used commercially [48,49].

2.3.3 Fischer-Tropsch Reactor

FT synthesis is highly exothermic. Therefore, efficient heat management in the reactor in order to maintain the desired operating temperature is the most important factor to be considered in the choice of a FT reactor for the given application [45]. The removed heat can be used internally, for steam production, or power generation. Catalyst features (e.g. size, activity and stability) and operation condition, which affect the present phases in the reactor, are other key factors in the selection of reactor design [48]. There are four main types of FT reactors [48,50]:

- *Circulating fluidized bed reactor:* Since only gas and solid phase can be present in fluidized reactors, this technology can only be used in HTFT. The syngas enters the reactor from the bottom and mixed with the solid circulating catalyst (Figure 10A). The syngas/catalyst mixture then flows into the riser in which the reaction takes part. Heat exchangers are installed within the riser to remove the produced heat from reactions and keep the temperature uniform. After that, the stream passes through a cyclone to capture the entrained catalyst particles which are collected and recycled back to the inlet syngas stream. However, high temperature in the reactor may cause carbon deposition leading to low catalyst life time of 40-45 days. Also, its complex design makes its control to be difficult [51].

- *Fixed fluidized bed reactor*: This reactor, also known as Sasol Advanced Synthol reactor, can be considered as an upgrade of circulating fluidized bed. It is constituted by a vertical vessel with gas distributor at the bottom, several heat exchange tubes on the inside and cyclones at the top for catalyst–product separation (Figure 10B). Because of the large density difference between the catalyst and gaseous product phase, cyclone separation is particularly efficient. Syngas velocity is calibrated so that a turbulent flow pattern is created inside the reactor. Consequently, it benefits from high heat exchange rates and efficient heat management. Besides, due to less complex design compare to circulating fluidized bed, it has a simplified control system and lower capital cost.

- *Multi-tubular fixed bed reactor*: Multi-tubular fixed bed reactor is shown in Figure 10C. like shell-and-tube heat exchangers; it consists of several concentric tubes, containing catalysts, surrounded by cooling water. Syngas enters at the top of the reactor while cooling water enters at the bottom. Therefore, it can be considered as a counter-current reactor. Produced syncrude is in the liquid form and easily run down the tube walls and is collected at the bottom of the reactor. Higher conversion rates can be achieved by using smaller catalysts particles. However, combination of narrow tubes, high gas velocity and small particles results in high

differential pressure in the reactor. On the other hand, heat management and bed temperature control become more complicated and difficult using catalysts with high activity. Since this reactor actually consists of multiple single-tube reactors in parallel, its scale-up is easier than other designs. Also, this design is proven to be stable and reliable throughout operation history of FT.

- *Slurry phase reactor*: Slurry phase, also known as slurry bubble-column reactor, has been developed to overcome some drawbacks of multi-tubular fixed bed design. As shown in Figure 10D, syngas enters from the bottom to the slurry bed consisting of suspended solid catalyst particles in a high thermal capacity liquid. Heat exchanger installed inside the reactor removes the produced heat during FT synthesis. The unconverted syngas and product gases leave the reactor at the top while mixture of wax and catalyst exits on the side. Unlike multi-tubular fixed bed reactor, pressure drop over the reactor is determined by the hydrostatic height of the slurry phase rather than particle size. Therefore, they can benefit from lower differential pressures by adjusting the hydrostatic height. Its design benefits from possibility of full temperature control. Moreover, it has the lowest installation and operation cost compared to aforementioned reactor types. Nevertheless, catalyst-product separation can be a challenge especially in case of industrial applications. Also, the high purity requirement of the syngas is more crucial since upon entry of any catalyst poisonous material all the catalyst particles presented in the reactor bed can be deactivated.

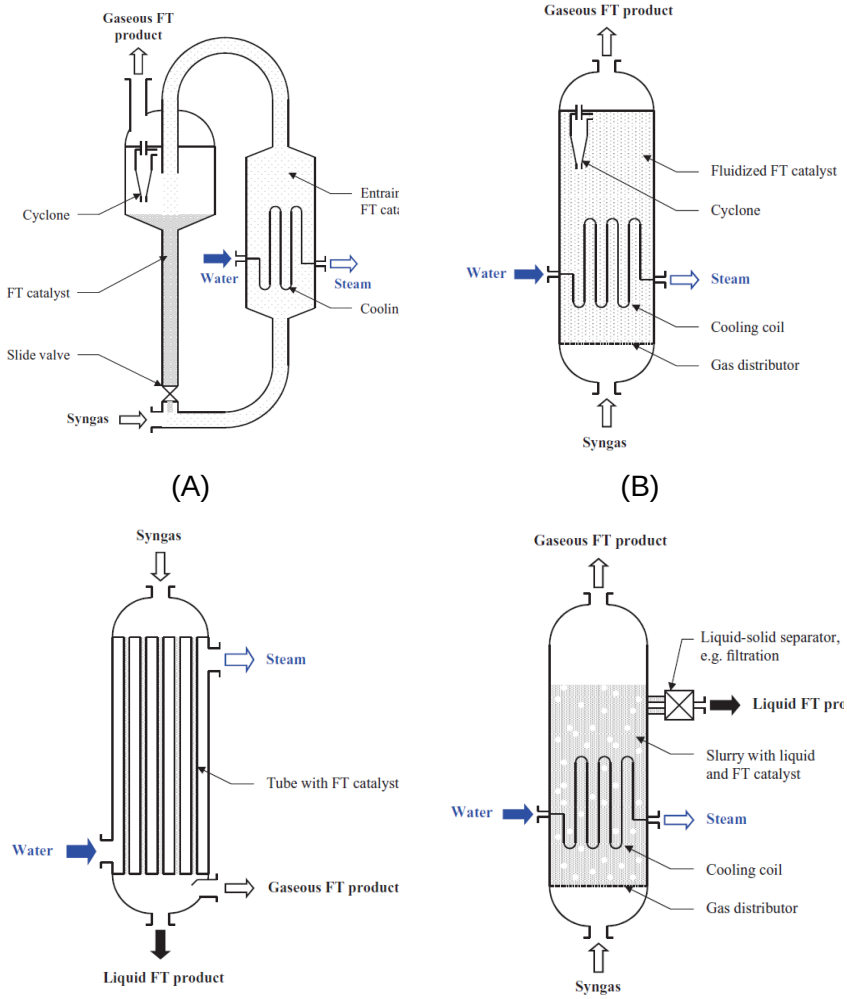

Figure 10- Diagram of A) circulating fluidized bed reactor, B) fixed fluidized bed reactor, C) multi-tubular fixed bed reactor, D) slurry phase reactor [48]

*2.3.4 Fischer-Tropsch System**

LTFT is considered here owing to its favorability for high cetane number-diesel production with negligible amounts of aromatic compounds.

Figure 11 shows Fischer-Tropsch subsystem including upgrading unit. Temperature and pressure of syngas stream first is adjusted to the desired operating condition prior to entering FT reactor. In other words, the syngas input (stream 1) is first pressurized to 25 bar and thereafter (stream 2) goes through a heat exchanger to reach the operating temperature of 240 ^{o}C. The system operation is once through; i.e., syngas (stream 3) passes through FT reactor once and the unprocessed syngas as well as light hydrocarbons (stream 14) are sent to the hydrogen recovery process. FT raw product in stream 4 (syncrude) is cooled down before being separated (stream 5) into three streams: gaseous products (stream 14), liquid products (stream 6), and water.

The gaseous products are sent to hydrogen recovery unit while the liquid part passes through an upgrading unit. The latter (Syncrude--stream 6) enters the first distillation tower where it is separated to naphtha, distillate (stream 7), wax (stream 8), and gaseous light hydrocarbons (stream 22). Naphtha and gaseous hydrocarbons leave the distillation tower at the top while wax (stream 8) is collected at the bottom of distillation tower and directed toward hydrocracking reactor. The gaseous part (stream 23) of the reactor outlet (stream 10) is separated from liquid products (stream 12) and water after being cooled down in HC heat exchanger. Like syncrude from FT reactor, the liquid part (stream 12) goes through a second distillation tower. The gaseous hydrocarbons are collected from the top stage (stream 24) and mixed with light hydrocarbon lines from other components. They can be considered as a by-product of the system, which can be used in a combustor to provide a heat source. The wax stream, collected at the bottom stage, may be considered as another by-product of the upgrading unit. Distillate stream (stream 13) and the distillates from the first distillation tower (stream 7) are sent directly to the diesel pool.

* This section is based on the third, fourth, and fifth papers.

The gaseous part of FT raw products (stream 14) is sent to the hydrogen recovery unit. This unit includes three subprocesses: auto-thermal reforming, water gas shift, and pressure swing adsorption. Stream 14, steam and pure oxygen enter an auto-thermal reformer where steam reforming of methane and partial oxidation of other hydrocarbons occur, resulting in an increase of H_2 and CO concentrations. To further increase of hydrogen content in the stream, the exhaust stream from reformer is sent to the two water gas shift reactors after cooling down in cooler I. The final step of this unit is separation of hydrogen through pressure swing adsorption. In this stage, hydrogen content of stream 20 is separated from gaseous light hydrocarbons and water. A fraction of this hydrogen will be used for hydrocracking process and the remaining can be consider as a by-product of the system. The gaseous hydrocarbon stream from separator is added to the gaseous hydrocarbon line.

The developed Aspen Plus flowsheet of FT and upgrading subsystem can be found in Appendix I- Aspen Plus Flowsheets.

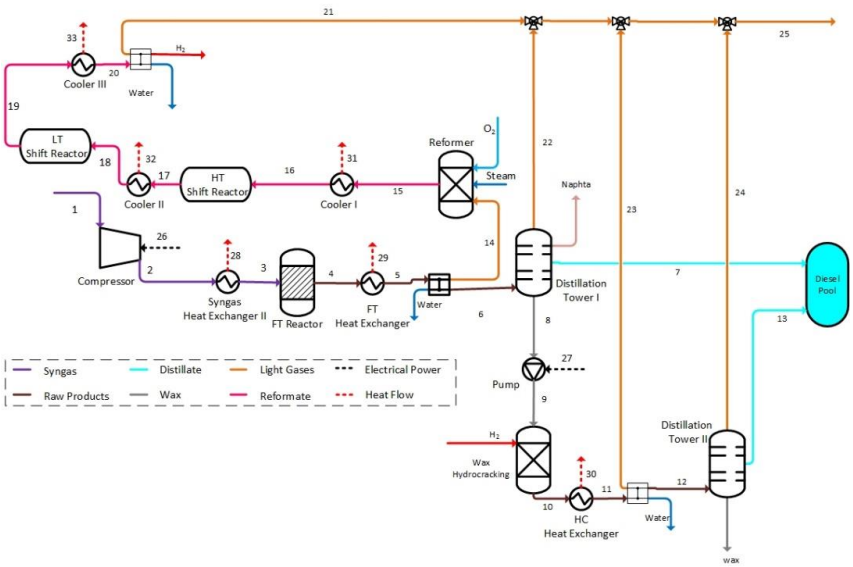

Figure 11- Schematic of Fischer-Tropsch System for Diesel Production

3 Model Description*

ASPEN Plus software (Aspen Tech) [52] is used to model and simulate the proposed integrated system. To facilitate and reduce the complexity of the modeling process, the integrated system is divided into three subsystems which have been modeled separately. A process flow sheet of each subsystem containing all of the necessary components to sustain its optimum operation is created. Standard components from ASPEN Plus library have been used to model all the components except for electrolysis unit and entrained gasifier, where no unique component is available in the library. The model and component parameters have been chosen and introduced to the software so that the desired operating condition for the FT diesel production process would be achieved. To exemplify, the hydrogen to carbon monoxide ratio at the electrolysis and gasification subsystem outlet is set to be 2.1 which is the desired value in the Fischer-Tropsch reactions using a cobalt catalyst [24,44,53].

This Chapter presents the developed model of each subsystem along with thermodynamic, economic, and emissions savings models that were used in the analysis. Governing equations and procedure that were used to model the renewable resources in the case studies are explained at the end of this Chapter.

3.1 Component Model

Chemical species that are accounted for in the system model can be divided in two main groups,

- Non-hydrocarbon elements such as H_2, CO, CO_2, H_2O, etc.

* The methodology presented in this Chapter is based on the published methodology in the first, second, third and fourth papers

- Hydrocarbons from C_1 to C_{30}, oxygenated compounds from C_1 to C_5, aldehydes and carboxylic acids (Appendix II- Fisher-Tropsch Components).

All in all, the process model includes 114 chemical components. In order to account for the products with carbon atom number higher than 30, a pseudo-component under name of WAX 30+ is defined in ASPEN. Since in this approach wax yield is represented by a single pseudo-component, it is vital to define its basic properties in ASPEN before executing the simulation, otherwise the vapor-liquid fraction of wax may be predicted incorrectly by the developed model [54]. To avoid this problem, the same values that are suggested in Bechtel [54] to model wax production are used here as well.

- Boiling Temperature (NBT): 974.3 °C
- API Gravity: 36.42 kg/m^3
- Molar Weight: 742.70 kg/kmol

3.1.1 Solid Oxide Electrolysis Unit

Table 7 lists the reactions that may occur in the solid oxide electrolysis unit. Reactions 1-3 are electrochemical reactions while the remainder are chemical reactions. Reactions 1 and 2 represent simultaneous reduction of steam and carbon dioxide at cathode electrode of electrolysis cells, respectively. The oxygen ions produced in these reactions pass through solid electrolyte to form oxygen at the anode electrode (reaction 3). Nonetheless, owing to presence of carbon content at the cathode, co-electrolysis not only entails electrochemical reduction of steam and carbon dioxide but also the water-gas shift reaction as shown in reaction 4. This reaction governs the relative contributions of each element in the inlet and outlet streams. The reverse water gas shift reaction would be enhanced at high operating temperatures (due to its endothermic nature) as well as electrochemical conversion of steam to hydrogen. Nevertheless, the main portion of carbon monoxide at the cathode outlet is produced from reversed water gas shift reaction rather than electrochemical reduction of carbon dioxide (owing to slower electrochemical reduction of CO_2 compared to steam electrochemical reduction and reverse water gas shift) [17,55].

In addition, a fraction of produced syngas may react internally to produce methane (reaction 5). This reaction is favored at higher operating pressures and lower operating temperature. Therefore, elevated operating pressure will

result in higher rate of methane production and consequently lower amount of syngas (hydrogen/carbon monoxide) in the cathode exhaust. Since syngas is the desired feed gas in the FT process, its reduced amount may cause lower performance of the whole system. Moreover, high operating pressures may enhance carbon deposition at the cathode electrode of electrolysis cells according to reactions 6 and 7 [18].

Table 7- Main reactions in the solid oxide electrolyser

No	Reaction	Heat of Reaction (kJ/mol)
1	$H_2O + 2e^- \rightarrow H_2 + O^{2-}$	+241.8
2	$CO_2 + 2e^- \rightarrow CO + O^{2-}$	+393.5
3	$2O^{2-} \rightarrow 2O_2 + 4e^-$	---
4	$CO + H_2O \rightleftharpoons H_2 + CO_2$	-41
5	$CO + 3H_2 \rightarrow CH_4 + H_2O$	-206.1
6	$CO + H_2 \rightarrow C(S) + H_2O$	-131.3
7	$2CO \rightarrow C(S) + CO_2$	-172.5

Co-electrolysis process in the SOEC is commonly modeled considering three consecutive stages: i) the reactant gases come to equilibrium with respect to the water-gas shift reaction, ii) the electrochemical reactions occur in the electrolysis cells, and iii) the produced gases again come into equilibrium according to reactions 4 and 5 before exiting the cathode compartment [56,57]. There is no single component in ASPEN Plus standard library to model the SOEC, hence three separate reactors are used to take these individual stages (occurring simultaneously) into account (Figure 12). In the first reactor (PRE-WGSR), the reactants (S13) will reach equilibrium based on reaction 4. Then this equilibrium mixture (S23) will go through the electrochemical reactions in the second reactor (SOEC) which results in production of syngas and oxygen. In reality, oxygen and syngas are produced separately in cathode and anode compartments, respectively. To take this fact into account, the exhaust from second reactor (S24) passes through a

separator where oxygen content of stream is separated (S26) from the remainder (S25). In the third and last reactor (POST-WGS), the gas mixture (S25) will reach the equilibrium based on the water gas shift and methanation reactions (reactions 4 and 5) [18,58]. This mixture is the electrolyser output, i.e. stream 14 in Figure 12 will be equivalent to stream 14 in Figure 5. The Gibbs reactor (RGibbs) is used to model the first and third reactors whereas stoichiometry reactor (RStoic) is selected for the second reactor.

In the case of steam electrolysis, where carbon contents are absent inside the electrolyser unit, PRE-WGSR and POST-WGSR are eliminated.

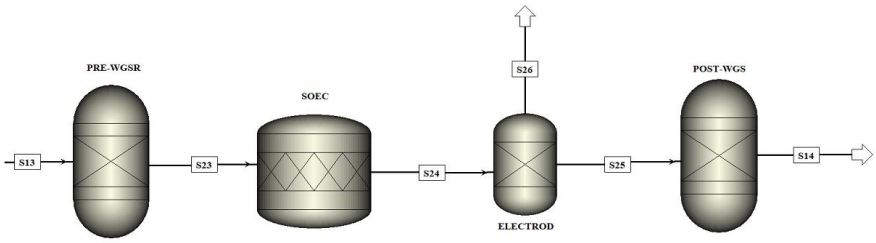

Figure 12- SOEC model in ASPEN

The reversible voltage of electrolysis cells, also known as Nernst voltage, depends on the operating temperature of electrolyser and partial pressures of the reactants. Nernst voltage, V_N, at the given operating condition in case of co-electrolysis is reported as the weighted average of steam and carbon dioxide reversible voltage values as shown in equation 1 [57]. Equation 2 is the reversible voltage of steam electrolysis.

$$V_{N,Co-electrolysis} = \frac{1}{y_{H_2O} + y_{CO_2}} \left(y_{H_2O} \left(\frac{-\Delta G_{f,H_2O(T)}}{2F} - \frac{RT}{2F} \ln \left[\left(\frac{y_{H_2O}}{y_{H_2} . y_{O_2}^{0.5}} \right) \left(\frac{P}{P_{std}} \right)^{-0.5} \right] \right) + y_{CO_2} \left(\frac{-\Delta G_{f,CO_2(T)}}{2F} - \frac{RT}{2F} \ln \left[\left(\frac{y_{CO_2}}{y_{CO} . y_{O_2}^{0.5}} \right) \left(\frac{P}{P_{std}} \right)^{-0.5} \right] \right) \right) \quad (1)$$

$$V_{N,Steam} = \frac{-\Delta G_{f,H_2O(T)}}{2F} - \frac{RT}{2F} \ln \left[\left(\frac{y_{H_2O}}{y_{H_2} . y_{O_2}^{0.5}} \right) \left(\frac{P}{P_{std}} \right)^{-0.5} \right] \quad (2)$$

$\Delta G_{f,H2O(T)}$ and $\Delta G_{f,CO2(T)}$ represent the Gibbs free energy of formation at SOEC operating temperature of steam and carbon dioxide respectively, y_i is the molar fraction of each component in the stream, P is the electrolyser pressure, T is the operating temperature and F is the Faraday constant. In

reality, the operating voltage of the electrolysis cells is higher than the reversible voltage owing to the internal resistance of the cells. The total loss mechanism in the operating cell is normally defined as area-specific resistance (ASR) which is assumed to follow an Arrhenius relationship to temperature [24,56]:

$$ASR(T) = ASR_{1100K} - 0.463 + 3.973\times10^{-5}\exp\left(\frac{10300}{T}\right) \quad (3)$$

The effect of operating pressure, however, is not considered in this equation. To include the effect of pressure in the model, *ASR* is calculated using the experimental relationship to operating temperature and pressure [59]:

$$ASR(P,T) = \begin{cases} 34.22e^{-0.0054T}.e^{-0.0217P} & co-electrolysis \\ 35.51e^{-0.0058T}.e^{-0.0217P} & steam-electrolysis \end{cases} \quad (4)$$

The operating voltage of the electrolysis cells at the operating condition can be estimated based on the values of V_N, *ASR*, and current density, i.

$$V_o = V_N + ASR(T).i \quad (5)$$

Current density is a design choice and normally is selected to be equal or close to the thermo-neutral current density of the electrolysis process at the given condition [18]. This is the point of operation where the supplied electricity is in the range of the thermal energy of endothermic electrochemical reactions [19]. In other words, the electrolyser neither requires nor releases heat. Hence, thermal management of SOEC would be less complex. A heat source would be necessary in cases that the electrolyser operates below this point, otherwise SOEC temperature will drop uncontrollably. On the other hand, not only heat management would be crucial when SOEC operates above thermo-neutral point but also electrolysis unit performance declines [18,19,60]. Thermo-neutral current density can be estimated as [59],

$$i_{TN} = \frac{V_{TN} - V_N}{ASR} = \frac{T.\Delta\bar{S}}{2.F.ASR} \quad (6)$$

where $\Delta\bar{S}$ is the entropy change of reactants taking part in the electrochemical reactions.

Electrical power consumption of SOEC can then be estimated according to equation 7:

$$P_{SOEC} = V_O . I_F \quad (7)$$

I_F is known as faradic current and directly depends on the consumption rate of reactants or production rate of products. During co-electrolysis there are two simultaneous electrochemical reactions occurring in which oxygen is the common by-product. Hence, here faradic current is estimated based on the production rate of oxygen, n_{O2}, on the anode compartment:

$$I_F = n_{O_2} . 4F \quad (8)$$

Table 8 shows the calculated values of open circuit voltage and area specific resistance from the theoretical model. Different operating temperatures are considered in the case of syngas production (eq. 1 and 4) while in case of electrolysis different operating temperatures and pressures are used (eq. 2 and 4). To validate the model results, these values are compared to the measured values from the experiments done by Ebbesen et al. [61] and Jensen et al. [62]. In the former case, the experimental values are presented for the thermodynamic equilibrium composition of the mixture at each temperature. In the latter, to be in agreement with the experimental conditions, the temperature is kept constant at 750 ^oC and stream composition was assumed to be comprised of 50% H_2 and 50% H_2O while pressure varied. As can be seen, the calculated values are quite comparable to the experimental ones, therefore the developed model is judged to fairly represent behavior of solid oxide electrolyser units.

Due to lack of experimental data in case of syngas production from pressurized SOEC unit, only hydrogen production simulation results can be validated at different pressures. Therefore, the empirical equations presented in equation 4 are only used whenever the operating pressure of SOEC is considered to be higher than atmospheric level, otherwise Arrhenius relationship to temperature (equation 3) is used to estimate the ASR. Strictly speaking, equation 4 is considered in SOEC model that is used in section 4.1 and Chapter 5 while equation 3 is used to produce results presented in Chapters 6 and 7. Although it may be proven that empirical equations presented here may require adjustment according to the experimental data which would be released in future, it most probably will not affect the trend of impact that pressure has on system performance. Hence, in this study these

equations are used to investigate possible impacts that elevated pressure may have on system performance.

Table 8- Comparison between the calculated open circuit voltage and area specific resistance with the measured values presented by Ebbesen et al. [61] *and Jensen et al.* [62]

Operating Condition	**ASR (Ω.cm^{-2})**		**Voc (V)**	
	Calculated	Experimental	Calculated	Experimental
Co-electrolysis				
Operating Temperature (ºC)				
750	0.50	0.51	0.832	0.843
800	0.38	0.37	0.825	0.869
850	0.28	0.26	0.812	0.890
Electrolysis				
Operating Temperature (ºC)				
750	0.44	0.41	0.97	0.982
800	0.33	0.27	0.968	0.967
850	0.25	0.19	0.965	0.951
Operating Pressure (bar)				
0.4	0.45	0.59	0.950	0.961
1	0.44	0.52	0.970	0.969
3	0.42	0.47	0.995	0.996
10	0.37	0.42	1.02	1.011

3.1.2 Sizing unit

Since the residence time in the entrained gasifier is small, fuel particles should be very small (in µm range) to achieve high conversion rates. Therefore, wood pellets are assumed to go through a sizing unit, which usually include granulators and hammer mill, prior entering the gasification. Weiland et al. showed that this unit has the highest power demand in the gasification system. Based on this study, it is assumed that the sizing unit electricity demand is 36 kWh_{el}/MWh_{th}.

3.1.3 Air Separation Unit (ASU)

Most entrained gasification systems use pure oxygen as an oxidant rather than air. The basic advantages of such designs are a) reduction in gasifier size, b) smaller downstream handling and clean up equipment, c) easier CO_2 recovery in absence of excess nitrogen in the stream, and d) higher heating value of the produced syngas. However, using pure oxygen in the system will add to the complexity and capital cost [41].

Oxygen can be produced in cryogenic plants with purity levels as high as 99.5%. Here, cryogenic air separation unit is used which provides oxygen with purity of 95% for the gasification process. A typical cryogenic plant usually consists of air compressor, air separation unit, and an optional oxygen compression system (the latter is not used for system operating near atmospheric pressures). Double column design is used in cryogenic plants since 1930's to efficiently produce oxygen with high level of purities [63]. According to Rubin et al. [63] the power consumption of ASU depends on the purity level of produced oxygen and can be calculated as shown in equation 9:

$$\begin{cases} P = 4.88\, e^{-3}.\eta_{ox} + 0.4238 & \eta_{ox} < 97.5 \\ P = \dfrac{7.361\, e^{-2}}{\left(100 - \eta_{ox}\right)^{1.316}} + 0.8773 & \eta_{ox} > 97.5 \end{cases} \tag{9}$$

where η_{ox} is the purity level of produced oxygen. The estimated power consumption includes the power required to operate the main air compressor, the refrigeration system, and auxiliary and control systems and is estimated based on kW per 100 cubic feet (2.8 m^3) of oxygen.

3.1.4 Entrained Gasifier

In an entrained gasifier, both fuel particles and oxidant enter at the top and travel to the bottom in a co-flow manner. Due to high temperature of the gasifier moisture content is released rapidly upon entering the gasifier. Dried fuel particles then go through pyrolysis reactions which results in production of volatile gases and char. Negligible amounts of tar will be produced owing to high operating temperatures, so it is neglected here. The volatile gases mostly include CO, CO_2, H_2, H_2O, and light hydrocarbons such as CH_4 [16,64]. The required heat for the endothermic gasification reactions is

provided via combustion of these volatile gases which rapidly are mixed with oxidant feed at the top of the gasifier.

Table 9 lists main reactions in the entrained gasifier. Reactions 1 to 4 represent combustion reactions that occur at the top of gasifier upon the oxidant agent entry. On the other hand, reactions 7 to 11 occur at the bottom of the gasifier, where gasification dominates (Char combustion (reactions 10 and 11) rarely occurs in this section of gasifier owing to rapid consumption of oxygen at the gasifier entrance [16]). Reactions 5 and 6 are water gas shift reaction and methane-steam reaction, respectively. The latter is responsible for increase in methane yield at the gasifier outlet provided that gasification process occurs at elevated pressures. The former can be used to adjust hydrogen to carbon monoxide ratio near the desired value. Sulfur oxides (SO_x) are absent in the syngas and sulfur content in the fuel is mostly converted to hydrogen sulfide (reaction 12), with the remainder in form of carbonyl sulfide (reaction 14). Besides, nitrogen oxides (NO_x) are produced in negligible amounts and nitrogen is mostly converted to ammonia (reaction 13) [21].

Table 9- Chemical reactions in the gasifier

No	Reaction	Heat of Reaction (kJ/mol)
1	$H_2 + 1/2\ O_2 \rightarrow H_2O$	-242
2	$CO + 1/2\ O_2 \rightarrow CO_2$	-283
3	$CH_4 + 1/2\ O_2 \rightarrow CO + 2H_2$	-36
4	$CH_4 + 2\ O_2 \rightarrow CO_2 + 2H_2O$	-803
5	$CO + H_2O \rightleftharpoons CO_2 + H_2$	-41
6	$CH_4 + H_2O \rightleftharpoons CO + 3H_2$	+206
7	$C(S) + CO_2 \rightleftharpoons 2CO$	+172
8	$C(S) + H_2O \rightleftharpoons H_2 + CO$	+131
9	$C(S) + 2H_2 \rightleftharpoons CH_4$	-75
10	$C(S) + O_2 \rightarrow CO_2$	-394
11	$C(S) + 1/2\ O_2 \rightarrow CO$	-111
12	$S + H_2 \rightarrow H_2S$	-20
13	$N_2 + 3H_2 \rightarrow 2\ NH_3$	-92
14	$CO + H_2S \rightarrow COS + H_2$	-139

Like solid oxide electrolysis unit, there is no single component in ASPEN Plus standard library to be used in modelling of the entrained gasifier. Hence, four different reactors, one separator, and a mixer were used to model different steps in the gasifier (Figure 13):

- DECOMP: Wood pellets first go through this yield reactor and are decomposed to its building elements according to the provided ultimate and approximate analysis.
- PYROL: Drying and pyrolysis reactions occur resulting in production of volatile matters and char.

- CHAR-SEP: Volatile matters are separated from char here. The former goes through combustion reactions.
- COMBUST: Volatile matters including light hydrocarbons are mixed with the oxidant flow (S30) and the heat released from their combustion provides the required heat for pyrolysis and gasification processes.
- MIX2: Combustion products (S7) are mixed with char (S6) here.
- GASIFIER: In the fourth and last reactor, gasification processes occur.

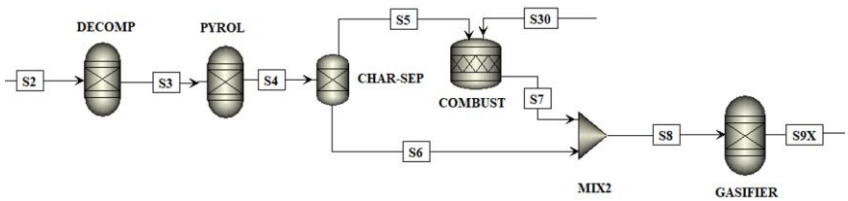

Figure 13- Entrained Gasifier model in ASPEN

Generally, methane content of syngas at the gasification outlet is much higher than what is estimated in the equilibrium model. This amount can be compensated for based on the empirical expressions in [65]:

$$\alpha = \frac{[CH_4]}{[CH_4]+[CO]+[CO_2]} \tag{10}$$

$$\alpha = 0.0029 e^{\left(\frac{3960}{T+27315}\right)} . P^{0.149} \tag{11}$$

where α is the relative mole fraction of methane, $[CH_4]$, $[CO]$ and $[CO_2]$ are the molar fractions of methane, carbon monoxide and carbon dioxide, respectively. T and P are operating temperature and pressure of the gasifier. Note that the presented expressions in Wu et al. [65] is based on the usage of mixture of high temperature air and steam as oxidant feed. Use of steam in the gasification process results in higher percentage of methane rather than pure oxygen [66]. Therefore, equation 11 is modified by modifying pre exponential factor to fit the methane content reported in the experiments [16].

The entrained gasification model is validated using the experimental results presented in Weiland et al. [67]. For the sake of comparison, the same

stem wood powder properties are used in the simulation. Table 10 shows the proximate and ultimate analysis of the selected wood pellets.

Table 10- Proximate and ultimate analysis of wood pellets [16]

Proximate Analysis (wt%)				**Ultimate Analysis (wt% dry)**					
Volatile	Fixed C	Moisture	Ash	C	H	N	Cl	S	O
76.9	16.0	6.7	0.34	50.8	6.2	<0.1	<0.01	<0.01	42.5

According to the experimental data fuel flow rate is set to 40 kg/h, oxygen flow rate to 24.6 kg/h, and operating pressure to 1.94 bar (abs) [67]. Table 11 shows the calculated values from simulation and measured values from experiment. As can be seen, the estimated values of syngas composition as well as predicted temperature of gasifier are quite comparable to the experimental ones.

Table 11- Comparison between the calculated composition of dry syngas and gasification temperature with the measured values [67]

Parameter	**Syngas Composition (%mol dry)**				**Temperature (°C)**	**H_2/CO**
	H_2	CO	CO_2	CH_4		
Calculated	28.5	48.3	19.9	2.6	1171	0.59
Experiment	27.8	48.7	20.4	2.3	~1200	0.57

3.1.5 Gasification Cooling Unit (Water Quench)

The produced syngas has high temperature (1200-1600 °C) which is harmful for the downstream equipment. In general, either radiant and convective heat exchangers or water quench is considered as the cooling system [68]. Although using heat exchangers will increase total efficiency of the system (through recovery of sensible heat of syngas), they are expensive especially at large scale. Water quench, on the other hand, is comparatively simple and inexpensive. Nonetheless, sensible heat of syngas is wasted in this case and consequently system efficiency will be lower [63]. In the quench

design, syngas and molten slag first goes through a water spray chamber before entering a water bath. The molten slag then quickly is passed through the critical temperature range where the ash becomes dry and consequently can be removed easily from the bottom of water bath. The syngas output from quench system is saturated with water vapor which may be enough to drive water gas shift reaction to achieve the desired hydrogen percentage in the syngas stream [16]. In this study, water quench design is considered and it is assumed that syngas is cooled down to reach 350 ^{o}C.

3.1.6 Water Gas Shift Unit

To achieve the desired hydrogen to carbon monoxide ratio of 2.1 in the output syngas from the EG subsystem, a water gas shift (WGS) reactor is included. Generally, WGS systems are classified into two types based on the type of catalyst which is used in the reactors, namely clean shift catalyst and sour shift catalyst. In the former, sulfur contents in the syngas are harmful while it is essential for the latter to keep the catalyst activation. In clean WGS system catalysts are usually iron and copper based but in sour WGS system they are normally of cobalt based [63].

In this study sour WGS has been selected, and consequently it is placed before selective removal of sulfur content from the stream. Normally, a steam to carbon monoxide ratio of 3 is required at the entrance of reactor to avoid carbon deposition which is achieved by injecting steam into the syngas stream [69]. In the present case, however, this extra stream is not necessary owing to the quench process.

3.1.7 Selexol Unit

The Selexol process for selective removal of sulfur content from gas streams has been in use since 1960's [63]. Selexol solvent is a mixture of dimethyl ethers of polyethylene glycols which is an excellent solvent for acid gases [70]. This process is based on the physical absorption and therefore depends on the temperature and partial pressure of gases. As can be seen from Table 12, solubility of hydrogen sulfide is much higher than carbon dioxide and consequently it is an ideal process for the selective removal of hydrogen sulfide followed by bulk removal of carbon dioxide.

Table 12 – solubility of gases in the Selexol solvent [71]

Component	H_2	CO	CH_4	CO_2	H_2S	COS	H_2O
Solubility Index	0.2	0.8	1.0	15	134	35	11000
Solubility, $Ncm^3/g.bar.@25^oC$	0.03	0.08	0.2	3.1	21	7.0	2200

Regardless of the system requirements for the level of H_2S/CO_2 selectivity and the necessity of bulk CO_2 removal, Selexol system always includes the following steps [63]

- Sour gas absorption
- Solvent regeneration and/or sour gas recovery
- Solvent cooling and recycle

Nevertheless, two separators are used to model Selexol system in this study. Power consumption of this section is estimated based on the molar flow rate of syngas, removed hydrogen sulfide and carbon dioxide. According to House et al., removing each mole of carbon dioxide requires actual work of about 23-26 kJ [72,73]. Power demand for selective removal of hydrogen sulfide, however, can be calculated according to equation 12.

$$W_{el} = 0.348 + 0.000478\left(453.6 M_{syn}\right)^{0.839} \quad (12)$$

More information regarding this system can be found in the literature [63,71,74,75].

3.1.8 Fischer-Tropsch Process

Slurry phase reactor design is selected owing to its efficient heat management as well as higher yield of long chain hydrocarbons. FT synthesis kinetic model and reaction system is defined in the ASPEN model by using dedicated kinetic sheets and reaction input forms. More information can be found in Appendix III- FT Synthesis Kinetic Model.

The introduced FT kinetic model is validated by comparing the simulation results with the experimental results presented by Todic et al. [76]. In Figure 14, the hydrocarbon formation rate versus number of carbon atoms in the

hydrocarbon is illustrated. The solid line is the calculated value from the simulation while the dots are the experimental values presented in ref. [76].

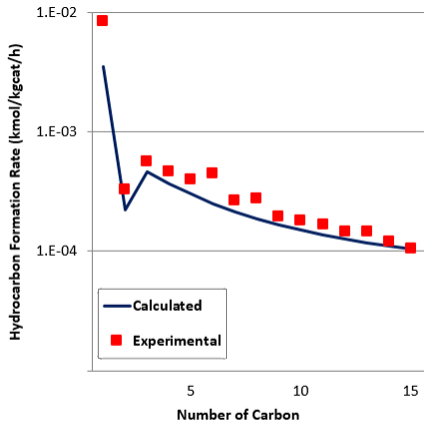

Figure 14- Comparison of calculated hydrocarbon formation rate with the experimental results from [76]

3.1.9 Upgrading Unit

This unit includes two distillation towers, hydrocracking reactor, and several heat exchangers and separators.

The distillation towers operation principle is based on the difference in boiling points of hydrocarbons (similar to the crude oil cracking tower). The first distillation tower separates syncrude into naphtha, distillate, wax, and gaseous light hydrocarbons. In the model, direct steam stripping tower composed of 54 stages with a lateral stripper of 12 stages, reflux ratio of 1.8 between every two consecutive trays and the bottom reboiler is selected to model this component. Naphtha and gaseous hydrocarbons leave the distillation tower at the top, while wax is collected at the bottom. The second distillation tower is responsible for separation of hydrocracking reactor products. Although the second distillation tower has the same arrangement as the first one, it is smaller and only consists of 15 stages.

The hydrocracking reactor, where wax is broken down to useful naphtha and middle distillates, operates at 340 ^{o}C and 45 bar which is in agreement with the literature data [77]. Like FT model, the hydrocracking reactions and kinetic model of the hydrocracking reactor is added to the ASPEN model.

More information regarding the kinetic model can be found in Appendix IV- Hydrocracking Kinetic Model.

3.1.10 Hydrogen Recovery Unit

This unit consists of three processes, auto-thermal reforming, water gas shift reaction, and pressure swing adsorption.

In the first step H_2 and CO content in the stream is increased by auto thermal reforming of gaseous part of FT products. RGibbs reactor, operating in adiabatic condition is chosen to model this component.

Two WGS reactor is further used to increase hydrogen content of the stream. The first water gas shift reactor (HT shift reactor) operating temperature is as high as 350 ^{o}C which has the advantage of high reaction kinetics. However, owing to exothermic nature of WGS reaction, it is thermodynamically limited causing incomplete conversion of carbon monoxide [78]. Therefore, the second WGS reactor operating at lower temperature of 200 ^{o}C is added to the unit to achieve high fraction of hydrogen in the stream. Like auto-thermal reformer, these reactors are modeled using RGibbs reactor.

Pressure swing adsorption is the final stage of hydrogen recovery unit where hydrogen content of the stream is separated. This stage is modeled using a separator block assuming to be able to recover 78% of hydrogen content of stream with purity of 99% [79,80]. A fraction of hydrogen is used for hydrocracking process and the remainder is considered as the by-product of the system.

3.1.11 Other Components

Other components, such as pressure changers and heat exchangers, are modeled using the available components from standard library of ASPEN Plus.

- ***Pressure changers:*** Standard isentropic compressor component is used to model every compressor in the integrated system. The discharged pressures are specified in each case considering the pressure loss in the system components as well as the desired operating pressure of each subsystem. The isentropic and mechanical efficiencies are set to the predefined values of 0.72 and 1, respectively. In case of pumps, efficiency and performance

curve are calculated by ASPEN based on the defined discharge pressure.

- ***Heat exchangers:*** Heater/cooler unit from ASPEN library is selected to model every heat exchanger that is included in the integrated system. In all heat exchangers, with exception of steam generator, output temperature is defined. The vapor fraction of outlet stream is defined for the steam generator and consequently ASPEN calculates the output temperature based on operating pressure.

- ***Mixer/ Separator:*** Mixer/separator unit from the ASPEN library is used here. The stream fractions leaving separators should be defined by the user while the outlet stream condition from mixers is estimated by ASPEN based on the temperature and pressure of the input streams.

3.2 Renewable Resources

3.2.1 Solar PV

Hourly power output of each PV panel is estimated based on the cell temperature and the average global irradiance in that hour according to euation 13,

$$P_{PV} = P_{PV,n} \frac{G}{G_{stc}} \left(1 + k\left(T_c - T_{stc}\right)\right) \tag{13}$$

where P_{PV}, is the power output of PV cells, $P_{PV,n}$, the nominal power output of PV cells, G, the average global solar irradiance, G_{stc}, irradiance at standard test condition, k, approximate effect of temperature on power, and T_c and T_{stc} are the cell temperatures at operating condition and standard test condition, respectively. Temperature of PV cells is calculated based on the equation presented by Migan [81]:

$$T_c = T_{air} + \frac{NOCT - T_{soc}}{G_{soc}} G \tag{14}$$

In equation 14, T_{air} represent the ambient temperature while $NOCT$ is the nominal operating cell temperature. T_{soc} and G_{soc} are the ambient temperature and irradiance at standard operating condition, respectively. The reported

hourly average global irradiance for 2-axis tracking planes and ambient temperature for a typical day of each month is extracted from the European commission database [82]. Other days of that month are assumed to follow the same trend as this typical day. Other parameters are selected based on the available commercial data of MSX-83 solar PV module from SOLAREX company [83] and can be found in Table 13.

Table 13 – MSX-83 PV module characteristics [83]

Parameter	Unit	Value
Maximum power, $P_{PV,n}$	W	83
Voltage at maximum power	V	17.1
Current at maximum power	A	4.85
Irradiance at standard test condition, G_{stc}	W/m^2	1000
Cell temperature at standard test condition, T_{stc}	^oC	25
Irradiance at standard operating condition, G_{soc}	W/m^2	800
Ambient temperature at standard operating condition, T_{soc}	^oC	20
Nominal operating cell temperature, *NOCT*	^oC	47
Approximate effect of temperature on power, *K*	$\%/^oC$	0.5

3.2.2 Wind

Guo [84] presented a method to downscale wind statistics to hourly wind data. According to this approach, the hourly wind speeds throughout a given day can be estimated by

$$U_n = U_{ave} + \frac{1}{\pi} U_{\max} \cos\left(\frac{n.\pi}{12}\right) \tag{15}$$

In this equation, U_n, U_{ave}, U_{max}, are the wind speed at hour n, daily average wind speed, and daily maximum wind speed, respectively. The daily average and maximum wind speed for a typical day of month in each location are

extracted from NASA database [85]. Similar to solar, other days of that month are assumed to have the same diurnal wind speed distribution.

NASA reported wind speeds at altitude of 50 meter and therefore the estimated hourly wind speeds are for the same altitude. Since wind speed depends on the altitude, these wind speeds should be scaled to the height of selected wind turbine (equation 16) [86].

$$\frac{U_Z}{U_{Z_r}} = \left(\frac{Z}{Z_r}\right)^a \tag{16}$$

where, U_z and U_{zr} are wind speeds at the hub height of Z and reference height of Z_r, respectively. wind shear exponent, a, can be estimated according to empirical correlation between wind speed and height [86]:

$$a = \frac{0.37 - 0.088\ln\left(U_{Z_r}\right)}{1 - 0.088\ln\left(\frac{Z_r}{10}\right)} \tag{17}$$

Hourly power production from wind depends on the wind speed. Generally, wind turbines are designed so that a minimum wind speed, also known as cut-in speed, U_{ci}, is required for them to start. On the other hand, wind turbines will be shut down during strong gusts that have higher speeds than their tolerable threshold to prevent any possible damage. The maximum designed speed is called cut-off speed, U_{co}. Rated wind speed, U_r, is another parameter that above its value wind turbine will generate the nominal electrical power independent of the wind speed. In other words, wind turbine produces constant power between rated wind speed and cut-off speed. Therefore, wind power production at each hour can be calculated based on equation 18 [87]:

$$P_{wind} = \begin{cases} 0 & U_Z \le U_{ci} \text{ or } U_Z > U_{co} \\ \frac{U_Z - U_{ci}}{U_r - U_{ci}}.P_t & U_{ci} \le U_Z \le U_r \\ P_t & U_r \le U_Z \le U_{co} \end{cases} \tag{18}$$

Variables P_{wind} and P_t are the potential wind power production and nominal power of wind turbine, respectively. Parameters used in the above equations are chosen based on the V90-3.0 MW wind turbine produced by Vestas and listed in Table 14 [88].

Table 14- fact and figures of wind turbine V90-3.0 MW [88]

Parameter	Unit	Value
Rated power, P_t	MW	3.0
Cut-in wind speed, U_{ci}	m/s	3.5
Rated wind-speed, U_r	m/s	15
Cut-off wind speed, U_{co}	m/s	25
Hub height, Z	m	105

3.3 Thermodynamic Model

The efficiency of the integrated system, η_s, is defined as the useful output from the system to the energy content of input streams,

$$\eta_S = \frac{\sum \dot{m}_k LHV_k}{\dot{m}_{biomass}\, LHV_{biomass} + W_{el,tot} + Q_{tot}} \tag{19}$$

where $\dot{m}$ and LHV represent the mass flow rate and lower heating value of each component, $W_{el,tot}$ is the total electrical consumption of the system, Q_{tot} is the total input heat to the system, and k, represents main product and different by-products of the integrated system.

Similarly, integrated system exergy efficiency, E_s, is defined as the ratio of outlet streams exergy content to the exergy content of all the inlet streams to the system (equation 20).

$$E_s = \frac{\psi_{P,sys}}{\psi_{F,sys}} \tag{20}$$

The exergy content of each stream is calculated by estimating share of its physical and chemical exergy according to equations (21-23) [89].

$$b\big|_{T,P} = b_{ph}\big|_{T,P} + b_{ch}\big|_{T_0,P_0} \tag{21}$$

$$b_{ph}\big|_{T,P} = \left(h\big|_{T,P} - h\big|_{T_0,P_0}\right) - T_0\left(s\big|_{T,P} - s\big|_{T_0,P_0}\right) \tag{22}$$

$$b_{ch}\big|_{T_0,P_0} = \frac{\sum y_i.\bar{b}_{ch,i} + \bar{R}T_0\sum y_i.Ln(y_i)}{M} \tag{23}$$

However, the exergy content of input biomass stream is calculated using the equations presented by Wu et al. [65]:

$$\Psi_{biomass} = \beta.\dot{m}_{biomass}.LHV_{biomass} \tag{24}$$

$$\beta = \frac{1.0414 + 0.0177\left(\frac{H}{C}\right) - 0.3328\left(\frac{O}{C}\right)\left[1 + 0.0537\left(\frac{H}{C}\right)\right]}{1 - 0.4021\left(\frac{O}{C}\right)} \tag{25}$$

where, [C], [H] and [O] are the molar fractions of carbon, hydrogen and oxygen in wood pellets, respectively.

3.4 Economic Model

Levelized cost of the produced FT diesel is estimated according to equation 26.

$$Levelized Cost\big|_{FT\,Diesel} = \frac{C_{ICP} + C_{O\&M} + C_U + C_{El.} + C_{Feedstock} - C_{income}}{Annual FT\,Diesel Production \times Capacity Factor} \tag{26}$$

where C_{ICP}, $C_{O\&M}$, C_U, $C_{El.}$, $C_{Feedstock}$, and C_{income} are the cost of installed capital of plant, operation and maintenance, utility, electricity, feedstock, and the income that is gained by selling the produced byproducts, respectively.

3.4.1 Installed Capital of Plant

Installed capital cost of plant depends on total plant cost (TPC), capital charge rate (CCR), and interest during construction of plant (IC) (equation 27). Table 15 lists CCR and IC values that are used.

$$C_{ICP} = (TPC + TPC \times IC) \times CCR \tag{27}$$

Table 15 – Economic parameters [90,91]

Parameter	Value	Description
CCR	15%	Fraction of total plant investment
IC	11.4%	Fraction of total plant cost

TPC equals to the sum of all the components' capital costs in the integrated system. Cost of each component is estimated based on its relevant scaling parameter and scaling factor, as shown by equation 28:

$$C_{component} = C_{base}\left(\frac{ECC}{BCC}\right)^{x} \tag{28}$$

where $C_{component}$ and C_{base} represent the capital cost of component and its base cost. *BCC*, is the base capacity of the component based on the scaling parameter, while *ECC* is the estimated capacity of that component in the system which is driven from simulation results; *x* is the cost scaling factor. Capital costs of components that were used in estimation including installation, manufacturing, labor, balance of plant, general facilities, engineering, overhead and contingencies are presented in Appendix V-Base Cost of Components [91–95].

Heat exchanger costs depends on the material and heat exchange area. Purchase cost of heat exchangers in the system, C_p, are estimated based on the base cost, C_B, pressure factor, F_P, and material factor, F_M, of that heat exchanger (equation 29).

$$C_P = F_P . F_M . C_B \tag{29}$$

The aforementioned factors are calculated using equations 30-32 for a floating head shell and tube heat exchanger constructed from stainless steel. Due to high operating temperatures of anode heat exchanger I and cathode heat exchanger in SOEC subsystem, however, Inconel is considered as heat exchanger material and therefore the material factor is different in the case of these heat exchangers [96,97].

$$C_B = \exp\left(10.106 - 0.4429\, Ln(A) + 0.09005\, (Ln(A))^2\right) \tag{30}$$

$$F_P = 0.9803 + 0.261\left(\frac{P}{100}\right) + 0.358\left(\frac{P}{100}\right)^2 \tag{31}$$

$$\begin{cases} F_M\big|_{S.S.} = 2.70 + 1.81\left(\dfrac{A}{100}\right)^{0.07} \\ F_M\big|_{Inconel} = 2{,}4103 + 0{,}50764\, Ln(A) \end{cases} \quad (32)$$

A is the heat exchange area and P is the pressure of heat exchanger.

The estimated purchase cost is multiplied by factor of 3.291 to include direct and indirect costs [96]:

$$C_{HX-Capital} = 3.291 C_P \quad (33)$$

3.4.2 Operation and Maintenance

Operation and maintenance cost of plant over an operation year is calculated as percentage of TPC (equation 34). O&M factors of 4-5 % usually is used for similar installations [90,91]. O&M factor, $F_{O\&M}$, of 4% is used in this study.

$$C_{O\&M} = TPC \times F_{O\&M} \quad (34)$$

3.4.3 Electricity

According to data presented by IRENA [98], solar photovoltaic (PV) electricity and onshore wind electricity has the highest and lowest global renewable electricity prices, respectively. Electricity price of other renewable technologies lies between these values. Therefore, two electricity prices of 0.23 $/kWh and 0.075 $/kWh are considered in the model, corresponding to the highest reported cost of solar PV electricity and the lowest reported cost of onshore wind, respectively [98].

However, different approach is used in estimation of electricity prices in Chapter 7. Different electricity costs of 0.16 and 0.08 $/kWh are considered to take to account the specific situation of solar PV and onshore wind electricity in Europe, respectively [98]. The cost of electricity at each hour then is presented as weighted average of these values and based on share of electricity that is produced either from solar or wind in that hour.

3.4.4 Feedstocks

Feedstock prices (water, carbon dioxide, and biomass) that are used in the estimation of the levelized cost of FT diesel are listed in Table 16. The price of water is selected based on the global water cost index reported by IBM research [99]. On the other hand, cost of carbon dioxide feedstock varies widely based on the source and the capture technology. To take these variations into account, the average levelized cost of CO_2 captured from five different pathways based on the data published by Rubin et al. [100] is used. The reported values do not consider the cost of transportation, so the suggested cost of transportation by Grant et al. [101] is included. The cost of wood pellets are estimated based on commercial pellets [102].

Table 16- Feedstock Costs

Utility	Unite	Cost ($/kwh)	Reference
Carbon dioxide	$/mt	52.65	[100,101]
Water	$/m^3	1.31	[99]
Biomass (wood pellet)	$/mt	248.96	[102]

3.4.5 Utility Cost

The operation cost of allocated heating and cooling utilities, C_U, is extracted directly from ASPEN Plus simulation results.

3.4.6 Income

C_{income} is the profit that is acquired by selling byproducts of the integrated system. Table 17 lists possible byproducts and their market prices. Note that, only pure oxygen, not diluted by sweep air, can be considered as a byproduct. Therefore, it is considered in the estimation of presented levelized cost of FT diesel whenever the air compressor is eliminated from the SOEC subsystem depicted in section 2.1.3.

Table 17- Byproducts market value

Byproduct	Unit	Value	Reference
Hydrogen	$/kg	4.6	[103]
LGHC	$/MJ	0.006	[104]
Naphtha	$/mt	400	[105]
Wax	$/mt	1000	[106]
Oxygen	$/kg	3	[107]
Heat	$/GJ	9.5	[108]

3.5 Emissions Model

The GHG emissions from the use of FT diesel is calculated based on the guidance provided by the European Commission. According to the EU directive 2009/28/EC, the GHG impact of FT diesel can be estimated according to equation 35 [109].

$$E_{FT\,Diesel} = e_{ec} + e_l + e_p + e_{td} + e_u - e_{sca} - e_{ccs} - e_{ccr} - e_{ee} \quad (35)$$

where,

$E_{FT\,\mathrm{Diesel}}$: total emissions from the use of FT diesel,

e_{ec}: emissions from the extraction or cultivation of raw materials,

e_l: annualized emissions from carbon stock changes caused by land-use change,

e_p: emissions from processing,

e_{td}: emissions from transport and distribution of fuel,

e_u: emissions from the fuel in use,

e_{sca}: emission saving from soil carbon accumulation via improved agricultural management,

e_{ccs}: emission saving from carbon capture and geological storage,

e_{ccr}: emission saving from carbon capture and replacement,

e_{ee}: emission saving from excess electricity from co-generation.

Emissions from extraction of raw materials, processing, transport and distribution, and carbon capture and replacement are relevant here; all others can be neglected, hence equation 35 will be reduced to

$$E_{FT\,Diesel} = e_{ec} + e_p + e_{td} - e_{ccs} - e_{ccr} \tag{36}$$

Emissions from extraction and cultivation and transport and distribution for farmed wood and waste wood were set to values that are already suggested in this directive and presented in Table 18 [109]. The emissions from processing are equal to the carbon dioxide that leaves the integrated system in the process of FT diesel production (e.g., emissions from cooling and heating utilities). These values as well as e_{ccr}, e_{ccs} are extracted directly from ASPEN model. Since FT diesel is produced from renewable sources, emission from its usage would be equal to zero [109]. There are other by-products and therefore the emission associated with the main product is the total emission multiplied by the allocation factor estimated using equation 37.

$$Allocation\,factor = \frac{Energy\,content|_{FT\,Diesel}}{Energy\,content|_{FT\,Diesel} + Energy\,content|_{byproducts}} \tag{37}$$

Emission savings of using FT diesel instead of fossil based fuel is calculated as shown in equation 38. E_f is the emission from using fossil based fuels and its value is set to 83.8 $gCO_{2,eq}$/MJ which is the recommended value by European Commission [109].

$$Emission\,savings = \frac{E_f - E_{FT\,Diesel}}{E_f} \tag{38}$$

Table 18- Default GHG emission values for FT diesel (gCO_{2eq}/MJ)

Type	e_{ec}	e_{td}
Waste wood	1	3
Farmed wood	4	2

4 System Operating Condition*

The first step towards better understanding of the integrated system operation is to estimate the optimum system operating condition to have the highest possible performance of the system for a given situation. Therefore the effect of operating condition on SOEC and EG subsystem performance is investigated. (Several studies related to the FT process and its optimum operating condition with respect to conversion efficiency have already been published [44,110–113]. Based on these findings the FT operating condition is set to 25 bar and 240°C.) Since hydrogen and carbon monoxide are the only components of syngas that will participate in the FT reactions, other possible products, such as methane, are treated as neutral components. So, for the purpose of correct demonstration of the effects of operating condition on the performance of SOEC and EG subsystems, the heating value of the products other than hydrogen and carbon monoxide in the outlet syngas stream are excluded from efficiency estimations.

4.1 Solid Oxide Electrolyser Subsystem

The main focus of this section is to quantify the effect of operating pressure and temperature on system performance. System target for production of precursor syngas is chosen based on the production possibility of about 150 l/h of FT diesel without using post-compression. To guarantee production of sufficient syngas at every given point, the amount of syngas output was kept constant in the model. The SOEC operation condition is set to 800 °C and 25 bar. The dry syngas, however, will be cooled down to 240 °C before leaving the subsystem which is desirable for low temperature FT processes. The hydrogen to carbon monoxide ratio at the system outlet is set to 2.1, which is the desired

* This Chapter is based on findings presented in the first and second papers.

value in the FT reactions using a cobalt catalyst [24,44,53]. The cathode inlet stream is composed of 50% steam, 30% carbon dioxide, 10% hydrogen, and 10% carbon monoxide and methane. Reactant utilization factor * of 70% was selected to eliminate any possibility of carbon deposition. On the anode side, the sweep air flow was varied to achieve 50% oxygen molar fraction at the anode outlet stream at any given operating point.

4.1.1 Pre-compression vs. Post-compression

The electrical demand and efficiency of the pressurized subsystem were compared with ones of a subsystem that operates at atmospheric level. The main difference here would be the need for including a syngas compressor in the latter case. For the sake of comparison, the same current density of 0.7, which is equal to the thermo-neutral value for the pressurized system, is considered.

According to the results (Table 19), in the pressurized subsystem an SOEC with nominal power of 3.6 MW and cell operating voltage of 1.18 V would be sufficient to assure achieving the target production of precursor syngas. As can be seen from the results in Table 19, the SOEC unit is the major consumer of electrical power in the subsystem. The required electrical power for the compression process in comparison to this value is negligible. Therefore, syngas compressor elimination from the system will not cause a dramatic variation of the total performance. For the same amount of syngas production, in case of post-compression, the electrolysis power demand drops to 2.0 MW (Table 19). The decrease in the SOEC power demand results in higher energy and exergy efficiency of the subsystem. The observed differences between performances of these systems can be explained by large amount of methane (consequently smaller amount of syngas) at the system outlet at elevated operating pressures.

* Reactant utilization factor is the measure of conversion rate of reactants to products.

Table 19- Comparison between performance of post-compression and pressurized systems

Parameter	Unit	Post-Compression	Pressurized
P_{SOEC}	MW	2.0	3.6
$P_{compression}$	MW	0.2	0.3
V_o	V	1.2	1.18
I	$A.cm^{-2}$	0.7	0.7
η	%	81.3	63.8
E	%	68.9	47.1

Temperature, pressure, and mixture composition at the cathode inlet, cathode outlet and system outlet are presented in Table 20. As can be seen, owing to internal production of methane from syngas (Table 7-reaction 5), methane content at the system outlet is quite high (14%). As a result, available syngas at the system outlet for further production of FT diesel is reduced which is an adverse effect of high operating pressure. Therefore a larger amount of reactants should be electrolyzed to produce the same amount of syngas in the pressurized system in comparison to atmospheric pressure operation. Strictly speaking, the conversion rate of reactants increases and consequently faradic current would be higher. This entails either larger number of electrolysis cells or active surface area should be considered at the same current density and operating voltage to produce the same amount of syngas. Consequently the SOEC stack will be heavier and bulkier at elevated operating pressures.

Table 20- Thermodynamic values of material streams of the SOEC system

Stream	Temperature (°C)	Pressure (bar)	Composition (Molar Concentration %)				
			H_2O	CO_2	CO	H_2	CH_4
Cathode inlet	800	25.3	53.6	27.6	5.13	10.3	3.2
Cathode outlet	800	24.7	24.2	13.1	17.2	34.6	10.9
System outlet	240	22.3	1.5	16.9	22.4	44.9	14.1

4.1.2 Pressure Effect

The effects of operating pressure on the production rate of syngas and methane as well as system performance from atmospheric pressure up to 36 bar are shown in Figure 15 to Figure 17. Primary operating parameters (e.g., temperature and current density) were kept constant. To guarantee production of sufficient syngas for further FT diesel production at all operating conditions, a constraint was imposed to the model maintaining a constant molar flow rate at the subsystem outlet.

As explained in the previous section, internal production of methane from syngas is favored at elevated operating pressures and consequently methane and syngas molar fractions at the cathode outlet would be higher and lower, respectively (Table 7-reaction 5). As can be seen in Figure 15, even small increase in operating pressure causes a drop in syngas molar fraction and therefore the effect of pressure on subsystem performance cannot be ignored. Nevertheless, the syngas molar fraction at the subsystem outlet reduces by more than 20% when operating pressure is increased from atmospheric to 36 bar. In order to compensate for this reduction, more reactants should be provided for the electrolysis process manifesting itself as higher faradic currents. On the other hand, according to the presented results in Figure 16, the operating voltage increases slightly up to 8 bar followed by a decrease. Nonetheless, operating voltage variations over this pressure range are small (less than 5%) and therefore can be considered as constant. This trend can be explained by two contradicting effects of pressure on the electrolysis unit: increase of Nernst voltage and decrease of ASR, both canceling each other out.

According to equation 7 (section 3.1.1), constant operating voltage and increase of faradic current results in higher electrical demand of electrolysis unit. Moreover, compressor and pump power demands increase at higher operating pressures. This results in an increase of total internal power demand of the SOEC subsystem as illustrated in Figure 16. Constant flow rate of syngas at the subsystem outlet along with the increase of both the electrical power demand and material input to the subsystem results in a gradual drop of 27 and 30 percentage points of energy and exergy efficiency, respectively.

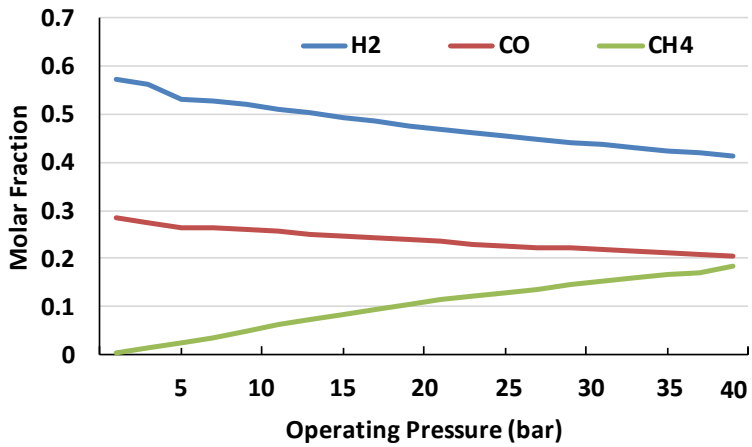

Figure 15- Effect of operating pressure on syngas and methane production (T=800°C)

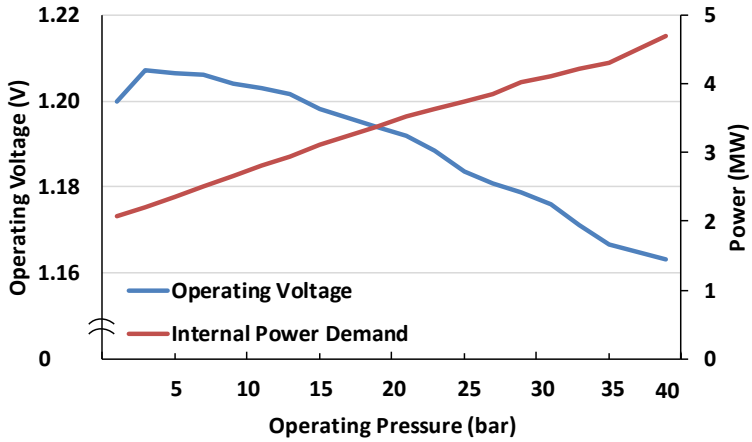

Figure 16- Effect of operating pressure on operating cell voltage and power consumption of the system (T=800°C)

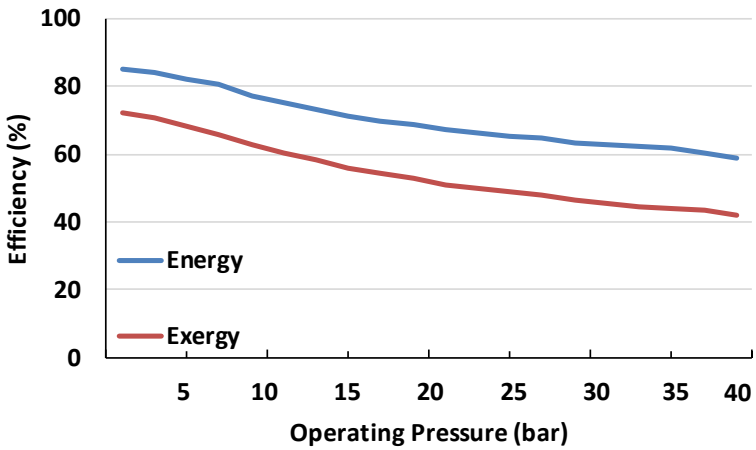

Figure 17- Effect of operating pressure on system energy and exergy efficiency (T=800°C)

4.1.3 Temperature Effect

The operating temperature was varied in the range of 700-900 °C while other operating parameters, such as operating pressure, were kept

constant. Internal production of methane from syngas is highly exothermic and consequently is disfavored at high operating temperatures. In other words, as also shown in Figure 18, the lower the operating temperature, the higher methane molar fraction at the subsystem outlet. Since molar flow rate of syngas is fixed in the model, lower internal methanation rates lead to higher syngas content, so a lower amount of reactants is necessary which in turn results in lower faradic currents. Moreover, elevated operating temperature causes not only more rapid reaction kinetics but also reduced internal cell resistance which ultimately cause operating voltage reduction (Figure 19). A simultaneous drop in faradic current and operating voltage results in eventual decrease in the electrical power demand of the SOEC unit. In addition, the electrical power demand of pressure changers reduces owing to the fact that lower flow rates pass through them. Hence, the dramatic drop in total internal power demand of SOEC subsystem is a result of drop in both SOEC unit and compression power demand, as illustrated in Figure 19.

As shown in Figure 20, subsystem energy and exergy efficiencies increase with temperature. Owing to the higher physical exergy content of streams, the increase of exergy efficiency is more dramatic than for energy efficiency. To exemplify: an increase of operating temperature from 700 to 800 ^{o}C will cause an increase of about 19 and 23 percentage point in SOEC subsystem energy and exergy efficiencies, respectively.

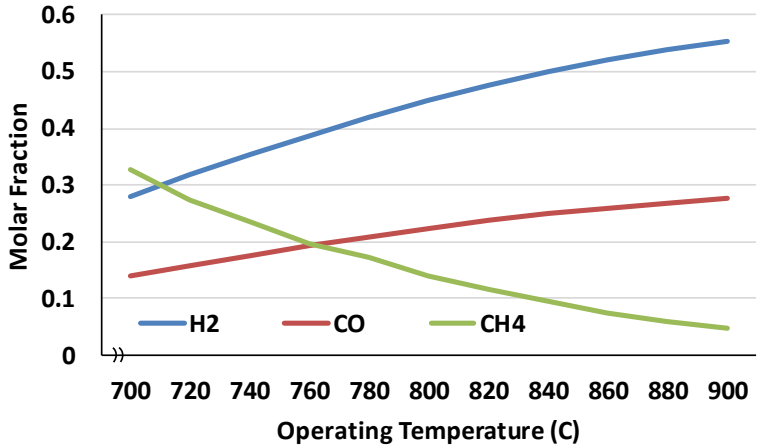

Figure 18- Effect of operating temperature on production of syngas and methane (P=25 bar)

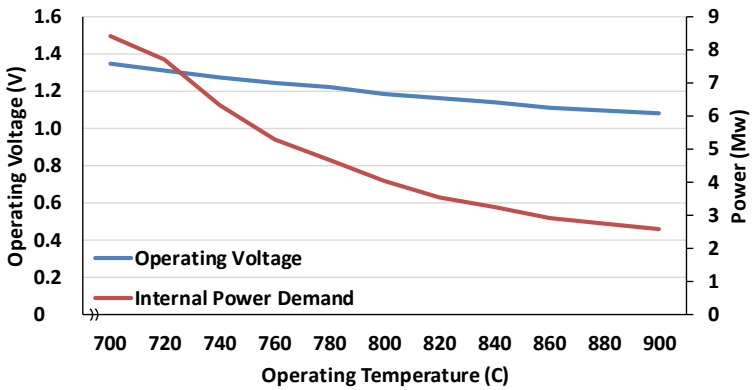

Figure 19- Effect of operating temperature on operating cell voltage and power consumption of the system (P=25 bar)

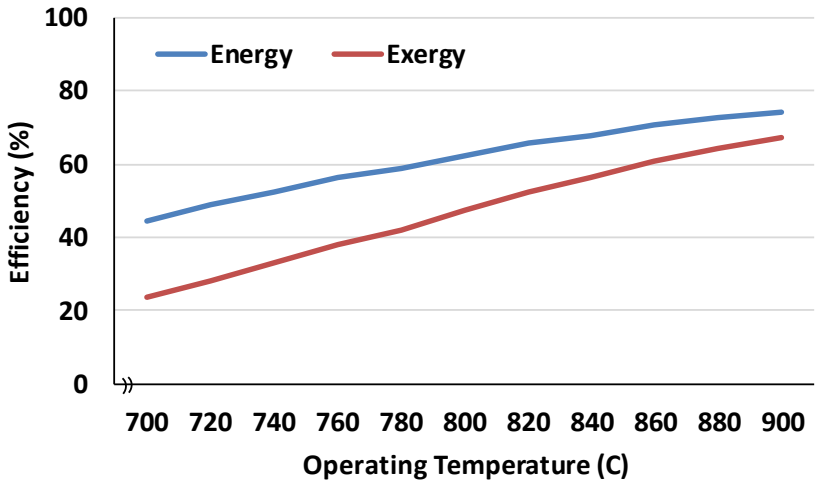

Figure 20- Effect of operating temperature on system energy and exergy efficiency (P=25 bar)

4.2 Entrained Gasification Subsystem

In this section an entrained gasification system, with production potential of sufficient precursor syngas for further production of 15 m^3/h Fischer-Tropsch diesel, is modeled and analyzed. Like SOEC subsystem, a constraint is defined in the model so that the production of certain amount of precursor syngas at every given operating condition is assured. In the base line design, EG reactor is assumed to operate at atmospheric level and 1200^{o}C. Since the FT subsystem is not included in this step of analysis, a syngas compressor and heat exchanger are considered to be located after the Selexol unit. Although the aforementioned components are usually included in the FT subsystem (Figure 11), they are added to the EG subsystem in this step so that the post-compression effect is taken into the consideration. Like SOEC subsystem, dry syngas leaves the EG subsystem at 240 ^{o}C, 25 bar, and with the hydrogen to carbon monoxide ratio of 2.1. As explained in section 3.1.4, wood pellet properties are used to model the lignocellulosic biomass input stream.

4.2.1 Pressure Effect

Effects of operating pressure on the syngas and methane content at the subsystem outlet and its overall performance are studied by varying operating pressure from atmospheric to 25 bar; gasification temperature was kept constant at 1200^{o}C.

As can be seen in Figure 21C, the molar fraction of methane at the subsystem outlet increases due to higher probability of methane production at elevated operating pressures. However, methane molar fracion in comparison to syngas is negligible owing to the high operating temperature of entrained gasification; i.e., 6% methane content (Figure 21C) compared to 63% hydrogen (Figure 21A) and 30% carbon monoxide (Figure 21B). Syngas content (hydrogen and carbon monoxide) at the subsystem outlet slightly decreases, which has a negligible effect on subsystem energy output. Although the energy output from the EG subsystem can be considered more or less constant, the total electrical power demand decreases with increase of pressure up to 6 bar due to the lower electrical demand of syngas compression, as shown in Figure 22. This effect is mainly negated by increase in ASU electrical power demand after 6 bar, since both oxygen volume flow rate and oxygen compression power demand increase. Hence, an initial increase followed by a slight drop in the subsystem energy and exergy efficiencies is observed. Strictly speaking, energy and exergy efficiencies have their highest values of 54.2% and 49.4%, respectively at 6 bar.

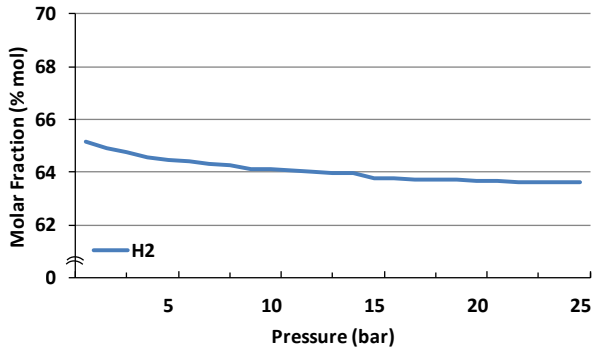

(A)

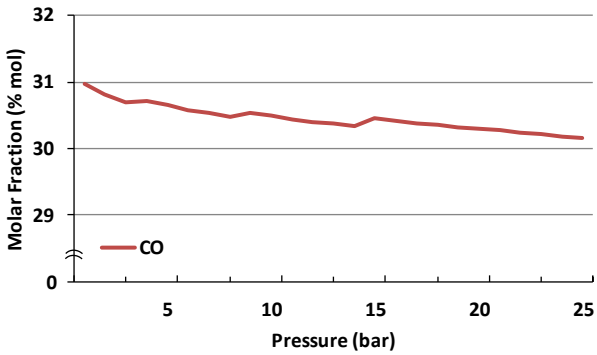

(B)

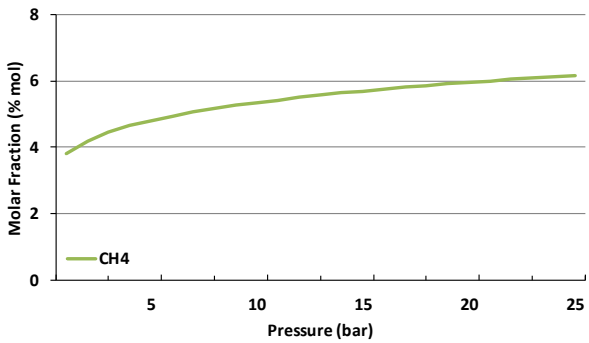

(C)

Figure 21- Effect of operating pressure on output stream content (T_G=1200 ^oC)

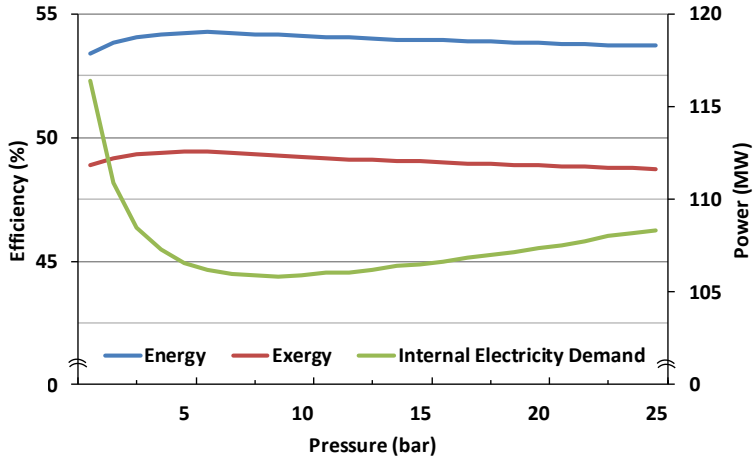

Figure 22- Effect of operating pressure on power consumption and energy and exergy efficiencies (T_G=1200 ^oC)

4.2.2 Temperature Effect

Figure 23 illustrates the effect of operating temperature on the stream composition at the subsystem outlet. The gasification temperature was varied from 1000 to 1400^{o}C while the operating pressure was kept constant at atmospheric level. As can be seen in Figure 23C, due to exothermic nature of methanation reaction, higher gasification temperatures result in lower methane content at the subsystem outlet. Similar to the operating pressure, variations in hydrogen and carbon monoxide molar fractions in the dry syngas are negligible and consequently output syngas energy content can be considered as constant (Figure 23A-B). Nonetheless, with increase in gasification temperature, the total internal electrical demand slightly decreases. Higher gasification temperatures can be achieved by increase of combustion rate which in turn causes an increase in oxygen flow rate. On the other hand, since lower molar fraction of methane is present at the subsystem outlet, lower raw biomass flow rate would be required to produce the same amount of syngas as when gasification temperature is lower. Therefore, to eliminate the possibility of combustion in the gasifier, oxidant flow should be reduced as well. These contradicting effects on oxidant flow results in a small change in ASU and consequently subsystem electrical power demand (Figure 24). Energy efficiency of the subsystem slightly

decreases (0.7 percentage point drop at higher temperatures) owing to the higher heat losses during quenching process. As shown in Figure 24, unlike energy efficiency, exergy efficiency exhibits a slight increase of one percentage point owing to the higher physical exergy of the streams at higher temperatures.

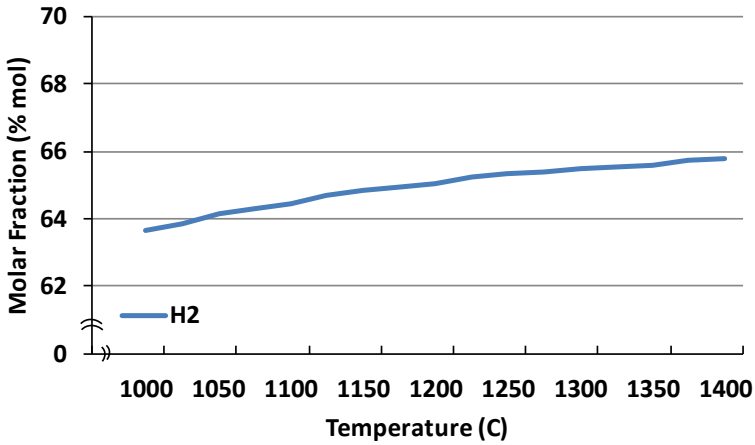

(A)

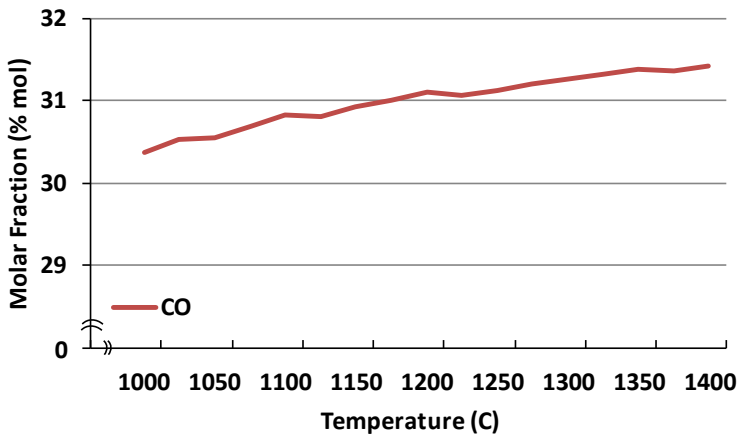

(B)

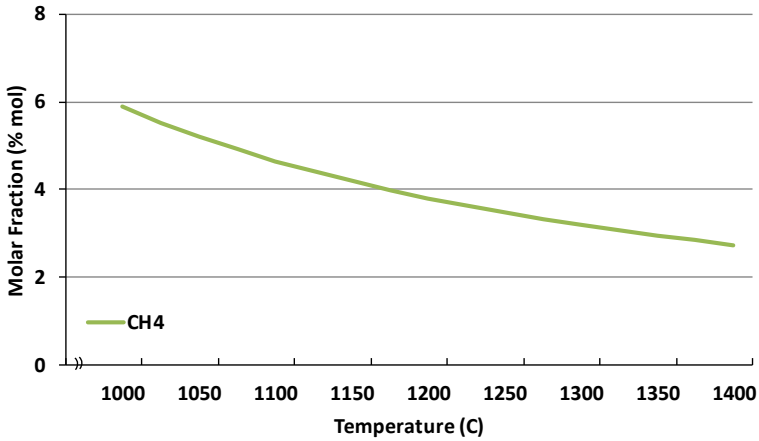

(C)

Figure 23- Effect of operating temperature on output stream content (atmospheric pressure)

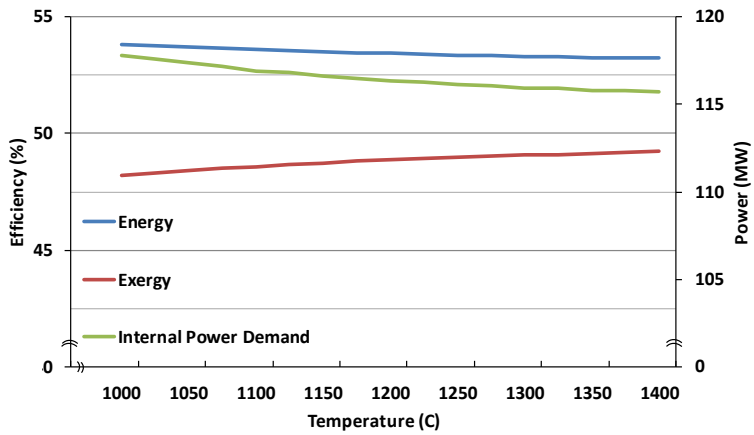

Figure 24- Effect of operating temperature on power consumption and energy and exergy efficiencies (atmospheric pressure)

4.3 Concluding Remarks

The main goal of this step was to define the range of operating conditions for both SOEC and EG subsystems to achieve high performance of the proposed integrated system. In both cases, the contribution of produced methane was neglected to portray the correct effect that each subsystem operating condition would have on the total performance of the system.

Results of SOEC analysis show that due to the internal production of methane from syngas at elevated operating pressure, atmospheric operation is more favorable than pressurized. Nonetheless, the effect of internal methane production can be balanced out at higher operating temperature. Since FT diesel is the desired final product of the integrated system rather than methane, atmospheric operating pressure and operating temperature of 800 ^{o}C (typical operating temperature of SOEC unit) seems a good operational choice for the SOEC subsystem.

Simulation results of EG subsystem showed that the role of other subsystem components in the final efficiency of the subsystem cannot be ignored. Moreover, due to high gasification temperature, methane content at the subsystem outlet in comparison to syngas is minuscule although its molar fraction increases with increase in operating pressure. It is also shown that the subsystem has its higher energy and exergy efficiencies at 6 bar. Unlike pressure, gasification temperature seems to not have prominent effect on the subsystem performance. All in all, it seems that EG subsystem operating at 6 bar and 1200^{o}C would be an acceptable choice.

5 Possible Integrations*

This Chapter is dedicated to find the answer to the second research question,

"What are the possible ways to integrate the selected technologies?"

In general, based on the operation mode of SOEC subsystem, two base line configurations can be suggested which are shown in Figure 25. In the first scenario SOEC operates in co-electrolysis mode and therefore precursor syngas is produced both from EG and SOEC (Figure 25A). In this step, it is assumed that both EG and SOEC subsystems have an equal contribution in providing the required precursor syngas for further production of 30 m^3/h of FT diesel. The allocated syngas production capacity is chosen as a compromise between benefits and drawbacks of EG and SOEC technologies, which will be discussed thoroughly in Chapter 6. In the second scenario (Figure 25B), the required carbon for FT diesel production is solely provided from gasification of stem wood. SOEC then is operating in electrolysis mode with the sole purpose of providing enough hydrogen to achieve a hydrogen to carbon monoxide ratio of 2.1.

Therefore, SOEC operation mode (co-electrolysis or electrolysis) is the main difference between the presented scenarios. Nevertheless, it causes slight variations in component configurations of SOEC and EG subsystems. The SOEC in the first scenario has a configuration according to Figure 5, while Figure 6 illustrates SOEC subsystem configuration in scenario 2. In the second scenario, the water gas shift reactor from EG subsystem (Figure 9) is eliminated.

In the previous Chapter, it was concluded that increasing pressure has adverse effect on performance of SOEC while EG showed its peak performance at 6 bar. Moreover, it was shown that an increase in SOEC

* The following Chapter is based on the findings that are presented in the third paper

temperature would results in higher performance of the system, while change in gasification temperature did not have any significant effect on total performance of EG subsystem. In this Chapter, these findings would be put in test to see if they are still significant. For example, it will be checked to see if any of these integrations would have their peak performance at 6 bar, or high performance of EG would be canceled out by other factors.

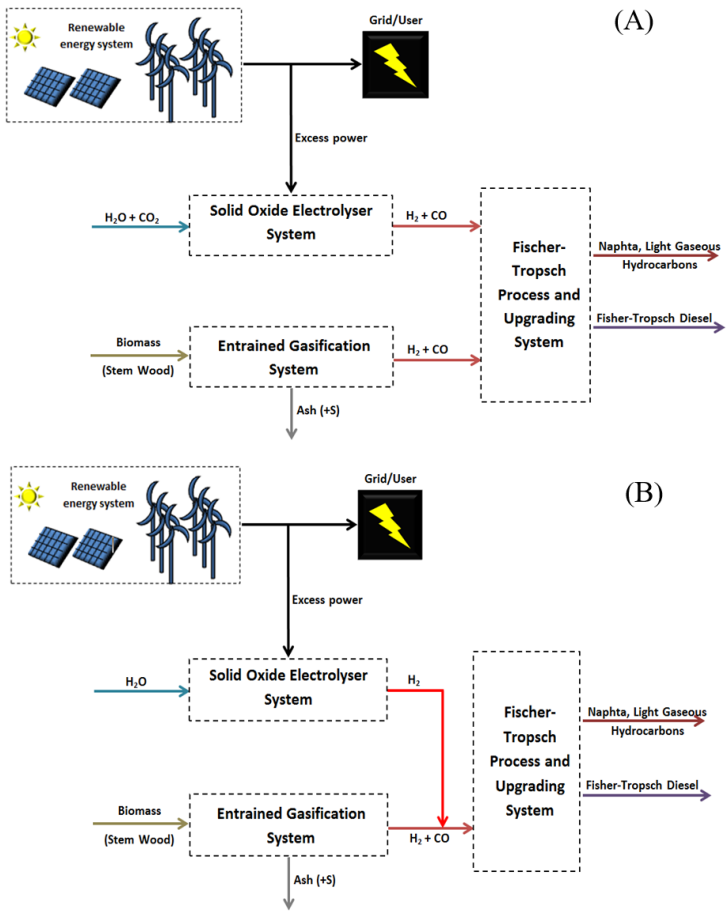

Figure 25- Different integrated system configurations A) scenario 1, B) senario 2

5.1 Effect of SOEC and EG Operating Pressure

The effect of SOEC and EG operating pressure on the integrated system energy and exergy efficiency in both scenarios is illustrated in Figure 26. Operating pressures of EG and SOEC subsystems are varied from atmospheric to 25 bar, respectively while operating pressure of FT reactor is kept constant at 25 bar. Naturally, no syngas compression would be required when SOEC and EG subsystem pressures reach 25 bar. As can be seen, increasing operating pressure results in a slight improvement of system efficiency while it has adverse effect in scenario 1.

The observed trend in scenario 1 can be explained by increase of the internal methane production at elevated pressures. As explained in section 4.1.2, the increase in methane content at the subsystem outlet in turn results in smaller syngas molar fraction (hydrogen and carbon monoxide), higher electrical power demand by SOEC, and consequently lower energy and exergy efficiencies. Similarly, elevated pressure results in higher level of methane at the gasifier outlet, although its molar fraction is negligible in comparison to the syngas molar fraction (section 4.2.1). Nevertheless, biomass input to the system increases about 1.3 percent with pressure (Figure 27). Therefore, the sizing unit (explained in section 3.1.2) requires more electrical power. The ASU electricity demand is also higher since it now provides compressed oxygen for the gasifier. On the other hand, electrical power demand of syngas compression (located before FT reactor) reduces with increase of the EG and SOEC subsystem pressures. However, this decrease cannot compensate the increase in electricity demand of other system components such as SOEC unit and therefore the total electrical power demand would be higher (Figure 28).

In the second case there will be no internal methanation in the SOEC cathode compartment; variations in operating pressure do not affect the steam input to the subsystem and consequently faradic current would be constant. Also, owing to elimination of slow carbon monoxide electrolysis reaction and higher reaction rates of steam electrolysis, internal power demand in this case is lower than the previous scenario; additionally the carbon dioxide compressor is eliminated and the internal power demand decreases further. Concurrently a higher input rate of biomass is required since all the required carbon should be provided from EG subsystem (Figure 27), causing the sizing unit in the EG subsystem to

have a higher power demand. As shown in Figure 28, these contradicting effects counterbalance each other so that the total internal power demand is lower here. In addition since changes in electrical power demand are almost constant, very slight changes in efficiencies are observed (Figure 26).

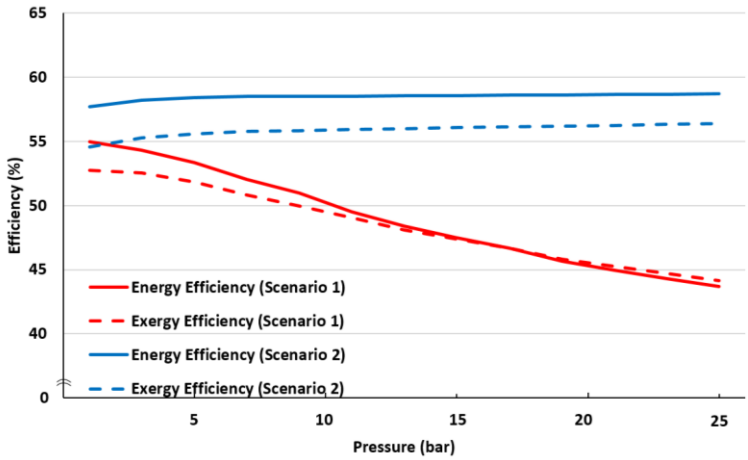

Figure 26- Effect of operating pressure on the energy and exergy efficiency in each scenario

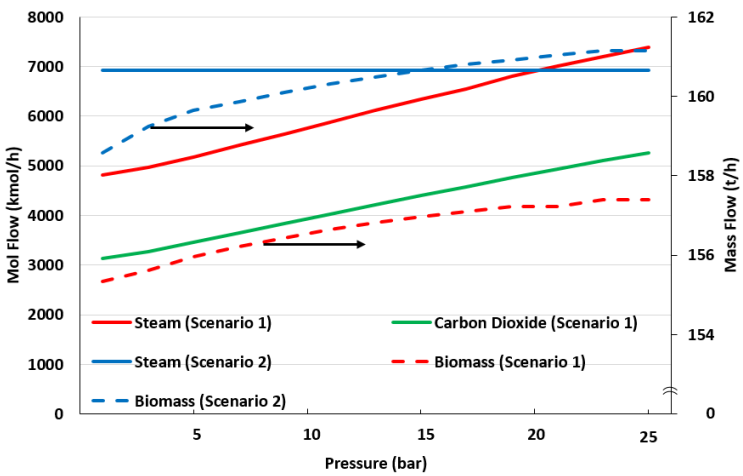

Figure 27- Effect of pressure on system feedstock inputs

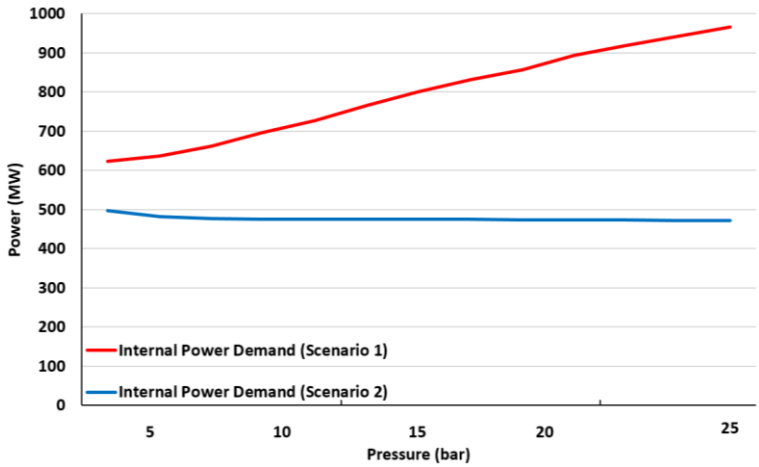

Figure 28- Effect of operating pressure on internal electrical demand in each scenario

5.2 Effect of Electrolyser operating Temperature

Operating temperature of electrolysis unit is varied from 700 to 900 ^{o}C while other operating parameters were kept constant.

As explained in section 4.1.3, for scenario 1 the exothermic methanation reaction occurring inside cathode compartment is favored at lower operating temperatures. Strictly speaking, the higher the temperature, the lower the internal methanation rate. As a result, lower reactant inputs are required to have the same molar flow rate of syngas at the subsystem outlet (Figure 29). Therefore, SOEC power demand would be lower. The eventual drop in the electrolysis power demand as well as lower demand of subsystem pressure exchangers (owing to reduction in their input mass flow rate) are manifested not only in the reduction of internal power demand of the integrated system (Figure 30) but also in the higher integrated system energy and exergy efficiencies (Figure 31).

Like pressure, in the second case, constant amount of water enters the system due to the absence of temperature-dependent chemical reactions (Figure 29). Although higher steam flow rate enters cathode compartment in this case than scenario 1, the total flow rate entering the cathode is lower. Therefore, total internal power demand of the integrated system is

lower than scenario 1, as shown in Figure 30. According to the presented equations in section 3.1.1, both the reversible voltage and ASR decrease by the operating temperature, resulting in the reduction of the total internal power demand as well as increase in system efficiencies.

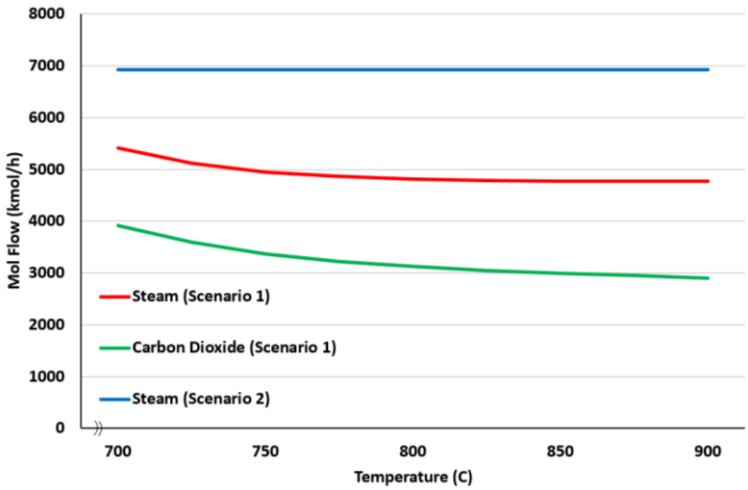

Figure 29- Effect of electrolyser operating temperature on system feedstock inputs

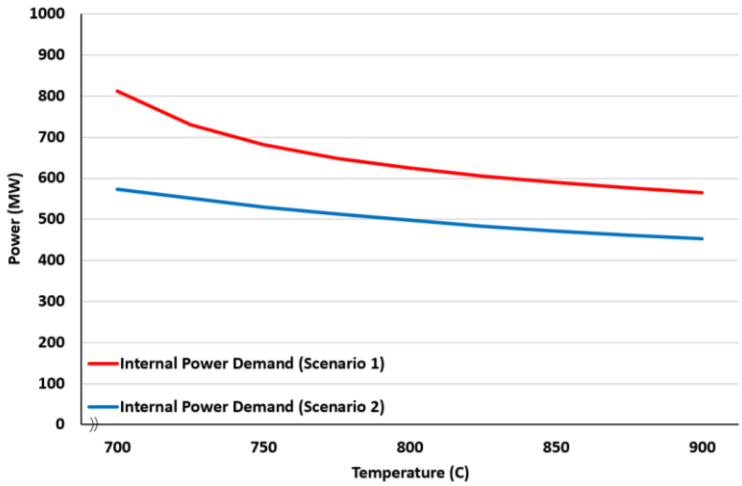

Figure 30- Effect of electrolyser operating temperature on internal power demand of each scenario

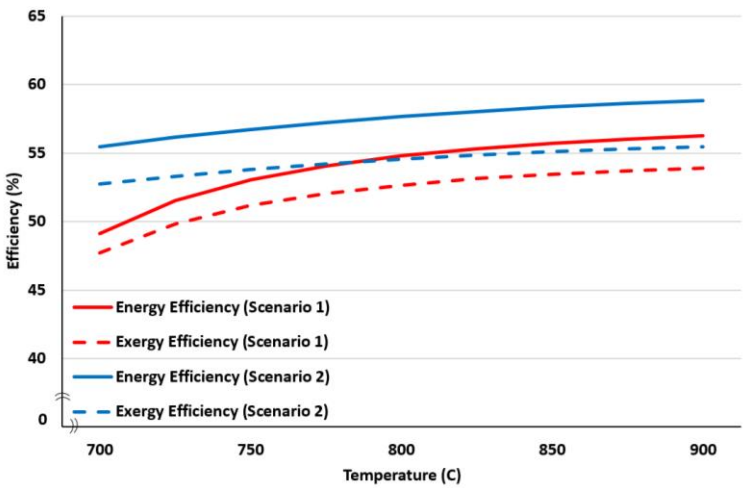

Figure 31- Effect of electrolyser operating temperature on energy and exergy efficiency of each scenario

5.3 Effect of Gasifier Operating Temperature

To investigate the possible effects of gasification temperature on the integrated system performance, gasification temperature was varied between 1000-1400 ^{o}C while the other system operating parameters are kept constant.

Like SOEC subsystem, higher operating temperatures result in lower rates of methane production from the precursor syngas. Therefore, with an increase in gasification temperature, biomass input rate to the system decreases (Figure 32). To achieve the desired hydrogen to carbon monoxide ratio, syngas passes through WGS reactor in the scenario 1 which seems to have a balancing effect on the system. Therefore, as can also be seen in Figure 32, biomass flow rate reduction is less dramatic in this case in comparison to the second scenario. As mentioned earlier, since all the required carbon for FT diesel production should be provided from gasification, the biomass flow rate is higher in scenario 2. Nevertheless, the sizing unit requires lower electrical power with an increase in temperature in both cases. This reduction in power demand, however, is negligible in comparison to total internal power demand of the system. Consequently, total internal power demand is barely affected by change in the gasification temperature, as shown in Figure 33. The combination of reduction of system input as well as constant system output and internal power demand results in higher system efficiencies (Figure 34). Nevertheless, energy and exergy efficiency of the integrated system in scenario 2 exhibit higher variations than scenario 1 due to the more significant drop in biomass input to the system in this case.

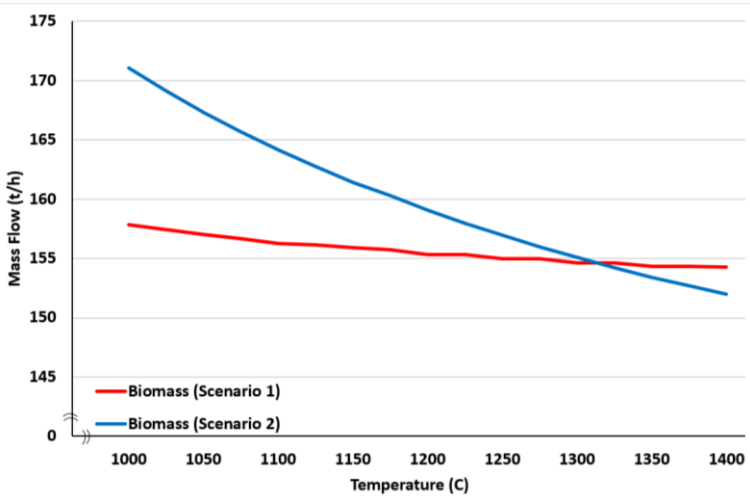

Figure 32- Effect of gasification temperature on the system feedstock input

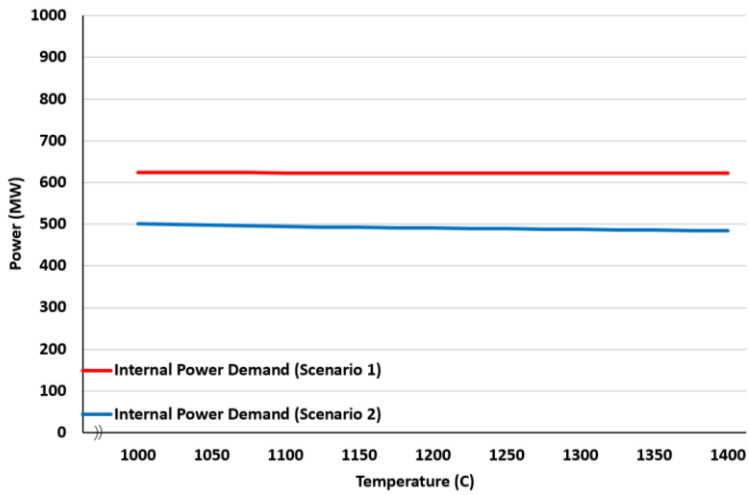

Figure 33- Effect of gasification temperature on internal power demand of each scenario

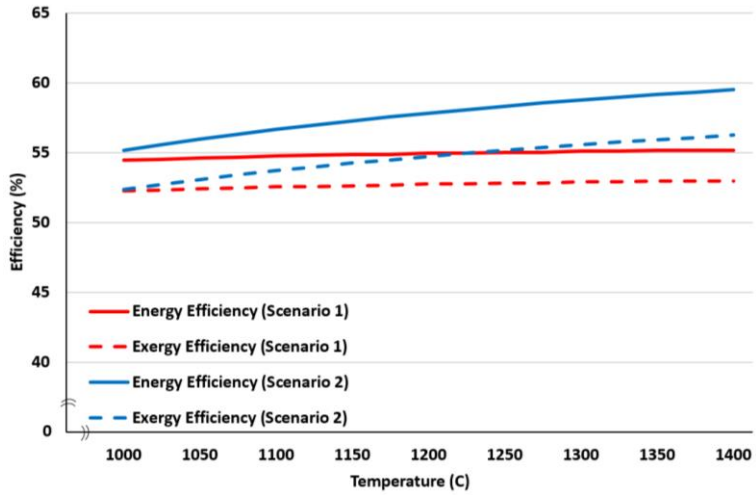

Figure 34- Effect of gasification temperature on energy and exergy efficiency of each scenario

5.4 Heating and Cooling Utilities

As shown in the presented subsystem schematics in Chapter 2, several heat exchangers are present in each subsystem. Different heating and cooling utilities are paired with these heat exchangers using Aspen Plus Energy Analyzer which considers both temperature requirements and the defined pinch temperature. The heating and cooling utilities along with their assigned heat exchangers are presented in Table 21, while Figure 35 shows the Sankey diagram of relation between subsystems and these utilities.

Cathode input flow rate in scenario 1 is higher and consequently anode heat exchanger I and cathode heat exchanger require more heat than scenario 2. However, the steam demand is higher in the second scenario which compromises the lower heat demand from combustion exhaust. Therefore, the integrated system heat demand is higher in the second scenario than first one. Similarly, more heat is released in scenario 2 (Table 21). Since higher flow rate of biomass and consequently syngas would go through EG subsystem, higher amount of heat is released from syngas cooler in this subsystem.

Table 21 – Assigned heating and cooling utilities

Utilities	Heat Exchanger	Utility Heat Duty (MW)	
		Scenario 1	Scenario 2
Medium pressure steam	Steam Generator	82.02	120.49
High temperature combustion exhaust	Anode Heat Exchanger I, Cathode Heat Exchanger	98.25	89.85
Total heating utilities		180.27	210.34
Medium pressure steam generation	Anode Heat Exchanger II, Syngas Heat Exchanger I, Syngas Heat Exchanger II, FT Reactor, Cooler I, Cooler II	393.95	391.28
Air	Condenser, HC Heat Exchanger	57.02	66.81
Cooling Water	Syngas Cooler, FT Heat Exchanger, Cooler III	386.59	415.65
Total cooling utilities		837.56	873.74

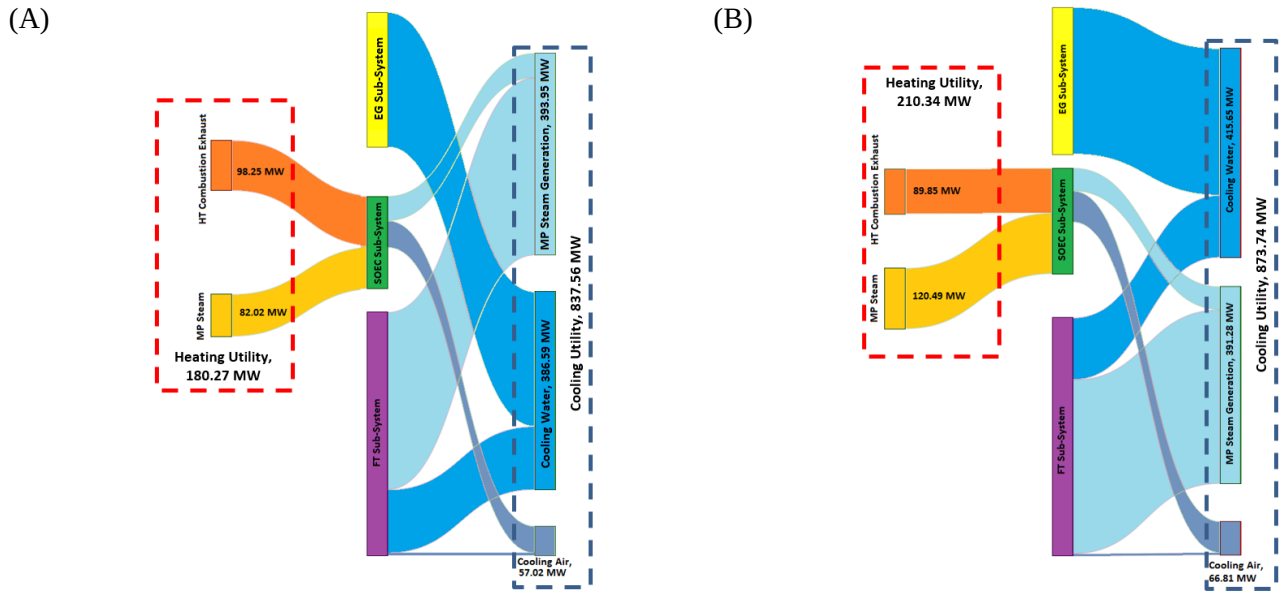

Figure 35- Sankey diagram of heating and cooling utilities A) scenario 1 and B) scenario 2

The produced medium pressure steam (MP steam) potentially allows for direct heat recovery. A quick glance at presented values in Table 21 shows that the amount of MP steam is sufficient to cover the medium pressure steam demand of the heating utilities. Including the remainder in the efficiency equation as a byproduct results in a remarkable boost of about 43 percentage points in both scenarios (Table 22). However, an increase of total exergy efficiency of the system would be much smaller (2 percent) owing to the low exergy content of MP steam.

Table 22- Comparison between integrated system performance with and without heat recovery in FT subsystem

Parameter	**Scenario 1**		**Scenario 2**	
	Energy Efficiency	Exergy Efficiency	Energy Efficiency	Exergy Efficiency
Without Heat Recovery	55.0	52.8	57.7	54.6
With Heat Recovery	78.9	54.2	82.6	56.1

5.5 Concluding Remarks

In this Chapter, two different configurations of the proposed integrated system based on the SOEC subsystem operation mode are analyzed. In other words, in the first scenario SOEC subsystem was used for the precursor syngas production while only steam electrolysis occurred in this subsystem in scenario 2.

Generally speaking, the integrated system had better performance and efficiency in the second scenario. Additionally, it was shown that variations in the operating pressures of EG and SOEC subsystems resulted in slight improvement of the integrated system performance in scenario 2 while it had an adverse effect on energy and exergy efficiencies of the integrated system in scenario 1. Considering operation

temperature, it seems that SOEC operating temperature has more prominent effect on the system performance than gasification temperature in scenario 1. On the other hand, in the second scenario, variations in both EG and SOEC operating temperature result in higher efficiencies. It is also mentioned that considering the produced MP steam as a byproduct of the system resulted in an increase of about 43 and 2 percentage point in system energy and exergy efficiencies, respectively.

6 Subsystems Sizes*

In Chapter 5, it was shown that including steam electrolysis in the integrated system instead of co-electrolysis results in better performance and higher efficiencies. Such configurations, however, would not have the possibility of the carbon dioxide recycling. In other words, including co-electrolysis adds another possible source of carbon for synthetic FT diesel production and therefore increase of the production potential of advanced biofuels. For the case of co-electrolysis, near closed-loop operation of the integrated system may be realized owing to the possibility of internal recovery of subsystems byproducts. To exemplify, oxygen (byproduct of co-electrolysis) can be used internally as the gasification agent. Therefore, the configuration featuring co-electrolysis process is considered hereafter. The main focus of this Chapter then is to quantify the effect of EG and SOEC syngas production capacity from thermoeconomic and environmental perspective. Furthermore, the effect of various internal recovery between subsystems are suggested and analyzed.

Like previous Chapter, the main output of the system is considered to be 30 m^3/h FT diesel. Naphtha, wax, light hydrocarbons, and hydrogen, which are produced in the FT subsystem are considered as possible byproducts. Based on the findings of previous Chapters, following operating conditions were selected for each subsystem:

- SOEC: 800 ^oC and atmospheric pressure
- EG: 1200 ^oC and atmospheric pressure
- FT: 240 ^oC and 25 bar

* The following Chapter is based on the findings that are presented in the fourth paper.

The baseline configuration of the integrated system is shown in Figure 36. Eleven different combinations of SOEC and EG syngas production capacity, based on the share of SOEC subsystem, are considered. These alternatives range from SOEC-only operation to EG-only operation, including combinations of SOEC/EG systems in 10% increments. The nominal syngas production capacity as a percentage of required syngas in each combination are presented in Table 23.

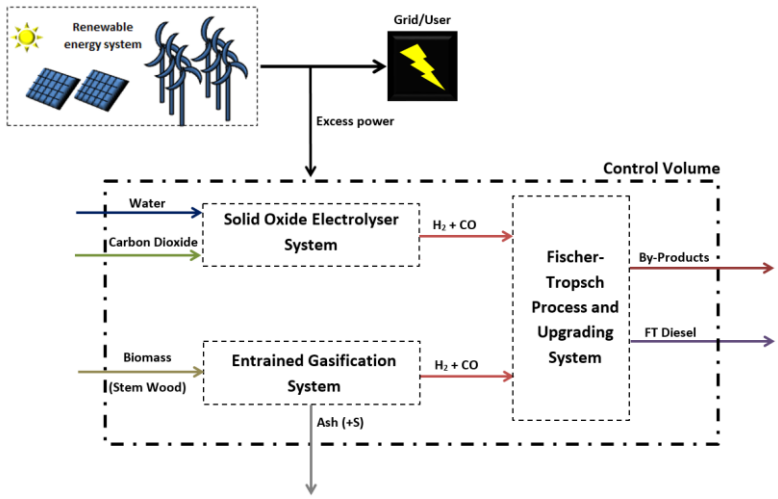

Figure 36- Schematic of SOEC-EG-FT integrated system (baseline integration)

Table 23- Nominal syngas capacity of SOEC and EG subsystems as percentage of final required syngas

Combination No.	Nominal Syngas production Capacity (%)	
	SOEC	EG
1	0	100
2	10	90
3	20	80
4	30	70
5	40	60
6	50	50
7	60	40
8	70	30
9	80	20
10	90	10
11	100	0

6.1 Baseline Integration Analysis Results

Efficiency of each combination is shown in Figure 37. SOEC subsystem has higher efficiency than EG subsystem and therefore the higher the share of syngas production in SOEC, the higher the energy and exergy efficiency of the integrated system. Energy and exergy efficiency rises from 47.5% and 44.7% in the first combination to 65% and 62.5% in the eleventh combination, respectively. Therefore it can be concluded that from the thermodynamic perspective, production of a higher share of precursor syngas in the SOEC subsystem is beneficial. However, increasing in syngas production capacity of SOEC results in drastic

increase of internal electrical power demand of the integrated system. Therefore, FT diesel levelized cost would be higher, as shown in Figure 38. Nevertheless, levelized cost of FT diesel when the integrated system just includes SOEC and FT in case of access to the low prices of renewable electricity, is in the same range of when only 60% of syngas is produced in the SOEC (2.07 $/liter in combination seven vs. 2.06$/liter in combination eleven). In this case, including EG subsystem in the integrated system with the nominal syngas production capacity of less than 40% does not seem a viable economical choice. Note that such a conclusion is not true in case of high prices of renewable electricity.

GHG emission savings from usage of produced FT diesel of each integrated system combination is shown in Figure 39. As can be seen, regardless of whether biomass is produced from waste wood or farmed wood, higher emission savings can be achieved by reducing the EG syngas production capacity. To exemplify, the GHG emission saving increased from 96% in the first combination to about 116% in the last combination. The observed trend is a result of not only a decrease in the amount of CO_2 emissions during preparation and processing of biomass but also an increase in CO_2 input to the SOEC subsystem. GHG emission savings higher than 100% implies that CO_2 input rate to the SOEC subsystem balances out other emission sources from cultivation to process to distribution. Hence, the GHG emission rate is negative.

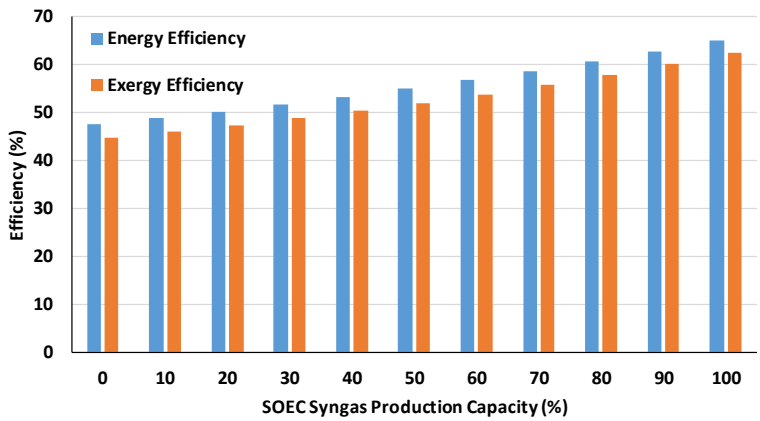

Figure 37- Effect of SOEC subsystem size on total efficiency of the system

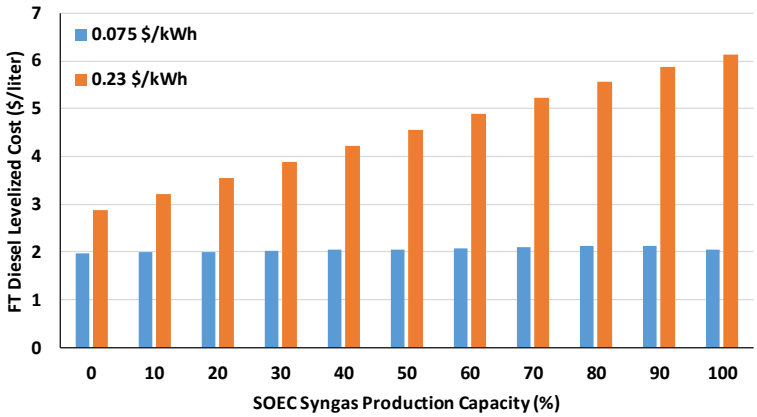

Figure 38- Effect of SOEC subsystem size on the levelized cost of produced FT diesel

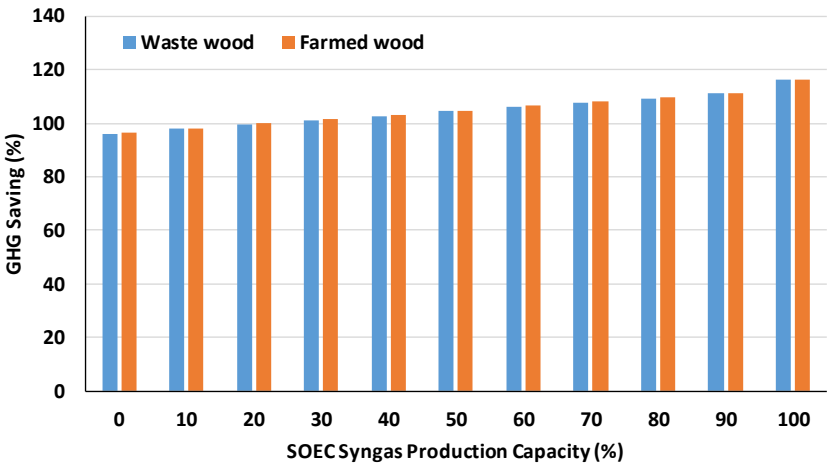

Figure 39- Effect of SOEC subsystem size on GHG saving

6.2 Internal Thermal Integration

As explained in section 5.4, Aspen Plus Energy Analyzer is used to assign the optimum heating and cooling utilities to each heat exchanger based on the streams content and temperature. Figure 40 depicts the

simplified integration between the chosen utilities and the system under study, while Figure 41 illustrates amount of each heating and cooling utility. As can be seen, in total two heating utilities and three cooling utilities are selected. Although SOEC is the only subsystem that requires a heating source, all subsystems require some type of cooling utility.

There are two ways of integrating heat flows in the system:

- Combustion of the produced gaseous light hydrocarbons
- Internal recovery of the generated MP steam

The following sections are dedicated to analysis of such heat flow integrations. List of heat exchangers and their assigned utilities can be found in Table 21 which is presented in section 5.4.

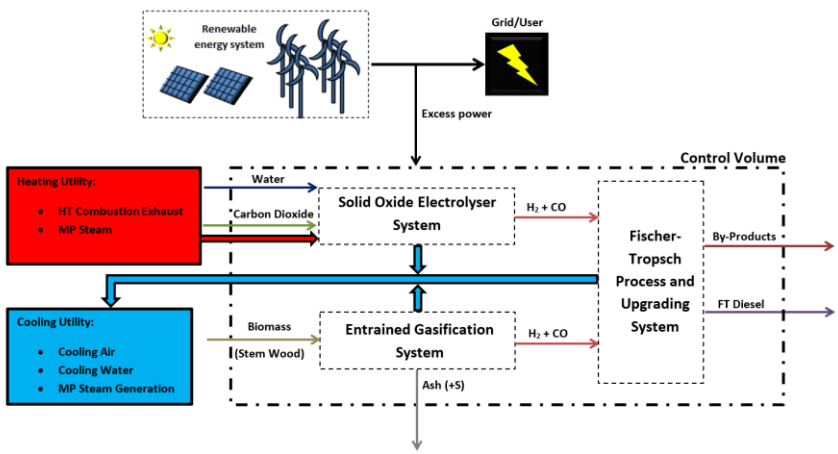

Figure 40- Schematic of heating and cooling utilities

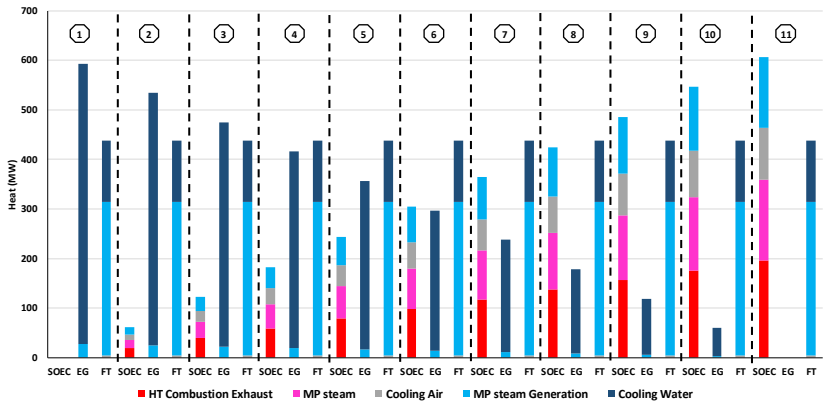

Figure 41. Heating and cooling utility requirements of each subsystem in each case

6.2.1 Combustion of Gaseous Light Hydrocarbons

Operation cost and GHG emission of HT combustion exhaust in the baseline design is estimated based on the combustion of natural gas. However, it is possible to replace natural gas with the gaseous light hydrocarbons that are produced in the system as a byproduct.

Energy and exergy efficiencies of each combination for both baseline design and with heat recovery are compared in Figure 42. As can be seen, this approach results in lower system efficiencies in all combinations. The observed trend can be explained by the fact that in the case of heat recovery, energy and exergy output from the system would be smaller. Although the energy and exergy flow input to the system also decreases, its effect is outbalanced with the former and therefore both energy and exergy efficiency decrease. Besides, the higher the share of syngas production in SOEC subsystem, the higher the amount of required heat flow to the subsystem and consequently the higher the combustion rate of gaseous hydrocarbons. Hence, system efficiency reductions are more severe in the cases that SOEC has higher share. For example, there is a 1 and 0.8 percentage point drop in energy and exergy efficiencies, respectively when SOEC has a share of 10% (the second combination). These values increase to 8 and 6 percentage point drop in the last combination.

As shown in Figure 43, FT diesel has a higher levelized cost when the heat recovery is introduced to the system. Similar to the efficiency, this increase becomes more severe with increase in share of SOEC subsystem syngas production owing to the lower income from selling the byproducts. From environmental perspective, since FT gaseous hydrocarbon can be considered as renewable fuel, the emission from its combustion would be zero. Therefore, the emissions from processing of the FT diesel reduce. On the other hand, due to lower rate of byproducts leaving the integrated system, the share of FT diesel emission increases having an adverse effect on the GHG emission when the demand of carbon dioxide is lower than its rate of supply. However, it has a positive effect on the emission savings where emission rate of the system is negative (combinations three to eleven in Figure 44).

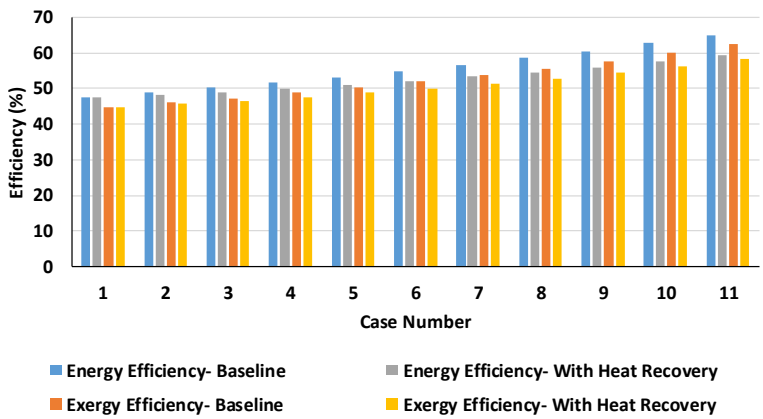

Figure 42- Effect of using FT gaseous light hydrocarbon instead of natural gas in heating utility on system performance

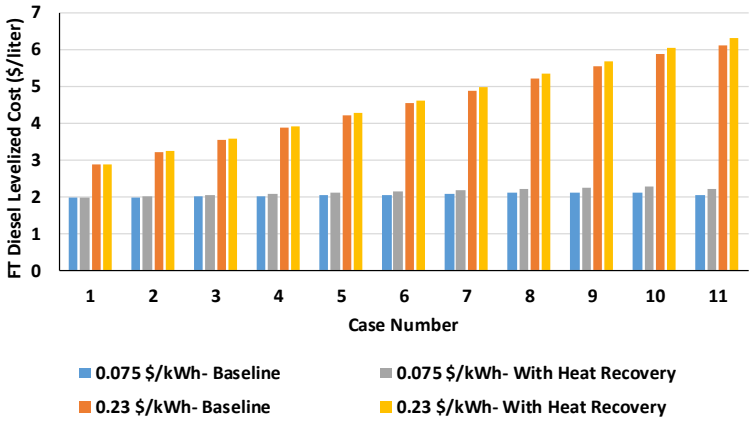

Figure 43- Effect of using FT gaseous light hydrocarbon instead of natural gas in heating utility on FT diesel levelized cost

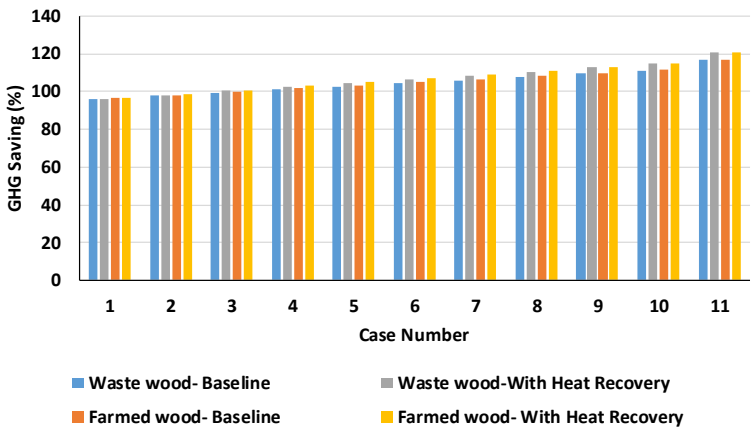

Figure 44- Effect of using FT gaseous light hydrocarbon instead of natural gas in heating utility on GHG saving

6.2.2 MP Steam Recovery

The other possible internal recovery of heat is to include the generated MP steam, used to meet the cooling requirements of system, in the calculations. As it is shown in Figure 40, MP steam is also a heating source which provides a part of the heating requirements of the SOEC

subsystem. Therefore, MP steam recovery not only allows elimination of MP steam heating utility but also the remainder steam can be considered as a byproduct of the integrated system. Therefore, in all of the combinations, energy and exergy outputs would be higher, while the energy and exergy inputs reduce. Consequently, both energy and exergy exhibit a boost (Figure 45). However, exergy efficiency enhancement is smaller owing to the fact that exergy content of heat flow is lower than its energy content. For example, while energy efficiency shows an increase of 40 percentage points in the sixth combination, exergy efficiency has an increase of 12 percentage points.

The effect of MP steam recovery on the FT diesel levelized costs is depicted in Figure 46. As can be seen, levelized cost of FT diesel is lower with including heat recovery than the baseline design. Two factors are responsible for this effect; a) lower operation cost of heating utility due to elimination of MP steam utility and b) higher generated income due to the addition of a new byproduct to the system.

Higher GHG emission savings are the other advantage of MP steam recovery. The heating utility emissions are lower since no MP steam is supplied from external sources resulting in decrease of GHG emissions and increase of emission savings in all of the combinations. The achieved emission saving through this integration is slightly lower compare to the previous proposed heat integration option owing to the lower emission rates of MP steam heating utility than HT heating utility. For example, in case eleven the emission saving reaches 119% compare to 120% that achieved by internal usage of FT gaseous hydrocarbons (Figure 47).

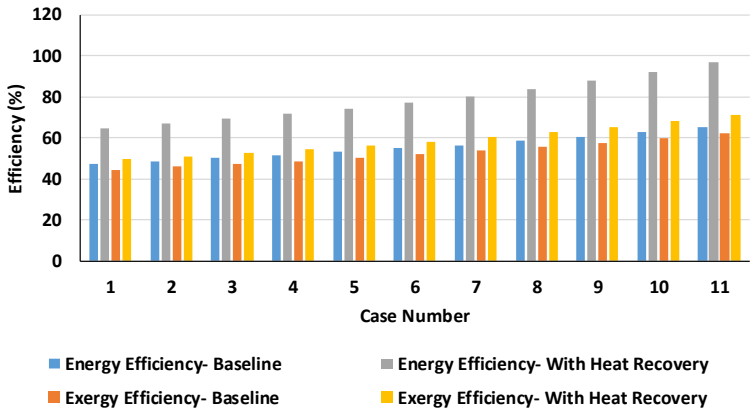

Figure 45- Effect of recovering generated MP steam on total efficiency of the system

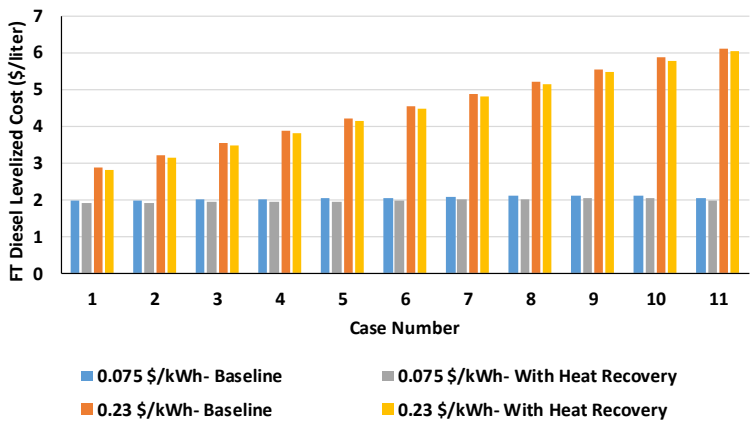

Figure 46- Effect of recovering generated MP steam on FT diesel levelized cost

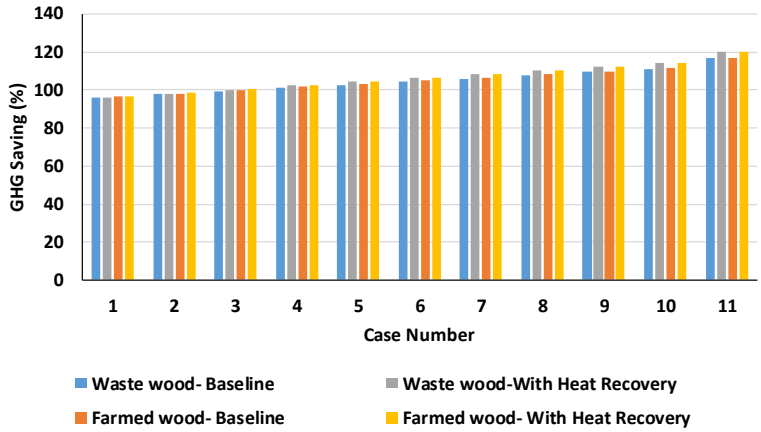

Figure 47- Effect of recovering generated MP steam on GHG saving

6.3 Internal Mass Integration

Besides heat, there is a possibility for internal recovery of some of the mass flows. There are four possible internal mass recoveries, namely: oxygen, carbon dioxide, hydrogen, and water recovery (Figure 48). Figure 49 illustrates the amount of specific mass stream that is available to be recycled internally (availability) versus consumption rate of that element. In other words, the ratio (not percentage) between availability and consumption rate of a certain mass stream are presented in this figure. As an example, the values shown for oxygen represents the amount of oxygen produced during co-electrolysis divided by oxygen consumption rate inside entrained gasifier. So, in combination 6 produced oxygen is about 1.3 times of its consumption rate in the gasifier. In the following sections the effects of each mass recovery from thermodynamic, economic, and environmental perspective are explained.

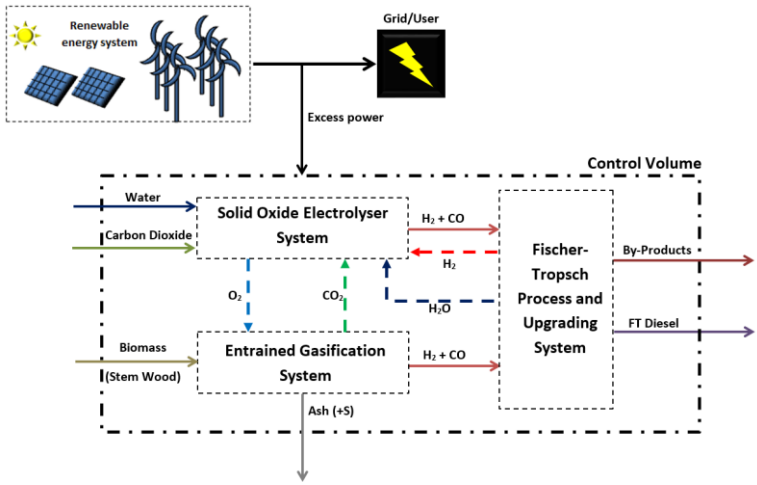

Figure 48- Possible internal mass integration between subsystems

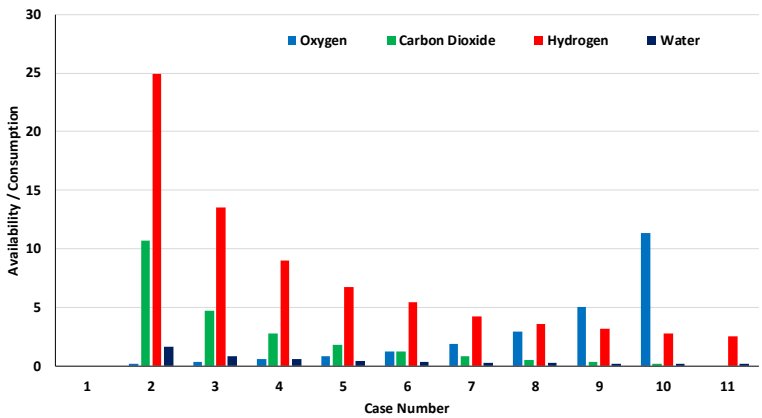

Figure 49. Availability of each recycled stream versus its consumption

6.3.1 Oxygen

Oxygen is a byproduct of co-electrolysis process. In the baseline design, the produced oxygen is released to the environment after being diluted using sweep-air (Figure 5). However, it is also possible to recover

it internally as an oxidizing agent for the gasification process. In this case, sweep air streams along with its related components are eliminated from SOEC subsystem. Nevertheless, the produced oxygen would not be sufficient to meet EG subsystem demand in combinations where SOEC supplies less than 50% of precursor syngas. In these combinations (2-5), ASU would have a smaller size while it is eliminated for the remaining combinations where internal oxygen recovery is possible (6-10). The capacity reduction or elimination of ASU from EG subsystem along with the elimination of sweep air compressor from SOEC subsystem result in lower electricity consumption of the integrated system. Moreover, the required heat input to the system is reduced owing to the elimination of anode heat exchanger I. Decrease in both power and heat demand of system boosts energy and exergy efficiencies (Figure 50). Internal oxygen recovery also results in reduction of both system capital cost and annualized cost of electricity and heating utility. Therefore, FT diesel levelized costs drop as can be seen in Figure 51. Furthermore, as can be seen in Figure 52, GHG emission savings exhibit a slight increase owing to decrease in emission from heating utility. To exemplify, GHG emission saving of the tenth combination increases by 0.7 percentage.

Note that internal oxygen recovery in the first and last combinations would not be possible and consequently no change is shown in the presented figures.

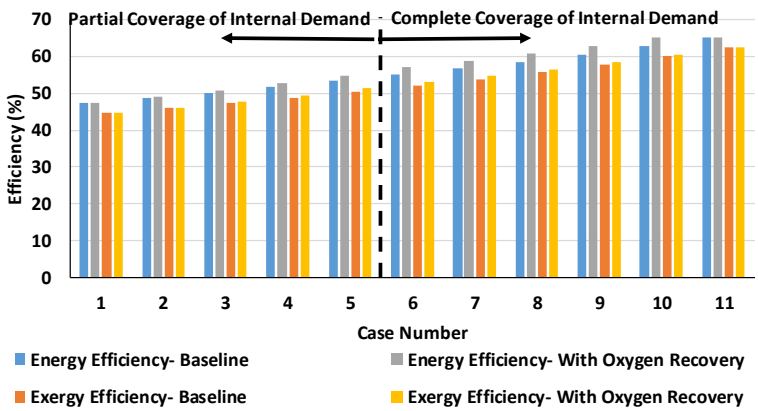

Figure 50- Effect of oxygen recovery on the total efficiency of the system

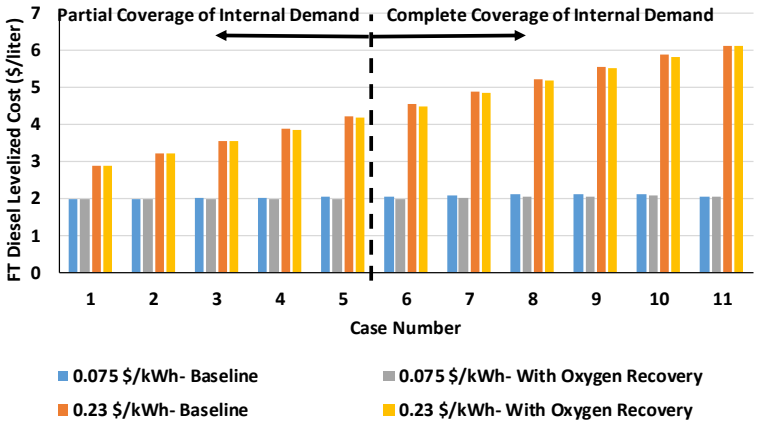

Figure 51- Effect of oxygen recovery on the levelized cost of FT diesel

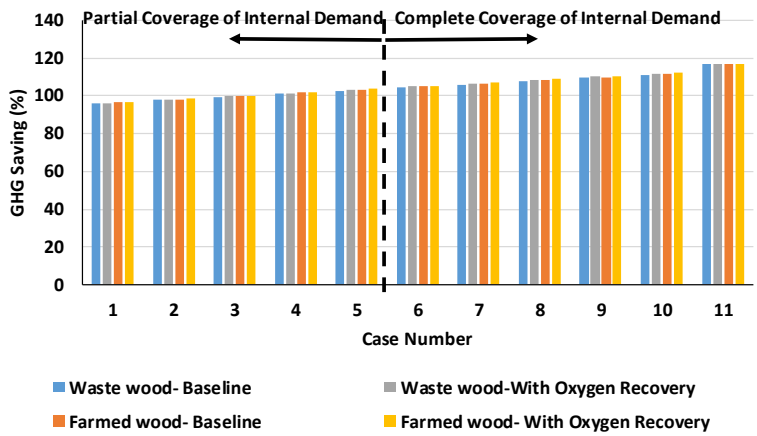

Figure 52-Effect of oxygen recovery on the GHG saving

6.3.2 Carbon Dioxide

The gasification output stream includes carbon dioxide which would be removed in the second stage of Selexol unit as explained in section 2.2.3. It is possible to reuse this carbon dioxide as the input to the SOEC subsystem. Like oxygen recovery, internal recovery of carbon dioxide cannot eliminate the dependency on an external source in all of the

combinations. Strictly speaking, complete elimination of system dependency on an external source is only possible in combinations where 50% or more of the required precursor syngas is produced from gasification of biomass. Since only exergy content of carbon dioxide is included in the thermodynamic analysis of the system, its internal recovery only affects the exergy efficiency of the integrated system (Figure 53). Due to reduction of exergy flow to the system, exergy efficiency shows a slight increases in all of the combinations. Internal recovery of carbon dioxide can also be considered as advantageous from economy perspective since it results in lower FT diesel levelized costs, as shown in Figure 54. Lower production costs of the FT diesel can be explained by the fact that smaller amount of carbon dioxide would be purchased in comparison to the baseline design. CO_2 internal recovery does not affect the GHG emission savings since its reuse is already considered in the emission estimation equation (section 3.5-equation 30).

Similar to the oxygen recovery, CO_2 internal recovery is not possible when either SOEC or EG subsystem is absent from the system integration.

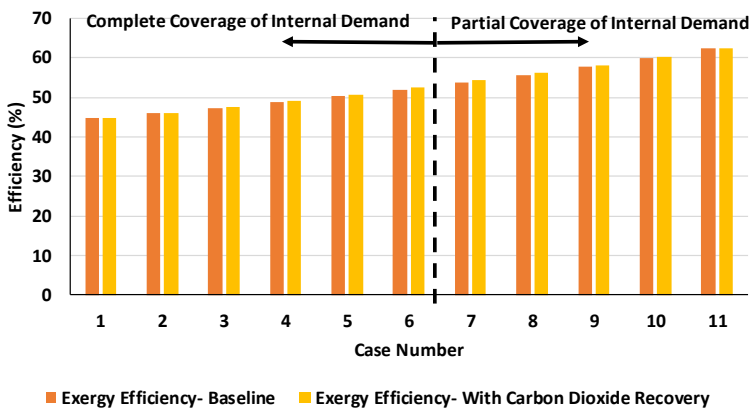

Figure 53- Effect of carbon dioxide recovery on the total exergy efficiency of the system

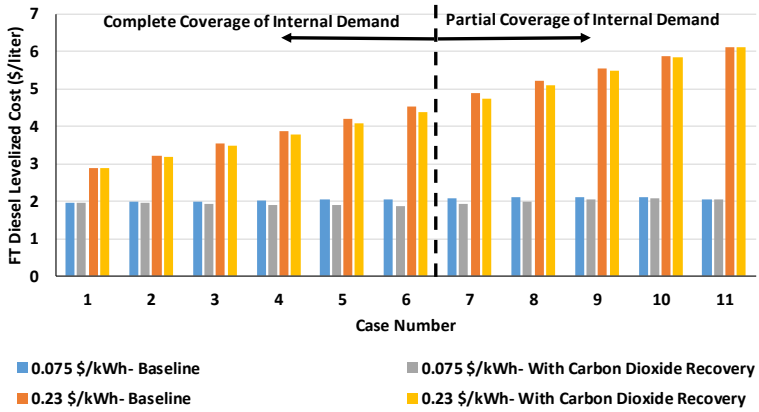

Figure 54- effect of carbon dioxide recovery on the levelized cost of FT diesel

6.3.3 Hydrogen

Hydrogen produced in the hydrogen recovery unit of FT subsystem is considered to be one of the byproducts of the integrated system. A fraction of the produced hydrogen is redirected to the hydrocracking reactor and the remainder is sold to the market. In this section the possibility of redirecting a small part of the produced hydrogen towards entrance of cathode compartment is investigated. Therefore, the recirculating compressor in the SOEC subsystem (section 2.1.3-Figure 5) is eliminated. Nevertheless, recirculating power demand is negligible in comparison to the total internal power demand of the integrated system, and therefore its elimination would not have a prominent effect on the system performance. The energy and exergy outputs decrease due to lower availability of hydrogen at the system outlet and consequently both energy and exergy efficiencies drop in combinations 2 to 10 (Figure 55). Additionally, as can be seen in Figure 56, production cost of FT diesel increases due to lower annualized income of the system.

The GHG emission savings also rise by internal recovery of the hydrogen (Figure 57). The observed trend in here can be explained by the fact that, based on the equation 30 (section 3.5), lower rate of hydrogen output as byproduct results in higher emission allocation factor of FT diesel. As explained in section 6.2.1, increased allocation factor will have

adverse effect on the GHG emission savings as long as the emission rate is positive. However, the emission rate is negative owing to the higher carbon dioxide input to the SOEC subsystem than other emission rates in the production chain.

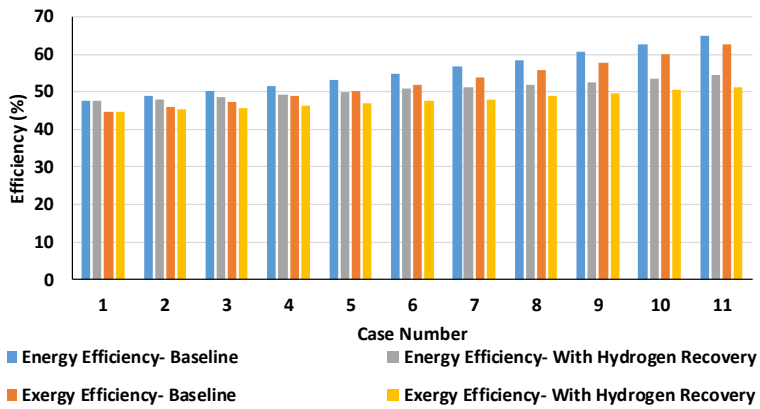

Figure 55- Effect of hydrogen recovery on total efficiency of the system

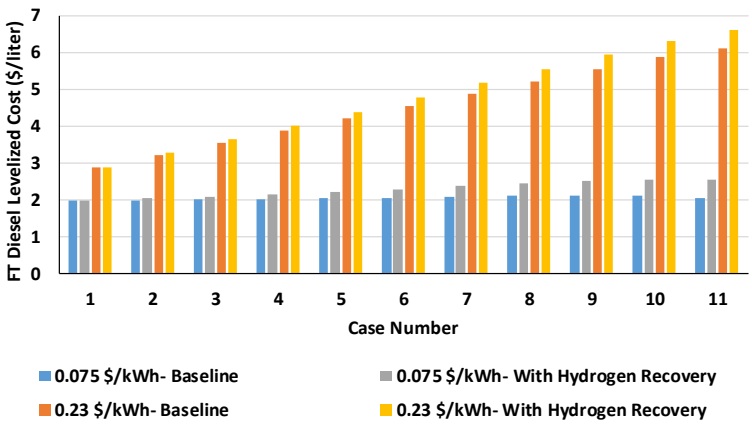

Figure 56- Effect of hydrogen recovery on the levelized cost of FT diesel

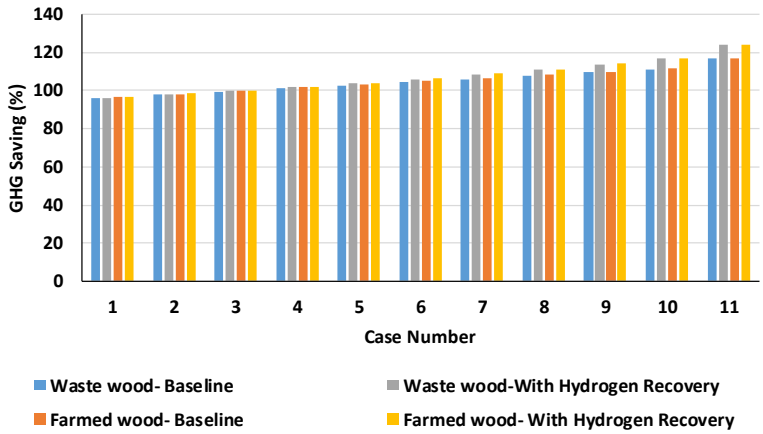

Figure 57- Effect of hydrogen recovery on the GHG saving

6.3.4 Water

The effect of internal recovery of water on the exergy efficiency as well as levelized costs of FT diesel is presented in Figure 58 and Figure 59, respectively. Water is the main byproduct of the FT reactions and syncrude upgrading processes. The produced water can be collected and used as input for co-electrolysis process to either reduce or eliminate the system dependency on external sources. Like CO_2 recovery, only exergy content of water is included in the thermodynamic analysis and consequently its internal recovery would only affect the system exergy efficiency. As can also be seen in Figure 58, internal recovery of water does not have any significant effect on the system exergy efficiency owing to its negligible exergy content in comparison to the system exergy inputs and outputs. It seems that the FT diesel levelized costs are also not affected by internal recovery of water, since water has the lowest price when is compared to other elements considered in the economy analysis (Figure 59).

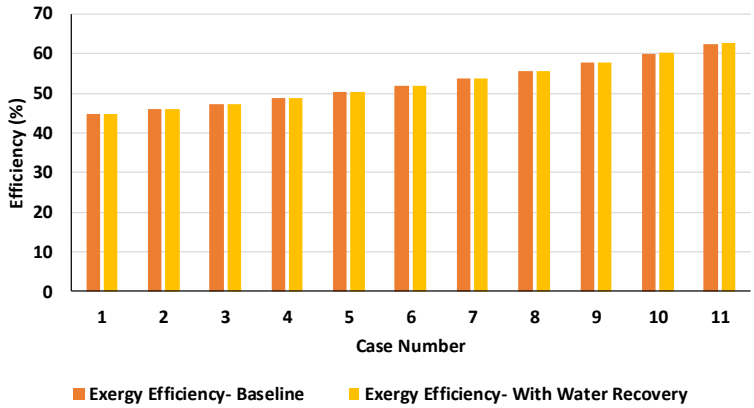

Figure 58- Effect of water recovery on total exergy efficiency of the system

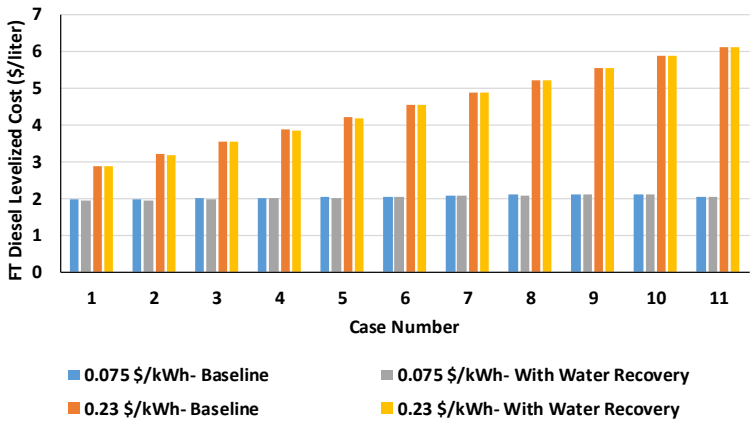

Figure 59- Effect of water recovery on the levelized cost of FT diesel

6.4 Concluding Remarks

The effect of EG and SOEC subsystem sizes on the integrated system performance was investigated in this Chapter. Eleven different combinations of the integrated system, based on the share of SOEC

subsystem in the precursor syngas production, were studied from thermoeconomic and environmental perspective. Results showed that in general higher share of co-electrolysis process results in the higher FT diesel levelized cost, GHG emission savings, as well as energy and exergy efficiency of the integrated system. However, continuous production of FT diesel may be proven to be impossible when system relies solely on the renewable electricity. It also was shown that equal precursor syngas production capacity of EG and SOEC subsystem would be a good compromise among the thermodynamic, economy, and environmental criteria.

Recovering produced MP steam, due to its positive effects, was shown to be the viable option and highly recommended. Amongst different possible internal mass recovery, oxygen and hydrogen recovery were the best and worst options, respectively. Although internal carbon dioxide and water recovery did not show any significant effect on the system performance, they may be proved beneficial owing to the reduction of the integrated system dependency on the external sources. Internal water recovery specifically would be advantageous if the integrated system is planned to be constructed and operated in dry regions where access to water is hard or not practical. Additionally, although combustion of produced FT gaseous hydrocarbons to provide the required heat source is not favorable from thermoeconomic perspective, it also will decrease system dependency on the external fuel sources.

7 Case Study*

So far steady state operation of subsystems was considered in the previous Chapters. However this may not be the most realistic approach especially in the case of the SOEC subsystem: renewable electricity will not be available all year around, leading to reduced capacity factors. This Chapter is dedicated to a case study and analysis of the proposed integrated system in specific regions under annual operating conditions.

7.1 Integrated System

The final configuration of the integrated system based on the findings of previous Chapter is illustrated in Figure 60. The SOEC subsystem operates only when excess electricity from renewables (solar and wind) is available, while the EG subsystem has continuous operation. Like before, FT diesel is considered to be the main product of the integrated system and other hydrocarbons such as naphtha and wax are the byproducts. Based on the findings in Chapter 6, FT gaseous hydrocarbons, water, oxygen, and carbon dioxide for internal use are recovered.

The first priority of the integrated system is to guarantee to meet the electrical demand of the city at any given point. Therefore, all or a fraction of FT diesel would be used in gas turbines to cover electricity shortage and the remainder (if any) is sent to meet the road transportation demands. Strictly speaking, the gas turbine is only in operation when the renewable electricity cannot meet the electricity demand of the users; i.e., SOEC subsystem is not in operation. Hence, the city electrical demand is met by the renewable electricity and is CO_2 free.

* The following Chapter is based on the findings that are presented in the fifth paper

The proposed integrated system in Figure 60 is modeled using both ASPEN Plus and Matlab software [52,114]. Renewable potentials (biomass, solar, wind) as well as electricity demand of the given locations first are estimated using Matlab. Size of subsystems then are selected based on these values. Based on the selected nominal size, operation of each subsystem is simulated using the developed models in ASPEN Plus. Finally, results from ASPEN Plus models are transferred back to Matlab in order to estimate the annual production potential of FT diesel in the given locations.

As explained in Chapter 6, SOEC and EG subsystems operate at atmospheric pressure and produce syngas with hydrogen to carbon monoxide ratio of 2.1. Operating temperature of these subsystems are 800 and 1200 ^{o}C, respectively. FT reactor, on the other hand, operates at 240 ^{o}C and 25 bar.

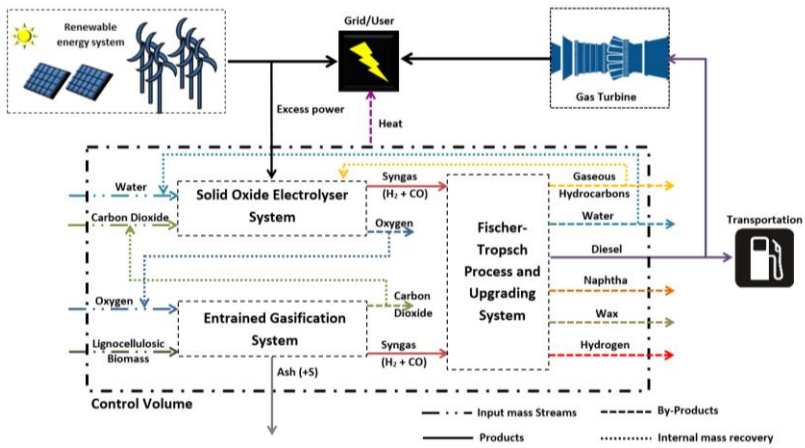

Figure 60- Integrated system schematic

7.2 Selected Locations

Theoretical feasibility of the proposed system is put into test in four different European locations, namely: Umeå, Stockholm, Turin, and Rome (Table 24). The selected cities represent a range of population size and geographic location, so renewables availability along with electricity, heat, and diesel demands vary. All locations are selected to ensure DH network accessibility.

Table 24- Name and specifics of the selected locations

City	Umeå	Stockholm	Turin	Rome
Region	Northern Sweden	Eastern Sweden	North-western Italy	Central Italy
Latitude	63°49′30″N	59°19′46″N	45°04′N	41°54′N
Longitude	20°15′50″E	18°4′7″E	07°42′E	12°30′E
Area (km^2)	2,317	6,519	1,127	5,352
Population	120,771	2,226,795	1,700,000	4,353,775

7.2.1 Electricity Supply and Demand

Hourly electricity demand (based on the bidding area) and production (based on the country profile) of each location in 2016 are estimated, as shown in Figure 61 A-D [102,115,116]. Considerable part of electricity demand in Sweden is met by nuclear electricity while electricity from fossil fuels is widely used in the Italian electricity market. In this study, it is assumed that the nuclear and fossil fuel share of electricity in the Italian and Swedish market is completely replaced by Solar PV and wind electricity.

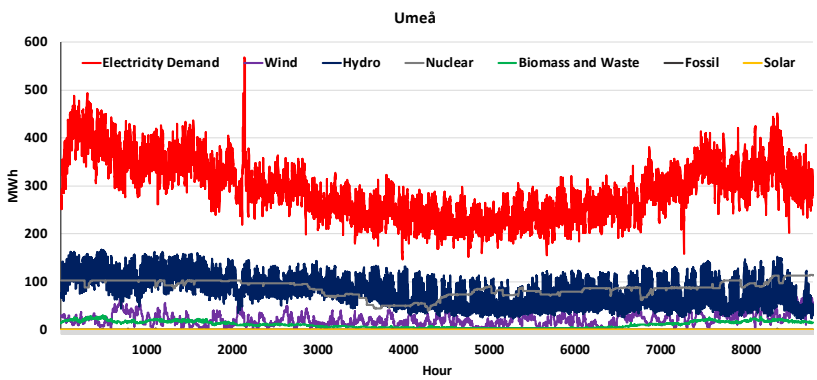

(A)

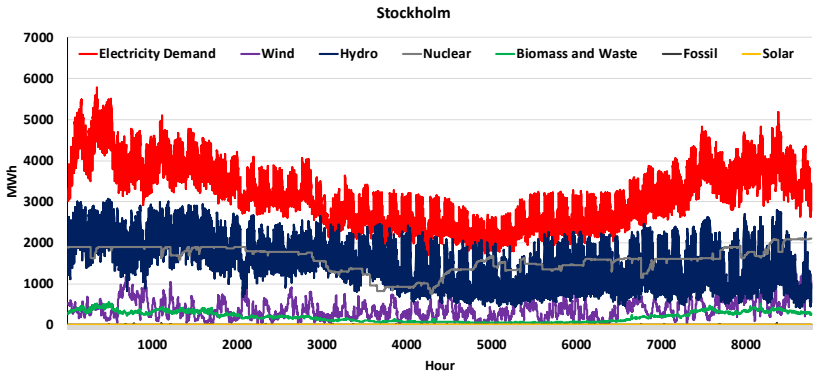
Stockholm
Electricity Demand
Wind
Hydro
Nuclear
Biomass and Waste
Fossil
Solar
MWh
Hour

(B)

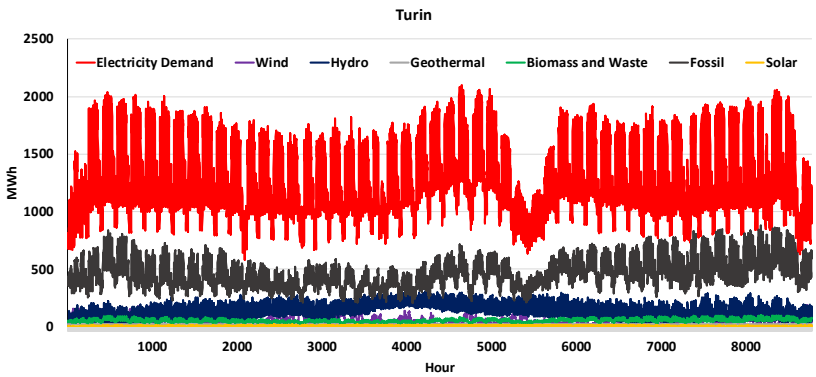
Turin
Electricity Demand
Wind
Hydro
Geothermal
Biomass and Waste
Fossil
Solar
MWh
Hour

(C)

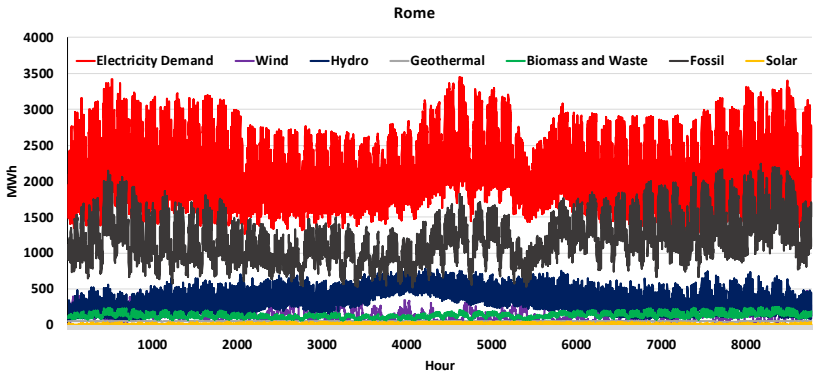

(D)

Figure 61- Electricity supply and demand of A) Umeå, B) Stockholm, C)Turin, D) Rome

7.2.2 Biomass Potential

Since each city is located in different region, base-potential of woody biomass is different.

Table 25 presents the sustainable technical potential of lignocellulose biomass, which is commercially viable to use for energy, for each region [115]. The share of selected cities from presented region base-potential is estimated in accordance with that city area.

Table 25- Base potential of biomass in each region (t/km^2) [115]

Country	**Sweden**				**Italy**			
Region	North		East		North-West		Center	
year	2012	2020	2012	2020	2012	2020	2012	2020
Final felling from non-conifer trees	5.1	5.8	10.8	12.8	45.07	42.6	44.9	44.4
Final felling from conifer trees	45.5	45.5	60.4	60.9	1.71	1.7	0.6	0.6
Thinning from non-conifer trees	4.4	4.4	10.8	10.5	6.32	6.0	6.3	6.0
Thinning from conifer trees	28.3	29.1	38.2	39.6	5.64	5.3	2.1	2.1
Total	83.3	84.8	120.1	123.8	58.75	55.7	53.8	53.0
Average	84.1		122.0		57.2		53.4	

7.3 Electrical Balance

As mentioned in section 7.2.1, nuclear and fossil fuel electricity share in the electricity market is assumed to be replaced by solar PV and wind. The viable size of each renewable power plant then is selected to fill the generated gap between the remaining electricity supply and cities demands presented in Figure 61 A-D. The hourly PV and wind electrical power production potentials are estimated based on their selected nominal size and according to the presented procedure in Chapter 3 and are included in the total electricity supply potential. Figure 62A-D presents electricity balance of each city where excess and shortage of electricity are presented by the positive and negative values, respectively. The SOEC subsystem is in operation when electricity balance has a positive value. In other words, annual syngas production potential from co-electrolysis process in each city is determined based on the excess electricity. As mentioned before, negative balance is covered using generated electricity in the gas turbines. Considering the electrical balance of the selected locations, continuous operation of SOEC subsystem is impossible.

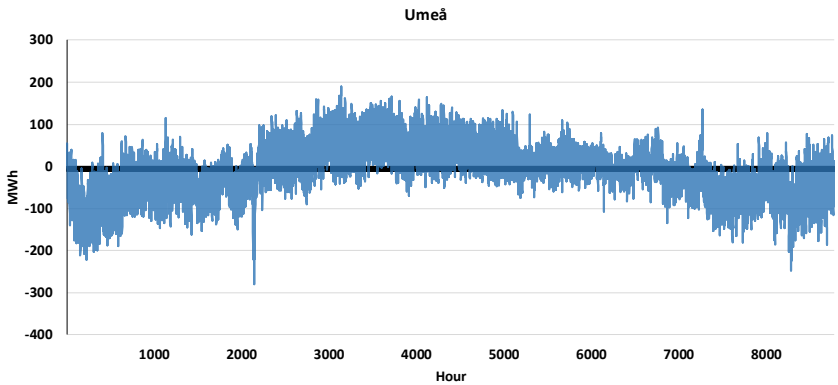

(A)

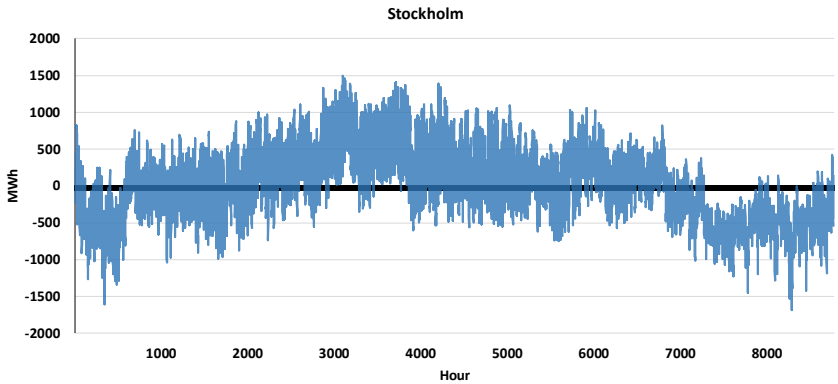
Stockholm
2000
1500
1000
500
0
-500
-1000
-1500
-2000
MWh
1000
2000
3000
4000
5000
6000
7000
8000
Hour

(B)

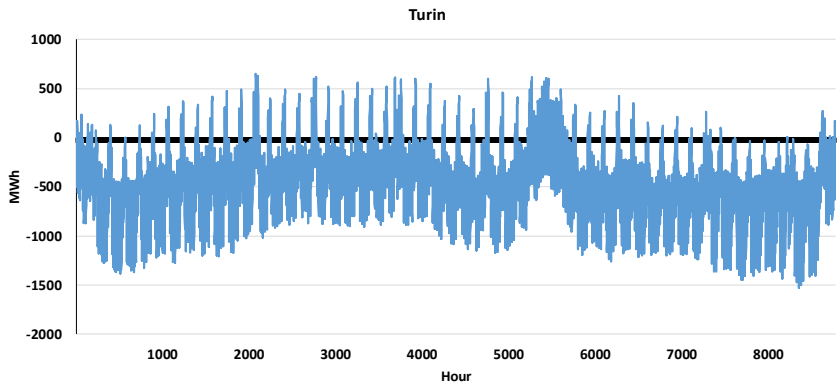
Turin
1000
500
0
-500
-1000
-1500
-2000
MWh
1000
2000
3000
4000
5000
6000
7000
8000
Hour

(C)

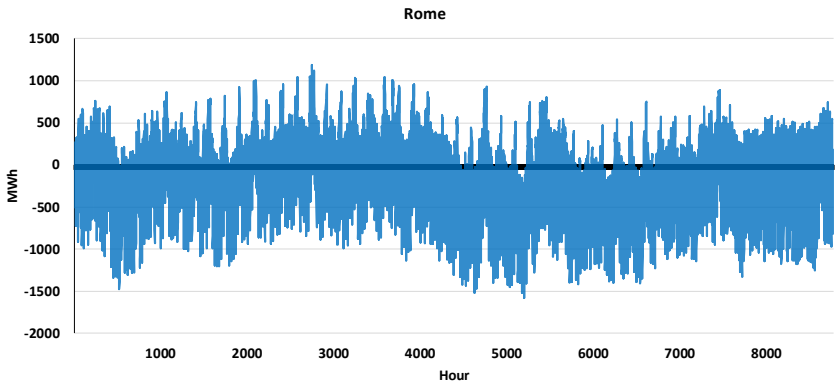

(D)

Figure 62- Electrical power production potential and consumption of A) Umeå, B) Stockholm, C) Turin, D) Rome

7.4 Diesel

FT diesel production potential and annual diesel demand of each location are listed in Table 26. The presented values of diesel demand are calculated in accordance with the reported road transportation demand of Italy and Sweden [117]. Sum of the SOEC and EG shares minus the amount of FT diesel that is used in the gas turbine (GTS) is presented as the annual diesel supply potential. In general, it seems that Stockholm and Turin have the highest and lowest potential for FT diesel production. The implemented system in Umeå has the highest possibility of meeting its diesel demand (32% of annual demand) owing to high base-potential of biomass in this region combined with a lower population. Comparing share of EG and SOEC subsystems in FT diesel production potential reveals that Rome is the city that can highly benefit from inclusion of the co-electrolysis process in the proposed integrated system (22% of total production). City ranks based on the SOEC subsystem share, from highest to lowest improvement in annual diesel production, are as Rome, Stockholm, Turin, Umeå. The same rank is valid to present the highest to the lowest possible GHG emission savings.

Table 26- FT diesel production potential and emission savings

City	Annual diesel demand , GWh	Annual diesel Supply, GWh				Percentage, (%)	Emission saving, (%)
		SOEC	EG	GTS	Total		
Umeå	553	12.2	165.6	0.2	177.6	32.1	98.0
Stockholm	10,202	104.0	665.7	1.4	768.3	7.5	99.6
Turin	6,969	9.9	54.7	3.4	61.2	0.9	100.2
Rome	17,848	69.0	241.4	1.9	308.5	1.7	102.0

Three different diesel levelized costs are estimated based on the availability of market to sell the byproducts. The first levelized cost, diesel cost 1, is estimated considering that no market is available to sell the byproducts. However, in the second cost estimation, diesel cost 2, it is assumed that there are suitable market for heat. This is a valid assumption since all of the selected cities have an existing DH network. Diesel cost 3 is estimated considering that FT diesel and every other byproducts are sold to the market. These estimated levelized costs are illustrated in Figure 63 for both fully integrated system as well as a system variant that excludes the EG subsystem. As can be seen, FT diesel production costs are higher in the former, emphasizing the importance of the EG subsystem from economical perspective. Nevertheless, FT diesel levelized cost in the case of Turin is the highest owing to its lowest base potential of biomass while Stockholm has the lowest levelized costs. Considering historical conventional diesel price (1.30-1.94 $/liter for Italy and 1.24-1.96 $/liter for Sweden), none of the cases presented here are competitive. Stockholm is the only city that shows a promise providing that all the byproducts are sold to the market.

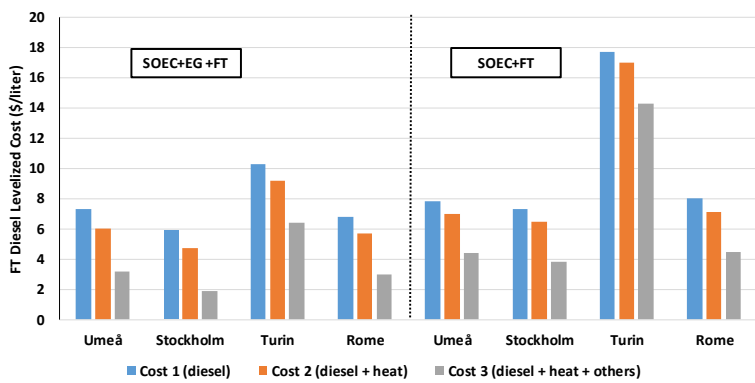

Figure 63- FT diesel production cost ($/liter)

7.5 Heat

Annual heat demand as well as the amount of heat that is provided by DH to the residential and service sector in Italy and Sweden are given in Table 27. Total space heating demand along with heating degree days (Appendix VI- Heating degree days) are used to estimate the monthly heat demand of each city. However, Italy has specific regulations regarding space heating via DH network. In accordance with country's objective on rational energy use and energy savings, Italy is divided in 6 climate subzones based on their typical heating degree days [118]. According to these regulations space heating in the selected cities should be as the following [118,119],

- Rome is located in zone D with maximum of 12 hr space heating per day between November 1st to April 15th

- Turin is located in zone E with maximum of 14 hr space heating per day between October 15th to April 15th

To take these regulations into account, heating degree days in Rome and Turin are set to zero for the months with no permission to have space heating. Monthly water heating demand, however, is estimated to be constant during each hour of the year, which is a usual approach in estimating the total heat demand of cities [119]. Total heat demand in a given month then is estimated as sum of both space heating and water heating demand. DH losses also should be taken into account since it is assumed that the heat demand will be covered from available DH network in the city. Network losses normally are accounted for over an operation year and added to the total heat demand. These losses are normally in the range of 14-16% of the base load and can be estimated from annual energy balances of the country. However, in case of unavailability of such information 15% would be a good assumption [119]. This value is used in this study as well.

Table 27- Heat demand and provided heat by district heating network [120]

Sector	Load	Demand (PJ)		District heating (PJ)	
		Italy	Sweden	Italy	Sweden
Residential	Space Heating	661.5	163.7	1.84	0.21
	Water Heating	101.8	62.4	91.77	17.31
Service	Space Heating	250.30	77.6	2.03	53.1
	Water Heating	66.0	22.7	0	0

Annual total heat demand of each city as well as heat production potential is presented in Table 28. Figure 64 A-D also illustrates amount of produced heat in the integrated system as percentage of total heat demand and DH network capacity. DH network capacity is estimated based on the difference between reported values of heat demand and provided heat from DH for Sweden (Table 27). However, the same approach would not give a realistic estimation for Italy since few cities in the country has access to DH while more than 50% of population in Rome and Turin has access to DH. In other words, the difference between country heat demand and provided heat from DH cannot paint a correct picture for these cities. Hence, DH network capacity for these cities are estimated based on the available rough data on the percentage of city residents that have access to DH [121]. Nevertheless, as can be seen from Figure 64 A-D, the amount of produced heat in each month is minuscule and almost negligible compared to either total heat demand or DH capacity and consequently may be accommodated easily into the existing DH network. Although no space heating is considered between mid-April to November for Rome and mid-April to mid-October for Turin, water heating demand is still much higher than the produced heat during these months. Since annual water heating demand is assumed to be scattered over the year equally, heat demand would be the same for these months. Hence, the visible drop in month July is only due to the increase in SOEC

operation which requires larger share of produced heat to be used internally as an example in the steam generator (Figure 5- section 2.1.3)

Table 28- Annual heat demand and production (TW)

City	Umeå	Stockholm	Turin	Rome
Annual heat demand	9981	184023	73387	187947
Annual available heat	0.65	2.9	0.23	1.14

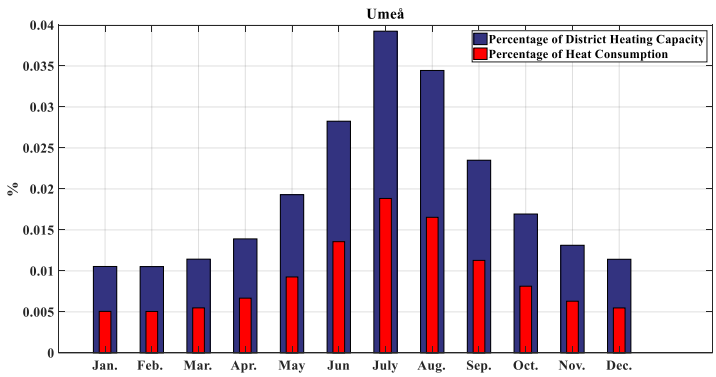

(A)

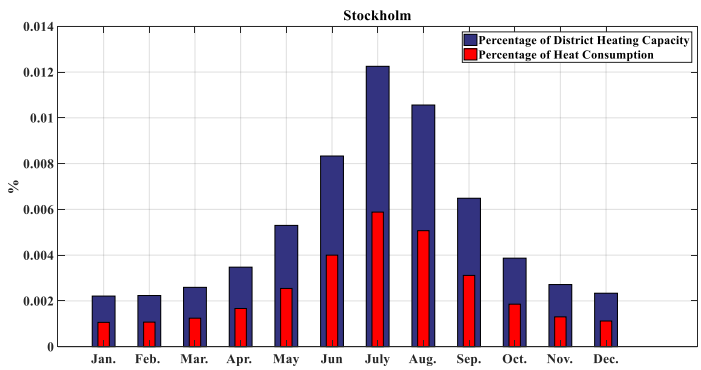

(B)

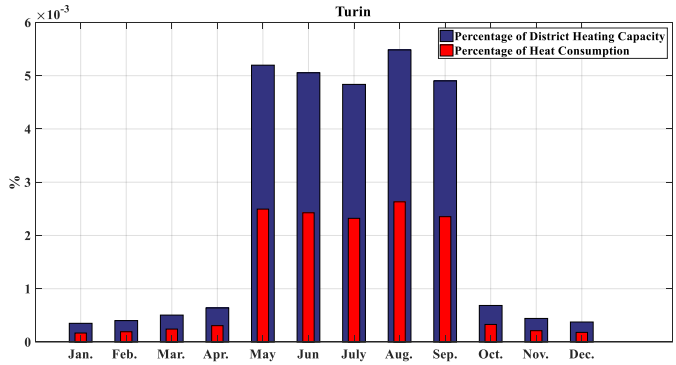

(C)

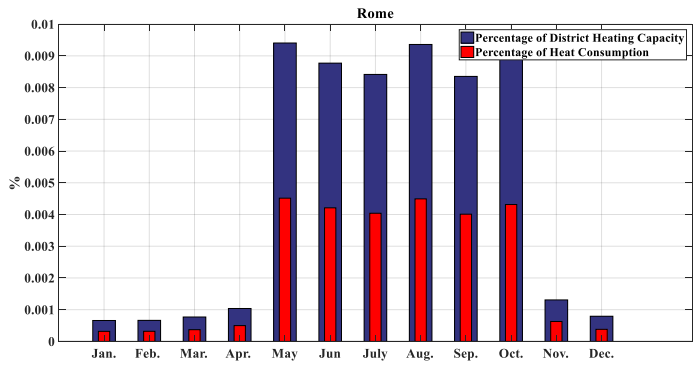

(D)

Figure 64- Heat production as percentage of total heat consumption and DH capacity

7.6 Mass Balance

Annual production and consumption rates of each internally recovered mass stream is shown in Figure 65A-D.

- *Oxygen:* Comparing annual oxygen consumption and production rates reveals that internal recovery cannot meet the internal demand and therefore the ASU unit should be included in the EG subsystem. However, by including the

internal recovery, the ASU unit size can be offset to a certain degree.

- *Carbon dioxide:* In all of the presented cases, there is no requirement to purchase carbon dioxide from external sources. In other words, CO_2 production rate during gasification and WGS reactions is greater than its consumption in the co-electrolysis process (Figure 65B).

- *Water:* Presented results in Figure 65C show that in case of Umeå, Stockholm, and Turin the produced water surpasses its consumption rate. Hence, neither of the presented cases, with the exception of Rome, depends on the external water source.

- *LGHC:* Like carbon dioxide, production of LGHC exceeds its consumption rate and consequently the integrated system is independent of external fuel sources (Figure 65D). The remainder of LGHC can be sold to the market as a system byproduct.

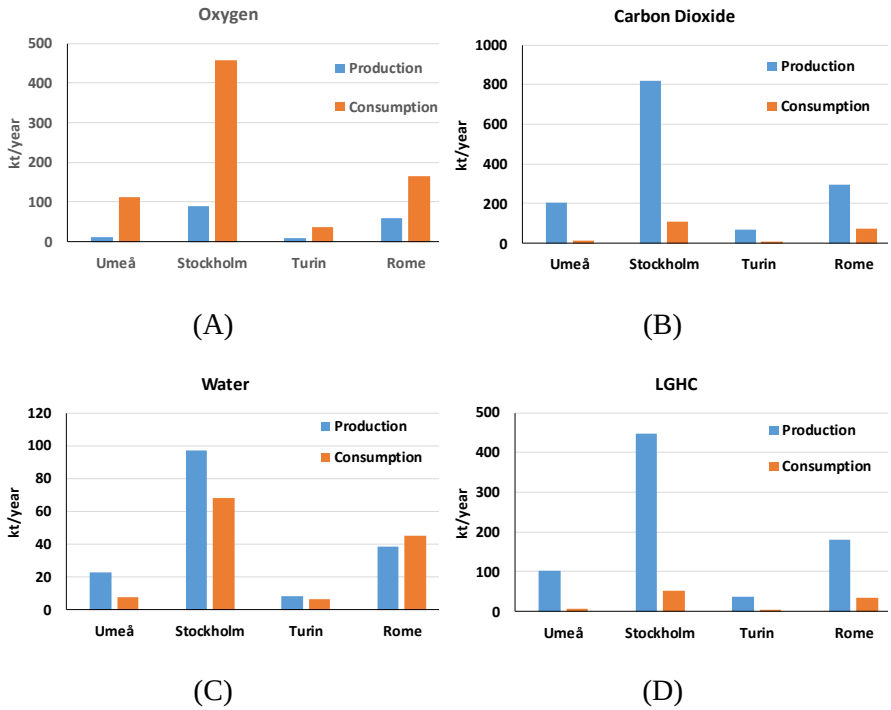

Figure 65- comparison between production and consumption of A) oxygen, B) carbon dioxide, C) water, and D) LGHC in the integrated system

7.7 Concluding Remarks

The feasibility of the proposed integrated system has been put in to the test. The performance of the final configuration of the integrated system, based on the findings of previous Chapters, in four European cities was investigated.

It was shown that based on the installation location, up to 32% of the diesel demand with the GHG emission savings as high as 102% can be met by including the proposed system in the existing energy system. Moreover, the electricity demand of each city was completely covered from renewable sources. Additionally, the recovered heat from the

integrated system was about 0.23 to 2.9 TW based on the installation location, although this amount is minuscule comparing to the total heat demand of these cities. Nevertheless, FT diesel production cost cannot compete with its conventional counterpart, even if all of the byproducts were sold to the market. Results also showed that carbon dioxide and LGHC internal recovery are sufficient to maintain system operation. Although providing external source of water was vital in case of Rome, no external water sources would be required for Umeå, Stockholm, and Turin cases. At last but not least, it was concluded that including the ASU unit in the EG subsystem was inevitable.

8 Policy

In the previous Chapter, potential integration of proposed system to energy system of four European cities were investigated. Although it showed great potential from environmental perspective, diesel production cost was not competitive with conventional diesel. Therefore, proper implementation of this system requires either taking advantage of existing support mechanisms or introduction of better support policies. Many countries initiated research plans, national targets and policy scheme to replace conventional fossil based hydrocarbons with CO_2-neutral bio-based or synthetic transportation fuels. Policy schemes defined to support integration of biofuels in the national energy matrix are usually driven by the possibility of oil price volatility reduction, increase of energy security, sustaining and/or improvement of the agriculture and forestry sector, and decarbonization of transportation sector [122]. The European Union first introduced a blending target of 5.75% renewable share in form of biofuels into the transportation sector by 2010. However, this target is later revised and changed in 2009 to 10% by 2020. In January 2014, EU published another communication report and stated that the biofuels produced from food based feedstock will not receive support after 2020, and consequently emphasizing more on advanced biofuels [123].

This Chapter is dedicated to investigate the policies that are currently in place in Italy and Sweden which are useful to promote and support implementing the proposed integrated systems. These countries are selected since the case study was performed on two cities of each one of them.

8.1 General Overview

Figure 66 shows the fossil based transportation fuels and liquid biofuels consumption in Italy (Figure 66A) and Sweden (Figure 66B). As can be seen, although diesel consumption in road transportation increased in past decade, total consumption of conventional fuels is slightly decreasing since 2007 owing to decrease of share of gasoline consumption. Nonetheless, these trends are more prominent in case of Italy than Sweden. Comparing reported annual production of liquid biofuels in each country reveals that Italy has larger capacity of liquid biofuels production than Sweden, 1065.6 versus 788.3 tonne of oil equivalent (TOE), although Sweden initiated including liquid biofuels in its transportation system earlier in 2001. Nevertheless, comparison between the reported numbers of total final energy consumption of fossil based fuel and liquid biofuels reveals that by 2014 Sweden was able to cover 12% of its total energy requirement for road transportation. On the other hand, for the same year Italy could only cover for 3.5% of its total fuel consumption which is much smaller percentage than Sweden. Therefore, although Italy has the capability to produce higher amount of liquid biofuels in general, its production rate per capita is less than Sweden.

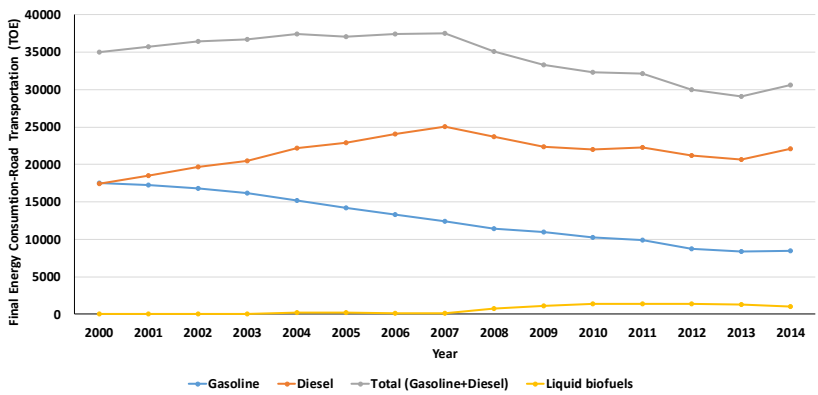

(A)

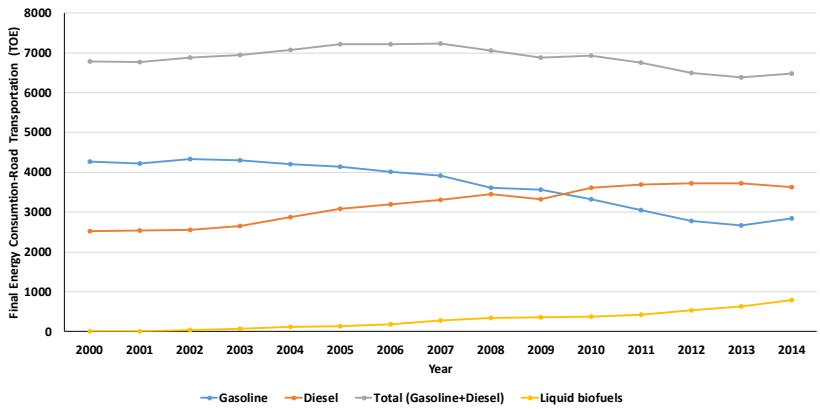

(B)

Figure 66- Final energy consumption of fossil based fuels and liquid biofuels for road transportation A) Italy, B)Sweden [117]

8.2 Current Policy

8.2.1 Italy

Annual production trend of liquid biofuels and biodiesel is shown in Figure 67. Italy started its liquid biofuel production plan by producing of 290 thousand tonne biodiesel in 2004. Since that time Italy has seen an increase in total production capacity. In 2008, production of biogasoline was initiated and therefore this capacity was also included in total liquid biofuel production. By 2013 biodiesel production contributed to about 87% of total national liquid biofuel production. Biodiesel is mainly produced from rapeseed oil which is imported from other EU countries. Soybean oil and palm oil also is used in production of biodiesel however to lesser extent [123,124]. In the 2011 decree, Italy set obligatory limits of 4%, 4.5%, and 5% of biofuels in the vehicle fuel mixture for 2011, 2012, and 2014, respectively [125]. From 2018, Italy mandates that gasoline and diesel should at least contain 1.2% of advanced biofuels. This requirement will increase to 2% by 2022. Hence, Italy is the first country in Europe that introduce legally binding requirements in support of advanced biofuels [123].

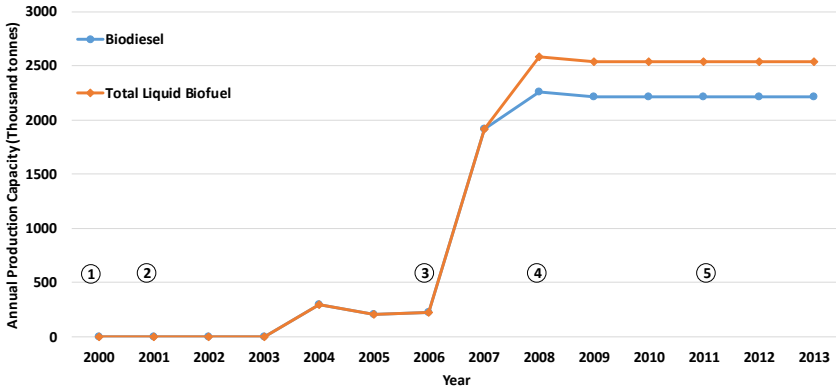

Figure 67- Italy annual production capacity of liquid biofuels and biodiesel [117]

According to IRENA policy database, Italy defined and introduced five different national policies to support integration of biofuels into its transportation system since 2000. Numbered circles in Figure 67 represents these policies and their initiating timeline [126]. The first ever defined policy specifically to support biofuels was presented in 2000. Table 29 lists these policy names and types. Although all of them can be used to promote the proposed integrated system, the last two are the most relevant since they set an obligatory limit for advanced biofuels and relevant GHG savings that they should have.

Table 29- Italian Policy scheme in support of biofuels for transportation [126]

No.	Title	Year	Policy Type
1	National plan for biofuels and biomass	2000	Policy Support > Strategic Planning
2	Biofuels tax exemption	2001	Economic Instruments > Fiscal/financial incentives >Tax relief
3	GHG emission trading	2006	Policy Support, Economic Instruments > Market-based instruments > GHG emission trading
4	Biofuels aid scheme	2008	Regulatory Instruments > Obligation schemes
5	National system of sustainability certification for biofuels	2011	Regulatory Instruments > Codes and standards

Italy has introduced a fairly new policy in 2015 on energy storage that may be used to gain support for implementation of this system. As explained in previous Chapters, the proposed integrated system can be considered as an energy storage facility for renewables. Therefore, it may lay in the category that is supported by this policy. This support mechanism includes technical specifications to integrate storage systems and defines a specific algorithm to calculate the electricity that is provided and fed to the grid from storage facilities.

8.2.2 Sweden

Figure 68 presents annual trend of liquid biofuel and biodiesel production capacity in Sweden between 2000 and 2014. As can be seen here, like Italy, the Swedish annual production capacity of liquid biofuels rapidly increased. In contrary to Italy, however, the total production capacity is much smaller. Moreover, biodiesel production contributes to only 46% of total produced liquid biofuels in 2013. Final target of Sweden is to have fossil free independent car fleet by 2030. Also, they plan to have net zero GHG emissions by half of the century which made Swedish strategy the most ambitious one between European countries

[127]. Their strategy mainly is based on general economical instrument such as setting a penalty for GHG emissions and favoring the cars with low environmental impacts.

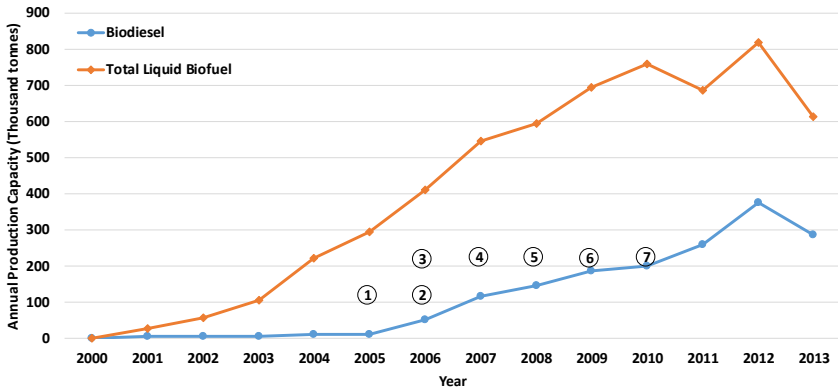

Figure 68- Sweden annual production capacity of liquid biofuels and biodiesel [117]

The numbered circles in Figure 68 represent each implemented support policy. Unlike Italy, Sweden introduced its first policy in support of biofuels later in 2005. However, from 2005 till 2010 almost one new policy in regards with biofuels were introduce each year [128]. Table 30 present the policies that can be useful in order to promote implementation of the aforementioned integrated system in Sweden.

Table 30- Swedish policy schemes in support of biofuels for transportation [128]

No.	Title	Year	Policy Type
1	Government vehicle procurement directives	2005	Regulatory Instrument > Obligation schemes Regulatory Instrument > Other mandatory requirements
2	Vehicle tax exemption for green cars	2006	Economic Instruments > Fiscal/financial incentives >Tax relief Economic Instruments > Fiscal/financial incentives >Tax
3	Requirement to supply renewable motor fuel	2006	Regulatory Instrument > Other mandatory requirements Regulatory Instrument
4	ECO car subsidy	2007	Economic Instruments > Fiscal/financial incentives > Grant and Subsidies
5	Vehicle conversion to alternative fuels	2008	Economic Instruments > Fiscal/financial incentives >Tax relief Regulatory Instruments > Monitoring Policy Support
6	A vehicle fleet independent of fossil fuel by 2030	2009	Policy Support > Strategic planning
7	Implementation of the sustainability criteria of the renewables directive	2010	Regulatory Instruments, Policy Support

8.3 Recommendations

As explained in previous sections, many support policies are already in place in both countries. However, almost all of these policies are designed and developed from consumption point of view. Considering that most of advance biofuel production technologies are not readily

available for the market, lack of enough support for R&D and biofuels production may prohibit the desirable transitions in transportation system. The following are key recommendations that can facilitate development of advanced biofuels such as production of FT diesel through the proposed integrated system:

- *Addressing data challenges for installed and planned projects*: the first step in developments of advanced biofuels is to have enough global accurate data of the installed projects which enables recognizing the short comings of each specific technology. Also data platform including system specific information, cost and performance can be used as base for the comparison between different technologies to find the best fit for the given climate and available biomass feedstock.
- *Removing obstacles from current regulations:* the minimum improvement that should be done in the regulations is to remove obstacles regarding market accessibility. In other word, facilitating market accessibility in each stage of the biofuel energy value chain, from production of biomass to consumption of biofuels, is one of the basic steps in order to increase their share in the transportation sector. This can be done for example through tariff structures and strategic planning. Moreover, governments should clarify the opportunities, limitations and conditions that the actors in each step of biofuel energy value chain will face.
- *Reducing fossil fuel support*: one obstacle in front of advanced biofuels integration into energy system is their high cost compared to fossil fuels. Governments may be able to increase share of biofuels in their energy system if they reduce the subsidies that they provide for fossil fuels. For example, fossil fuel support in Italy was about 3631 million euro in 2014 of which 62% was for some type of land transportation using fossil fuels. These numbers for Sweden are about 1291 million euro and 64% [129]. So, it may be beneficial to redirect some of these allocated funds toward development and production of advanced biofuels. Such an approach should be considered with cautious to assure that it will not

interfere drastically with other national goals especially economic growth of country.

- *Introducing new regulations:* besides removing the obstacles and clarifying the existing energy regulations, new supporting laws should be created. As mentioned earlier in this section, no support mechanism for R&D, production of feedstock commodities, and intermediary suppliers yet introduced [130]. The most advanced biofuel production technologies are still immature and developing strategic clear support scheme for these sectors will greatly affect speed of transition to the environmental friendly transportation system. For example, introducing economic instruments such as providing grants for research and development of new pathways for production of environmental friendly transportation fuels may speed up the process. Moreover, governments can facilitate the transition from fossil based transportation system by introducing clear and well developed measuring instruments.
- *Providing support during initial phase:* like other stages in biofuel production chain, no defined support mechanisms for producers exist in Italy nor Sweden [130]. Providing financial support especially during the initial phase of advanced technology instalment results in reduction in the cost and consequently facilitate integration of such technologies in the energy market. Such financial incentives also may lead to attract more investment for construction of advanced biofuel plants. This is the same approach that helped development of renewable energy technologies like solar photovoltaic or wind. Investment tax credit, production and operation grants, soft loans, property tax reduction or exemption, and underpricing access to government lands are among many support mechanisms that may help growth of investment and installation of advanced biofuel production plants.

8.4 Concluding Remarks

The historical trend of biofuel production and defined support policies of Italy and Sweden were discussed in this section. Italy's annual biofuel

production rate can meet small percentage of its road transport fuel demand. In addition, the major part of biomass feedstock is imported from other European countries. Although biofuel production in the Italian transportation system is more sustainable, it definitely was not helpful toward gaining independency from energy imports. Moreover, the major part of produced biofuel is of the first generation biofuel, which its further development may be in conflict with food production industry. On the other hand, Sweden's biofuel production can meet about 12% of its road transportation demand. Although both countries introduced regulatory schemes and support policies, all of them are for the consumption side. Currently, no scheme or policy is in place to support other stages of advance biofuel production such as R&D, feedstock production, biofuel production, and intermediary suppliers. A few recommendations were suggested which may accelerate transition of transportation system towards CO_2-neutrality.

9 Conclusion

An integration between solid oxide electrolysis cells (SOEC), entrained gasification (EG), and Fischer-Tropsch (FT) technologies was proposed and investigated. The main purpose of this integration is to produce FT diesel that can replace conventional diesel in transportation. The other advantage of such integration is the role that it can play in integration of renewable electricity to the existing energy system. Providing that electricity for co-electrolysis is coming from renewables, the proposed integrated system then can be considered as energy storage. In this case, some part of produced FT diesel would be used to cover shortage of electricity. Since FT diesel is produced from renewables and recycled/reused carbon dioxide, it can be considered as renewable fuel and consequently electricity network would have high GHG emission savings.

It was shown that to achieve high performance and efficiency, it is better to produce syngas in atmospheric pressure and then compress it to the high pressures required by FT process. The reason is simply higher rates of methane that exists in the outlet streams of SOEC and EG subsystems at elevated operating pressures. In other words, lower amount of hydrogen and carbon monoxide mixtures would be produced for the same rate of steam, carbon dioxide, electricity, and biomass to the integrated system. Since methane does not participate in any of FT reactions, it is a neutral element in FT reactor. Hence a higher rate of methane supply, owing to elevated pressure, affects system performance dramatically. Although operating SOEC and EG subsystems at elevated pressure implies smaller or total elimination of syngas compressor before FT reactor, the effect of former on the system performance cannot be counterbalanced by lower electricity demands due to latter. Consequently, it is advised to operate these subsystems at atmospheric levels. Note that this conclusion is true only in cases that production of other hydrocarbons than methane is the main target of the system. If methane would be the desired final product, then operating at elevated pressures would affect system positively owing to the internal production of methane.

In addition, results showed that integrated system would have better performance in case of steam electrolysis than co-electrolysis. The difference between these cases is that EG subsystem in the former provides all the carbon content required for FT diesel production, while this requirement is divided between SOEC and EG in latter case. Therefore the co-electrolysis option has the benefit of increased potential of FT diesel production, and it provides an opportunity to achieve closed-loop operation via recycling carbon dioxide produced in the gasification process. Hence, to have the highest possible effect on transportation sector, this operation mode is strongly suggested regardless of its lower system performance.

In general, to have a good balance between the strength and shortcomings of SOEC and EG subsystems, a 50-50 share of syngas production in each subsystem is recommended. This sizing option also provides a reasonable compromise between operational, economical, and environmental perspectives. Nevertheless, sizing of integrated system should be done considering the specific requirements of a given application as well as priorities that set by the plant developer. Moreover, in practice, it would not be possible to operate SOEC subsystem at all time if the required electricity is produced from renewable sources. In general, two options can be suggested to optimize sizing of SOEC subsystem,

- FT diesel production: in this case the only concern would be production of high rates of FT diesel. SOEC subsystem then is designed to have continuous operation alongside EG. However, extra care should be given to take to account the emission associated with provided electricity so that final production of FT diesel would not have higher emission rate than their conventional counterpart.

- FT diesel production and energy storage: in this case the co-electrolysis process can occur when excess electricity from renewables available. Therefore, selecting size of SOEC is limited by the maximum available excess renewable electricity. Unlike previous option, it would not be possible to have continuous co-electrolysis process. Strictly speaking, SOEC would operate at its nominal level only during some parts of operational year while it would totally be shut down in others. Although the produced FT diesel would be enough

to cover electricity shortage, the remaining part would cover a minuscule percentage of transportation requirements. Moreover, SOEC would have higher rate of degradation when operates at on/off mode rather than continuous operation. One solution to increase duration that SOEC operates at its nominal level is to size renewable power plants to produce electricity in rates much higher than actual demand. In this case, amount of available electricity increases and consequently larger amount of FT diesel would be available. Nonetheless, increase of RES size would require through analysis of possibilities and limitations for a given location, e.g. addition installation cost and/or land availability, which is beyond the scope of this study.

The integrated system simulation results showed good promise of high performance and GHG emission savings. On the other hand, investment on its implementation cannot be justified from economic point of view since the produced diesel has a high production cost that is not currently competitive in most cases even by considering selling all other byproducts to the market. Development and implementation of this integrated system requires introduction of detailed and precise support policies by governments. Currently, considering Italy and Sweden as an example, no support policy for R&D, investment, or operation of sustainable fuel production plants are in place. However, both countries set strict targets for including sustainable fuels such as FT diesel in their energy system and have support mechanisms for consumers that may guarantee market availability. Taking investors and producers into account while developing new support schemes would have considerable positive effect on pushing the transportation system towards a more environmental friendly and sustainable one. Considering the renewable potential as well as current defined target and policy structure, it seems that implementation of proposed integrated system in Italy may be more attractive than in Sweden owing to,

- Higher potential of solar electricity production
- Lower national lignocellulosic biomass potential and consequently necessity to include other renewable sources in synthetic fuel production

- Higher rate of fossil fuel import
- Higher GHG emission rate in both road transportation (98.2 vs. 16.6 million tonne CO_{2eq}) and electricity network (71.8 compare to 6.8 million tonne CO_{2eq}) [131].
- More demanding and strict targets for including advanced biofuels in the road transportation system
- Benefit from overlap between current support mechanism (biofuel and energy storage)

Besides providing governmental support, another possibility to tackle the current issue of system economy is to choose another hydrocarbon as final product of the system from wide range of possible FT products rather than diesel. The main difference in the integrated system then would be configuration of upgrading subsystem. High temperature FT products may also be a better option than FT diesel from economic perspective. The short chain hydrocarbons produced during high temperature FT process can be used in chemical industry and therefore has the possibility to increase share of renewables in this sector.

10 Appendix I- Aspen Plus Flowsheets

Figure 69 to Figure 71 show the Aspen Plus flowsheet of each subsystem of the integrated system.

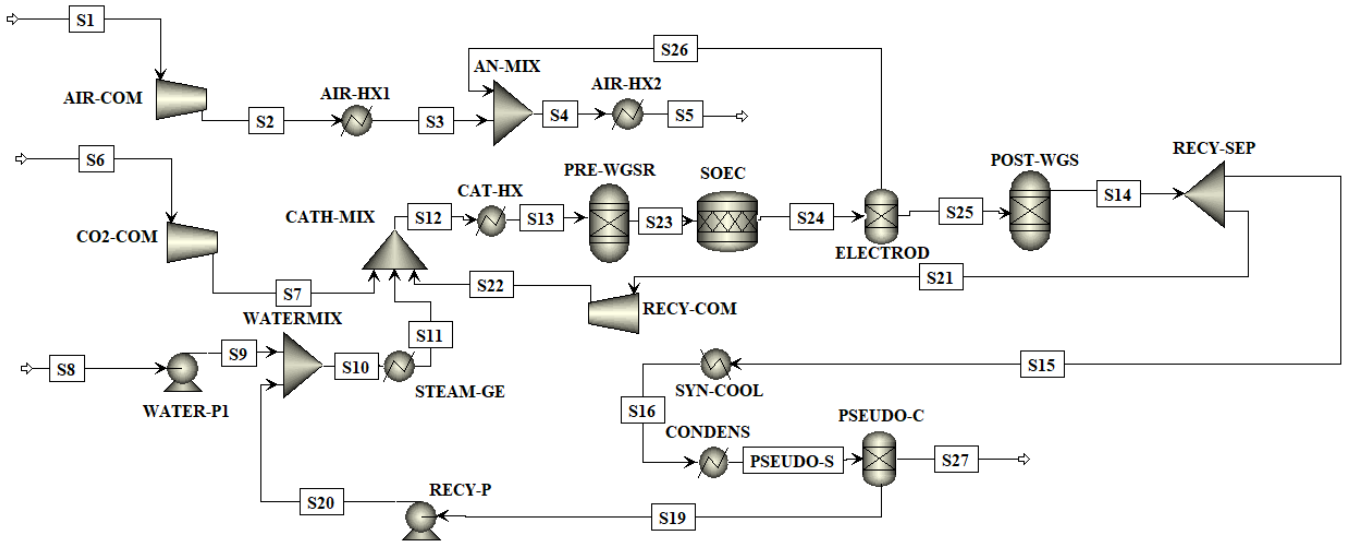

Figure 69- SOEC ASPEN flowsheet

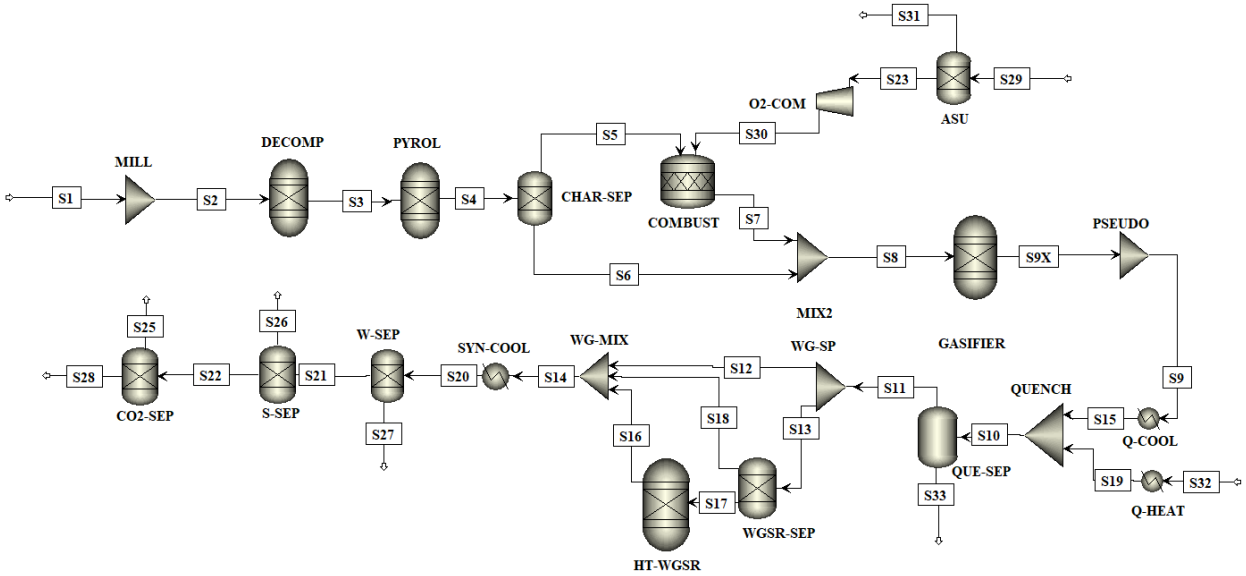

Figure 70-EG ASPEN Plus flowsheet

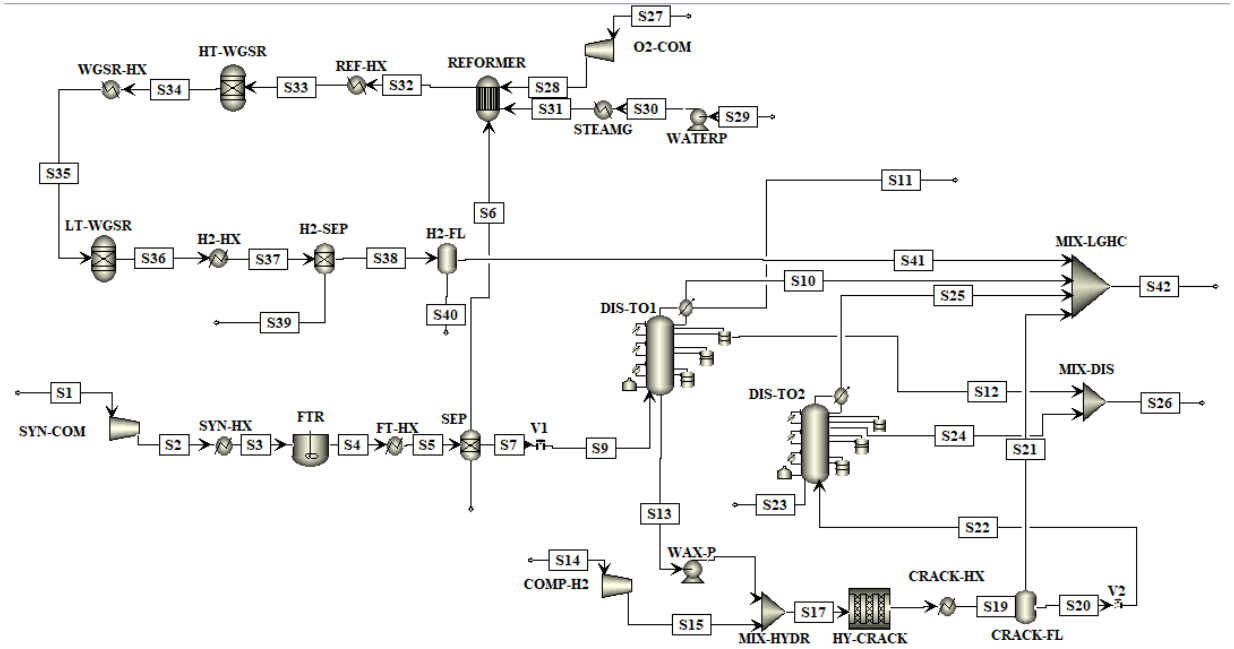

Figure 71- FT ASPEN Plus flowsheet

11 Appendix II- Fisher-Tropsch Components

Table 31- Fisher-Tropsch components

Carbon Atoms	Olefins	Paraffins	Alcohols	Aldehydes	Carboxylic Acid	Methyl - Alkanes
1	-	CH_4	CH_3OH	-	-	-
2	C_2H_4	C_2H_6	C_2H_5OH	CH_3CHO	CH_3COOH	-
3	C_3H_6	C_3H_8	C_3H_7OH	$CH_3(CH_2)CHO$	$CH_3(CH_2)COOH$	
4	C_4H_8	C_4H_{10}	C_4H_9OH	$CH_3(CH_2)_2CHO$	$CH_3(CH_2)_2COOH$	C_4H_{10}
5	C_5H_{10}	C_5H_{12}	$C_5H_{11}OH$	$CH_3(CH_2)_3CHO$	$CH_3(CH_2)_3COOH$	C_5H_{12}
6	C_6H_{12}	C_6H_{14}				C_6H_{14}
7	C_7H_{14}	C_7H_{16}				C_7H_{16}
8	C_8H_{16}	C_8H_{18}				C_8H_{18}
9	C_9H_{18}	C_9H_{20}				C_9H_{20}
10	$C_{10}H_{20}$	$C_{10}H_{22}$				$C_{10}H_{22}$
11	$C_{11}H_{22}$	$C_{11}H_{24}$				$C_{11}H_{24}$
12	$C_{12}H_{24}$	$C_{12}H_{26}$				$C_{12}H_{26}$
13	$C_{13}H_{26}$	$C_{13}H_{28}$				$C_{13}H_{28}$
14	$C_{14}H_{28}$	$C_{14}H_{30}$				$C_{14}H_{30}$
15	$C_{15}H_{30}$	$C_{15}H_{32}$				$C_{15}H_{32}$

Carbon Atoms	Olefins	Paraffins	Alcohols	Aldehydes	Carboxylic Acid	Methyl-Alkanes
16	$C_{16}H_{32}$	$C_{16}H_{34}$				$C_{16}H_{34}$
17	$C_{17}H_{34}$	$C_{17}H_{36}$				$C_{17}H_{36}$
18	$C_{18}H_{36}$	$C_{18}H_{38}$				$C_{18}H_{38}$
19	$C_{19}H_{38}$	$C_{19}H_{40}$				$C_{19}H_{40}$
20	$C_{20}H_{40}$	$C_{20}H_{42}$				$C_{20}H_{42}$
21	$C_{21}H_{42}$	$C_{21}H_{44}$				$C_{21}H_{44}$
22	$C_{22}H_{44}$	$C_{22}H_{46}$				$C_{22}H_{46}$
23	$C_{23}H_{46}$	$C_{23}H_{48}$				$C_{23}H_{48}$
24	$C_{24}H_{48}$	$C_{24}H_{50}$				$C_{24}H_{50}$
25	$C_{25}H_{50}$	$C_{25}H_{52}$				$C_{25}H_{52}$
26	$C_{26}H_{52}$	$C_{26}H_{54}$				$C_{26}H_{54}$
27	$C_{27}H_{54}$	$C_{27}H_{56}$				$C_{27}H_{56}$
28	$C_{28}H_{56}$	$C_{28}H_{58}$				$C_{28}H_{58}$
29	$C_{29}H_{58}$	$C_{29}H_{60}$				$C_{29}H_{60}$
30	$C_{30}H_{60}$	$C_{30}H_{62}$				$C_{30}H_{62}$
30+	**C_{30+}**	**pseudo-component WAX**				

12 Appendix III- FT Synthesis Kinetic Model

Among the possible kinetic mechanisms for the FT synthesis, the carbide mechanism is widely used in kinetic modeling. Its main feature is based on formation of hydrocarbons by successive addition of a building unit with one carbon atom and no oxygen into the growing chain [111]. This reaction pathway is defined by the series of elementary reaction steps shown in Table 32. This reaction pathway is coupled with the chain-length-dependent olefin desorption concept. Thus, the obtained kinetic model allows simultaneous evaluation of both reactant conversion and product distribution.

Following the methodology explained by Todic [76] and Selvatico [132], Langmuir-Hinshelwood-Hougen-Watson (LHHW) mechanism model approach was used to relate the hydrocarbons formation rates with the partial pressures of reactant species and rate and equilibrium constants of elementary reactions. LHHW represents a simplified model, according to which the surface of the catalyst is described as a continuum array of equivalent sites with the assumption of interacting only in the chemisorption of the reactant species [133]. Integration of LHHW with hydrocarbon selectivity model based on a chain-length-dependent olefin desorption effect makes it possible to accurately predict product distribution compare to experimental observation possible.

Table 32- FT synthesis carbide mechanism reaction pathway [76]

Step	Type	Elementary reaction	Kinetic/Equilibrium constant
1	RDS	$CO + H\text{-}\sigma \rightarrow H\text{-}\sigma\text{-}CO$ $CO + CH_3\text{-}\sigma \rightarrow CH_3\text{-}\sigma\text{-}CO$ $CO + C_nH_{2n+1}\text{-}\sigma \rightarrow C_nH_{2n+1}\text{-}\sigma\text{-}CO$	k_1
2	EQS	$H\text{-}\sigma\text{-}CO + H_2 \leftrightarrow H\text{-}\sigma\text{-}C + H_2O$ $CH_3\text{-}\sigma\text{-}CO + H_2 \leftrightarrow CH_3\text{-}\sigma\text{-}C + H_2O$ $C_nH_{2n+1}\text{-}\sigma - CO + H_2 \leftrightarrow C_nH_{2n+1}\text{-}\sigma - C + H_2O$	K_2
3	EQS	$H\text{-}\sigma\text{-}C + H_2 \leftrightarrow H\text{-}\sigma\text{-}CH_2$ $CH_3\text{-}\sigma\text{-}C + H_2 \leftrightarrow CH_3\text{-}\sigma\text{-}CH_2$ $C_nH_{2n+1}\text{-}\sigma - C + H_2 \leftrightarrow C_nH_{2n+1}\text{-}\sigma - CH_2$	K_3
4	EQS	$C_nH_{2n+1}\text{-}\sigma - CH_2 \leftrightarrow C_nH_{2n+1}\ CH_2\text{-}\sigma$	K_4
5	RDS	$CH_3\text{-}\sigma + H_2 \rightarrow CH_4 + H\text{-}\sigma$ $C_nH_{2n+1}\text{-}\sigma + H_2 \rightarrow C_nH_{2n+2} + H\text{-}\sigma$	k_{5M} k_5
6	RDS	$C_2H5\text{-}\sigma \rightarrow C_2H_4 + H\text{-}\sigma$ $C_nH_{2n+1}\text{-}\sigma \rightarrow C_nH_{2n} + H\text{-}\sigma$	k_{6E} $k_{6,n}$
7	EQS	$H_2 + 2\sigma \leftrightarrow 2H\text{-}\sigma$	K_7

In this model three basic elementary reactions are considered, chain growth, chain desorption (forming olefins), and chain hydrogenation (forming paraffins). The main assumptions are

- Chain growth rate and chain hydrogenation to paraffin rate is independent from chain length
- Chain desorption to olefin is a function of carbon number

The linear increasing of strength of olefin adsorption to the catalyst surface with carbon number is usually explained by weak Van der Waal's interaction [134] as expressed as follows,

$$\Delta H_{ads,o}^{n} = a_0 + a_1 n \tag{39}$$

Where a_0 and a_1 are constants while $\Delta H_{ads,o}^{n}$ is the heat of adsorption of an olefin molecule with n carbon atoms.

According to Evans-Polanyi relation, it is possible to assume that the activation energy of desorption step is also linearly dependent on carbon numbers. For information regarding Evans-Polanyi relation refer to [135]. So, activation energy of desorption can be formulated as,

$$E_{d,o}^{n} = E_{d,o}^{0} + \Delta E\, n \tag{40}$$

where $E_{d,o}^{n}$ is activation energy of the desorption step of 1-olefin molecule with n carbon atoms, $E_{d,o}^{0}$is desorption energy independent of chain length, and ΔE is the reduction in desorption energy contribution per every CH_2 group. Applying this formulation of the activation energy in the Arrhenius equation, the 1-olefin desorption rate constant ($k_{d,n}$) can be expressed as,

$$k_{d,n} = A_d\, e^{-\frac{E_{d,o}^{n}}{RT}} = A_d\, e^{-\frac{E_{d,o}^{o}}{RT}} e^{-\frac{\Delta E\, n}{RT}} \tag{41}$$

Equation 41 can be explained more simply as equation 42 by defining constants as follows,

$$\begin{aligned} k_{d,n} &= k_{d,o}.e^{nc} \\ k_{d,o} &= A_d\, e^{-\frac{E_{d,o}^{o}}{RT}} \quad , \quad c = e^{-\frac{\Delta E\, n}{RT}} \end{aligned} \tag{42}$$

Hence, it is possible to set up the complete scheme to derive a rate equation for each hydrocarbon product of the FT.

Considering the carbide mechanism in the form of the stepwise pathways illustrated in Table 32, the assessment of rate equations follows the LHHW approach under these assumptions [76]:

- Elementary steps involved in CO monomer formation or in chain propagation for the formation of n-paraffins and 1-olefins are rate-determining steps (RDS)

- All other elementary steps are considered to be rapid enough to be quasi-equilibrated
- According to experimental data presented in literature, methane and ethene have different formation rate constants than other n-paraffin and 1-olefins
- Rate constants of chain propagation and hydrogenation to n-paraffin are independent of carbon number
- Rate constants of chain desorption to form 1-olefin is exponentially dependent on carbon number
- Total number of active sites on the catalyst surface is constant
- On the catalyst surface only one type of FT active site is present
- Concentrations at surface intermediates and vacant sites are at steady state.

Rates of formation of n-paraffin and 1-olefin with carbon number n then can be estimated using equation 43 and 44.

$$n \geq 2 \qquad R_{C_nH_{2n+2}} = k_5 \left[C_nH_{2n+1} - \sigma\right] P_{H_2} \tag{43}$$

$$n \geq 3 \qquad R_{C_nH_{2n}} = k_{6,n} \left[C_nH_{2n+1} - \sigma\right] P_{H_2} \tag{44}$$

where, $[C_nH_{2n+1}\text{-}\sigma]$ is the surface fraction of adsorbed specie, P_{H2} is the hydrogen partial pressure, k_5 is the kinetic constant of the n-paraffin formation, and $k_{6,n}$ is the kinetic constant of 1-olefin formation which is equal to $k_{6,0}\, e^{nc}$.

On the other hand, as mentioned before, methane and ethene are assumed to have different formation rate constants:

$$R_{CH_4} = k_{5M} \left[CH_3 - \sigma\right] P_{H_2} \tag{45}$$

$$R_{C_2H_4} = k_{6E} \left[C_2H_5 - \sigma\right] P_{H_2} \tag{46}$$

where, k_{5M} is kinetic constant of the methane formation and k_{6E} is the kinetic constant of ethene formation which is equal to $k_{6E,0}\, e^{2c}$.

The introduction of growth probability factor allows to relate the surface fractions of various growing chain intermediates $[C_nH_{2n+1}\text{-}\sigma]$ to

kinetic constants, partial pressures of carbon monoxide, hydrogen and water and fraction of vacant sites [σ].

The chain growth probability factor for a molecule having n carbon atoms (α_n) is defined by equation 47.

$$n \geq 3 \qquad a_n = \frac{\left[C_n H_{2n+1} - \sigma\right]}{\left[C_{n-1} H_{2n-1} - \sigma\right]} \tag{47}$$

The assumption that concentrations of surface intermediates and vacant sites are at steady state is applied for the fraction of [C_nH_{2n+1}-σ] surface intermediate:

$$n \geq 3 \qquad -\frac{dc_n}{dt} = -k_1 P_{CO} c_{n-1} + k_1 P_{CO} c_n + k_5 P_{H_2} c_n + k_{6,n} c_n = 0 \tag{48}$$

where, c_n is equal to [C_nH_{2n+1}-σ], c_{n-1} is [$C_{n-1}H_{2n-1}$-σ], k_1 is the kinetic constant of CO monomer formation, P_{CO} and P_{H2} is partial pressures of carbon monoxide and hydrogen, respectively. Combining equations 47 and 48 results in equation 49:

$$n \geq 3 \qquad a_n = \frac{\left[C_n H_{2n+1} - \sigma\right]}{\left[C_{n-1} H_{2n-1} - \sigma\right]} = \frac{k_1 P_{CO}}{k_1 P_{CO} + k_5 P_{H_2} + k_{6,n} e^{nc}} \tag{49}$$

where, a_n depends on n through the exponential term in the denominator.

Since methane and ethene have different termination rate constants (k_{5M} and k_{6E}, respectively), their growth probabilities are defined separately as shown in equations 50 and 51.

$$a_1 = \frac{\left[CH_3 - \sigma\right]}{\left[H - \sigma\right]} = \frac{k_1 P_{CO}}{k_1 P_{CO} + k_{5M} P_{H_2}} \tag{50}$$

$$a_2 = \frac{\left[C_2 H_5 - \sigma\right]}{\left[CH_3 - \sigma\right]} = \frac{k_1 P_{CO}}{k_1 P_{CO} + k_5 P_{H_2} + k_{6E,0} e^{2c}} \tag{51}$$

Since LHHW approach deals with surface coverage, the method of evaluation of the fraction of vacant sites [σ] is fundamental. According to the site balance, [σ] is related to partial pressures and kinetic constants. It is assumed that deactivation is negligible and total number of active catalytic sites is constant over time [76]. Therefore, the fraction of vacant sites can be calculated as follows,

$$[\sigma] = B\left(1 + \sqrt{K_7}\left(2 + 1\frac{1}{K_4}\right)\sqrt{P_{H_2}} + \frac{\sqrt{K_7}}{K_3K_4}\frac{1}{\sqrt{P_{H_2}}} + \frac{\sqrt{K_7}}{K_2K_3K_4}\frac{P_{H_2O}}{P_{H_2}^{1.5}}\right) \quad (52)$$

where, factor B can be estimated by the following expression,

$$B = a_1 + a_1a_2 + a_1a_2\sum_{i=3}^{n}\prod_{j=3}^{i}a_j \quad (53)$$

And the equilibrium constants of elementary reaction steps presented in Table 32 (K_2, K_3, K_4, and K_7) are calculated according to equation 54.

$$K_i = A_i e^{-\frac{\Delta H_i}{RT}} \quad (54)$$

where, A_i is the pre-exponential factor of the ith elementary reaction step and ΔH_i is the enthalpy of ith elementary step and adsorption reaction step.

Finally, the resulting reaction rate equations for methane, ethene, n-paraffin, and 1-olefin can be expressed in kmole of FT product over kilogram of catalyst consumed,

$$R_{CH_4} = \frac{k_{5M}\sqrt{K_7}P_{H_2}^{1.5}a_1}{[\sigma]} \quad (55)$$

$$R_{C_2H_4} = \frac{k_{6E,0}e^{2c}\sqrt{K_7 P_{H_2}}a_1}{[\sigma]} \quad (56)$$

$$R_{C_nH_{2n+2}} = \frac{k_5\sqrt{K_7}P_{H_2}^{1.5}a_1a_2\prod_{i=3}^{n}a_i}{[\sigma]} \quad (57)$$

$$R_{C_nH_{2n}} = \frac{k_{6,0}e^{nc}\sqrt{K_7\ P_{H_2}}a_1a_2\prod_{i=3}^{n}a_i}{[\sigma]} \quad (58)$$

In order to simplify the integration of the kinetic model in the Aspen Plus input reaction scheme, the obtained reaction rates have been uniformed to the conventional LHHW form which is

$$r = \frac{(kinetic factor)(driving force expression)}{(adsorption expression)} \quad (59)$$

where,

$$(kinetic factor) = a e^{-\frac{b}{RT}} \quad (60)$$

$$(driving force expression) = \sqrt{K_7} P_{H_2}^{d} \quad (61)$$

$$(adsorption expression) = 1 + \sqrt{K_7}\left(2 + 1\frac{1}{K_4}\right)\sqrt{P_{H_2}} + \frac{\sqrt{K_7}}{K_3 K_4}\frac{1}{\sqrt{P_{H_2}}} + \frac{\sqrt{K_7}}{K_2 K_3 K_4}\frac{P_{H_2O}}{P_{H_2}^{1.5}} \quad (62)$$

Parameters that are used in these equations are presented in Table 33, while the estimated parameters values for FT model can be found in Table 34.

Table 33- Parameter expression of equation 60

Product	*a*	*b*	d
Methane	$\frac{\alpha_1 A_{5M}}{B}$	E_{5M}	1.5
Ethene	$\frac{\alpha_1 \alpha_2 A_{6E}}{B}$	$E_{6E}^{0} + 2c$	0.5
n-paraffin with *n* carbon atoms	$\frac{\alpha_1 \alpha_2 \prod_{i=3}^{n} \alpha_i A_5}{B}$	E_5	1.5
1-olefin with *n* carbon atoms	$\frac{\alpha_1 \alpha_2 \prod_{i=3}^{n} \alpha_i A_6}{B}$	$E_6^{0} + nc$	0.5

Table 34- Estimated parameters for FT model [76]

Parameter	Value	Unit	Parameter	Value	Unit
$\boldsymbol{A_1}$	$1{,}83 \times 10^9$	$\frac{\text{kmol}}{\text{kg}_{\text{cat}}\ \text{h bar}}$	$\boldsymbol{E_1}$	$1{,}00 \times 10^5$	$\frac{\text{kJ}}{\text{kmol}}$
$\boldsymbol{A_2}$	5,08	-	$\Delta\boldsymbol{H_2}$	$8{,}68 \times 10^3$	$\frac{\text{kJ}}{\text{kmol}}$
$\boldsymbol{A_3}$	2,44	$\frac{1}{\text{bar}}$	$\Delta\boldsymbol{H_3}$	$9{,}44 \times 10^3$	$\frac{\text{kJ}}{\text{kmol}}$
$\boldsymbol{A_4}$	2,90	-	$\Delta\boldsymbol{H_4}$	$7{,}90 \times 10^3$	$\frac{\text{kJ}}{\text{kmol}}$
$\boldsymbol{A_5}$	$4{,}49 \times 10^4$	$\frac{\text{kmol}}{\text{kg}_{\text{cat}}\ \text{h bar}}$	$\boldsymbol{E_5}$	$7{,}24 \times 10^4$	$\frac{\text{kJ}}{\text{kmol}}$
$\boldsymbol{A_{5M}}$	$8{,}43 \times 10^4$	$\frac{\text{kmol}}{\text{kg}_{\text{cat}}\ \text{h bar}}$	$\boldsymbol{E_{5M}}$	$6{,}30 \times 10^4$	$\frac{\text{kJ}}{\text{kmol}}$
$\boldsymbol{A_6}$	$7{,}47 \times 10^8$	$\frac{\text{kmol}}{\text{kg}_{\text{cat}}\ \text{h bar}}$	$\boldsymbol{E_6^0}$	$9{,}72 \times 10^4$	$\frac{\text{kJ}}{\text{kmol}}$
$\boldsymbol{A_{6E}}$	$7{,}03 \times 10^8$	$\frac{\text{kmol}}{\text{kg}_{\text{cat}}\ \text{h}}$	$\boldsymbol{E_{6E}^0}$	$1{,}09 \times 10^5$	$\frac{\text{kJ}}{\text{kmol}}$
$\boldsymbol{A_7}$	$1{,}00 \times 10^{-4}$	$\frac{1}{\text{bar}}$	$\Delta\boldsymbol{H_7}$	$-2{,}50 \times 10^4$	$\frac{\text{kJ}}{\text{kmol}}$
$\Delta\boldsymbol{E}$	$1{,}12 \times 10^3$	$\frac{\text{kJ}}{\text{kmol}\ (\text{CH}_2)}$			

13 Appendix IV- Hydrocracking Kinetic Model

In a crude oil refinery, hydrocracking process is usually considered merely as a residue conversion technology, but in LTFT wax treatment is an essential step which effectively maximize the overall middle distillate yield and quality [77,136]. Considering cobalt-based catalyst in slurry LTFT reactor and according to chain growth mechanism, product distribution is shifted toward heavier paraffin. Hence, product consists of a large fraction of wax with a boiling point temperature higher than 370 °C and rather limited distillate yields with high cetane number but poor cold flow properties. While the former is an added value, the latter makes its direct and indirect (as diesel blend component) use as transportation fuel challenging [136]. Therefore, hydrocracking process is used to solve these problems.

Generally, hydrocracking process consists of two different reactions,

- Hydro-isomerization which improves cold flow properties
- Hydrocracking of paraffinic chains which results in higher total yield of middle distillate

According to Baltanas et al. alkanes can participate in cracking reaction as iso-alkanes [110]. So, in the hydro-isomerization reaction, alkanes first are dehydrogenated to alkenes and then the isomerized alkenes can be hydrogenated to iso-alkanes and cracked to lighter components. Thus, catalysts used in hydrocracking reactors are characterized by the presence of two active sites, metal sites for hydrogenation/dehydrogenation, and acidic sites for isomerization/cracking. Further explanations of the process can be found in [43].

In this study, hydrocracking process of FT wax and its product distribution was modeled by the approach presented by Pellegrini et al using LHHW method [77,132]. First, it is assumed that only alkanes with carbon number larger than 4 are involved in the hydrocracking process. Then, the reaction model for hydro-isomerization and hydrocracking is

deduced. For the sake of simplicity and considering the available experimental data, only mono-methyl alkanes are considered in isomers class.

For every n-alkane heavier than butane, the hydro-isomerization reaction equation has the following expression,

$$n \geq 4 \quad C_nH_{2n+2} \leftrightarrow CH_3CH(CH_3)C_{n-3}H_{2n-5} \tag{63}$$

where it is clear that each linear alkane reaches the equilibrium with its branched isomer.

In hydrocracking process, it is necessary to make distinction between isopentane, methyl-alkane with odd or even carbon number in the longer chain,

$$n = 2 \quad CH_3CH(CH_3)C_2H_5 + H_2 \leftrightarrow \frac{1}{2}CH_4 + \frac{1}{2}C_2H_6 + \frac{1}{2}C_3H_8 + \frac{1}{2}C_4H_{10} \tag{64}$$

$$odd\ n \geq 3 \quad CH_3CH(CH_3)C_nH_{2n+1} + H_2 \leftrightarrow 2CH_3CH(CH_3)C_{\frac{n-3}{2}}H_{n+1} \tag{65}$$

$$even\ n \geq 4 \quad CH_3CH(CH_3)C_nH_{2n+1} + H_2 \leftrightarrow CH_3CH(CH_3)C_{\frac{n-4}{2}}H_{n-3} + CH_3CH(CH_3)C_{\frac{n-2}{2}}H_{n-1} \tag{66}$$

These reactions formulations are defined base on the assumption that iso-alkanes are supposed to break in the middle of the chain. This assumption is based on the experimental results of primary hydrocracking of light hydrocarbons reported in [137,138]. It was shown that the hydrocarbon fragments (with the exception of C_1, C_2, and C_3) are apparently produced nearly in the same amounts. According to this mechanism C_1 and C_2 are not produced, while C_3 is produced at a low rate. Nevertheless, formation of a small fraction of these lightest hydrocarbons is possible and should be taken into account. Hence, the reaction scheme presents a different way of cracking for iso-pentane which is shown in reaction 64 [77].

The isomerisation reactions are considered to be in equilibrium, while cracking reactions are rate-determined. Hence, linear and branched alkanes with *n* carbon number are characterized according to the following equations,

$$r_{isom}(n) = \frac{k_{isom}^0(n)e^{-\frac{E_{isom}(n)}{RT}}\left(fug_{n-C}(n) - \frac{1}{K_{eq}(n)}fug_{iso-C}(n)\right)}{ADS} \tag{67}$$

$$r_{cr}(n) = \frac{k_{cr}^{0}(n) e^{-\frac{E_{cr}(n)}{RT}} fug_{iso-C}(n)}{ADS} \quad (68)$$

where,

$k_{isom}^{0}(n)$: Pre-exponential factor of isomerization of n-alkane with n carbon atoms;

$E_{isom}(n)$: Activation energy of isomerization of n-alkane with n carbon atoms;

$k_{cr}^{0}(n)$: Pre-exponential factor of hydrocraking of iso-alkane with n carbon atoms;

$E_{cr}(n)$: Activation energy of hydrocraking of iso-alkane with n carbon atoms;

$K_{eq}(n)$: Equilibrium constant between isomerization direct and backwards reactions;

$\text{fug}_{n-C}(n)$: Fugacity of the n-alkane with n carbon atoms;

$\text{fug}_{iso-C}(n)$: Fugacity of the iso-alkane with n carbon atoms;

ADS: adsorption factor

The adsorption factor is estimated according to equation 69. $K_{L_{n-C}}(n)$ and $K_{L_{iso-C}}(n)$ in this equation are the Langmuir constants that govern the adsorption of n-alkanes and iso-alkanes, respectively.

$$ADS = \text{fug}_{H_2}\left[1 + \sum_{i=1}^{30+} K_{L_{n-C}}(n)\,\text{fug}_{n-C}(n) + \sum_{i=4}^{30+} K_{L_{iso-C}}(n)\,\text{fug}_{iso-C}(n)\right] \quad (69)$$

The kinetic parameters are estimated based on the following experimental equations [77].

$$K_{L_{n-C}}(n) = 10.3 e^{0.4n}\ (1/Pa) \quad (70)$$

$$K_{L_{iso-C}}(n) = 20.0 e^{0.1n}\ (1/Pa) \quad (71)$$

$$K_{cr}^{0}(n) = 1.52n^{7.63} \times 10^{16} \ (kmol/kg_{cat}h) \quad (72)$$

$$K_{isom}^{0}(n) = 3.88n^{7.7} \times 10^{17} \ (kmol/kg_{cat}h) \quad (73)$$

$$K_{eq}(n) = 1.24n^{2} - 1.15 \times 10^{-2} + 5.20 \times 10^{3} \quad (74)$$

$$E_{cr}(n) = (3.06\ln(n) + 8.75) \times 10^{4} \ (kJ/kmol) \quad (75)$$

$$E_{isom}(n) = 2.23\ln(n) \times 10^{4} + 1.20 \times 10^{5} \ (kJ/kmol) \quad (76)$$

14 Appendix V-Base Cost of Components

Table 35 lists base cost of components. In this table *BCC* is the base capacity of the component based on the scaling parameter, while *ECC* is the estimated capacity of that component in the system which is driven from simulation results. *x* is the cost scaling factor. The presented values here are overnight capital costs of other components that were used in estimation including installation, manufacturing, labor, balance of plant, general facilities, engineering, overhead and contingencies [91–95]. Since SOEC technology is not yet mature, most researchers use estimates based on the state-of-the-art solid oxide fuel cells (SOFC) [24,92]. So, such estimates are also used here. Note that the presented base cost in the mentioned references were reported based on the dollar values in different years. To unite all the reported costs to a unique year, all of them are modified to dollar value in 2016 based on the US inflation rate.

Table 35- Base cost of components

Component	Scaling Parameter	Unit	x	BCC	C_{base} (M_{2016}$/Unit)	Reference
Air Compressor	Air flow	kmol/s	1	53.78	85.70	[91]
CO_2 Compressor	Compressor power	MWe	0.67	10	7.38	[93]
Cathode Recycle Compressor	Recycled syngas flow	kmol/s	1	4.27	0.58	[91]
SOEC	SOEC active area	m^2	1	1	0.00351	[92]
Biomass storage, prep, handling	Biomass feed	wet t/hr	0.77	64.6	17.79	[94]
ASU	Pure O2 output	t/hr	0.5	76.6	62.35	[93,94]
O2 Compressor (ASU)	Compressor power	MWe	0.67	10	9.71	[93,94]
Gasifier	Biomass feed	MW_{th} (LHV)	0.5	482.8	281.99	[95]
Cyclone	Syngas inlet flow	m^3/s	0.7	68.7	1.65	[95]
Water gas shift reactor	Syngas to WGSR	MW_{th} (LHV)	0.67	1377	21.44	[95]
Selexol (H2S)	S input	t/day	0.67	66.8	52.299	[93]
Selexol (CO2)	CO2 Captured	t/hr	0.67	234.3	58.27	[93]
Syngas Compressor	Compressor power	MWe	0.67	10	11.19	[94]

Component	Scaling Parameter	Unit	x	BCC	C_{base} (M_{2016}$/Unit)	Reference
FT reactor	FT input Volumetric Flow rate	MM SCF/hr	0.75	2.52	22.17	[94]
Distillation tower	FT flow to HC	Mlb/hr	0.7	14.44	1.17	[94]
Wax hydrocracking	Inlet Flow	Mlb/hr	0.55	8.984	15.16	[94]
Auto-thermal reformer	ATR output SG	kmol/hr	0.9	31000	119.88	[94]
H2 recovery (PSA)	FT H2 recovery plant,	MM CF/hr	0.7	0.033	1.35	[94]
Other (pumps/mixer/separator)	-		-		0.04	[92]

15 Appendix VI- Heating degree days

Although hourly heat demand is usually available in cities with district heating network, such information is not available to public [119]. Hence, to take the possible fluctuations in heat demand during each month, concept of heating degree day has been used in this study. Heating degree day is the difference between outdoor temperature at certain location and base temperature [119,139]. The logic behind such approach is that inside temperature of a typical building is generally 2-3 ^{o}C is higher than outside temperature. In other words, indoor temperature would be around 21-22 ^{o}C when outdoor temperature is 18 ^{o}C. Any drop in outdoor temperature consequently results in decrease of indoor temperature below comfort temperature and therefore heating system requires to cover the differences. So, heat demand of a building can be estimated based on the outdoor temperature difference from base temperature [119]. Since heating degree days take the outdoor temperature fluctuations into account, it can portray effect of extreme conditions better than other simplified methods that use mean outdoor temperature [139]. Table 36 shows heating degree days for four locations used for the case study. This values are reported by NASA as average of 22-year values. The base temperature for calculation of these degree days is 18 ^{o}C [85].

Table 36- Heating degree days [85]

Month	Umeå	Stockholm	Turin	Rome
January	718	612	685	247
February	673	564	586	233
March	650	540	507	204
April	493	400	385	146
May	339	254	226	37
Jun	178	115	116	2
July	91	41	49	0
August	115	55	50	0
September	231	167	170	0
October	391	323	328	17
November	529	462	512	108
December	651	576	640	207

16 References

[1] World Energy Council. European Climate Change Policy Beyond 2012. London: 2009.

[2] Kaltschmitt M, Streicher W, Wiese A, editors. Renewable Energy - Technology, Economics and Environment. 1st ed. Berlin/Heidelberg : Springer Berlin Heidelberg; 2007.

[3] Trainer T. Renewable Energy Cannot Sustain A Consumer Society. Dordrecht: Springer Netherlands; 2007. doi:10.1007/978-1-4020-5549-2.

[4] Connolly D. A Review of Energy Storage Technologies 2009.

[5] Barnes FS, Levine JG. Large Energy Storage Systems Handbook. CRC Press Book; 2011.

[6] Demirel Y. Energy - Production, Conversion, Storage, Conservation, and Coupling. 1st ed. Springer-Verlag London; 2012. doi:10.1007/978-1-4471-2372-9.

[7] AGRAWALA S, BASHMAKOV IA, BLANCO G, BRUCKNER T, BRUNNER S, BUSTAMANTE M, et al. Fifth Assessment Report - Mitigation of Climate Change. New York: 2014. doi:ISBN 978-1-107-05821-7 / ISBN 978-1-107-65481-5.

[8] Tijmensen MJA, Faaij APC, Hamelinck CN, Van Hardeveld MRM. Exploration of the possibilities for production of Fischer Tropsch liquids and power via biomass gasification. Biomass and Bioenergy 2002;23:129–52. doi:10.1016/S0961-9534(02)00037-5.

[9] Trippe F, Fröhling M, Schultmann F, Stahl R, Henrich E, Dalai A. Comprehensive techno-economic assessment of dimethyl ether (DME) synthesis and Fischer-Tropsch synthesis as alternative process steps within biomass-to-liquid production. Fuel Process Technol 2013;106:577–86. doi:10.1016/j.fuproc.2012.09.029.

[10] Swain PK, Das LM, Naik SN. Biomass to liquid: A prospective challenge to research and development in 21st century. Renew Sustain Energy Rev 2011;15:4917–33. doi:10.1016/j.rser.2011.07.061.

[11] HAMELINCK C, FAAIJ A, DENUIL H, BOERRIGTER H. Production of FT transportation fuels from biomass; technical options, process analysis and optimisation, and development potential. Energy 2004;29:1743–71. doi:10.1016/j.energy.2004.01.002.

[12] Prins MJ, Ptasinski KJ, Janssen FJJG. Exergetic optimisation of a production process of Fischer–Tropsch fuels from biomass. Fuel Process Technol 2005;86:375–89. doi:10.1016/j.fuproc.2004.05.008.

[13] Buragohain B, Mahanta P, Moholkar VS. Thermodynamic optimization of biomass gasification for decentralized power generation and Fischer–Tropsch synthesis. Energy 2010;35:2557–79. doi:10.1016/j.energy.2010.03.003.

[14] Leibbrandt NH, Aboyade AO, Knoetze JH, Görgens JF. Process efficiency of biofuel production via gasification and Fischer–Tropsch synthesis. Fuel 2013;109:484–92. doi:10.1016/j.fuel.2013.03.013.

[15] Kim K, Kim Y, Yang C, Moon J, Kim B, Lee J, et al. Long-term operation of biomass-to-liquid systems coupled to gasification and Fischer-Tropsch processes for biofuel production. Bioresour Technol 2013;127:391–9. doi:10.1016/j.biortech.2012.09.126.

[16] Weiland F. Pressurized entrained flow gasification of pulverized biomass. 2015.

[17] Graves C, Ebbesen SD, Mogensen M, Lackner KS. Sustainable hydrocarbon fuels by recycling CO2 and H2O with renewable or nuclear energy. Renew Sustain Energy Rev 2011;15:1–23. doi:10.1016/j.rser.2010.07.014.

[18] Sun X, Chen M, Jensen SH, Ebbesen SD, Graves C, Mogensen M. Thermodynamic analysis of synthetic hydrocarbon fuel production in pressurized solid oxide electrolysis cells. Int J Hydrogen Energy 2012;37:17101–10. doi:10.1016/j.ijhydene.2012.08.125.

[19] Bierschenk DM, Wilson JR, Barnett SA. High efficiency electrical energy storage using a methane–oxygen solid oxide cell. Energy Environ Sci 2011;4:944–51. doi:10.1039/C0EE00457J.

[20] Rüdlinger M. Thermal and chemical utilization of carbonaceous materials, in particular for emission-free generation of energy, 2012. doi:US20120238645 A1.

[21] Manganaro J, Chen B, Adeosun J, Lakhapatri S, Favetta D, Lawal A, et al. Conversion of residual biomass into liquid transportation fuel: An energy analysis. Energy and Fuels 2011;25:2711–20. doi:10.1021/ef200327e.

[22] Baliban RC, Elia JA, Floudas CA, Gurau B, Weingarten MB, Klotz SD. Hardwood biomass to gasoline, diesel, and jet fuel: 1. Process synthesis and global optimization of a thermochemical refinery. Energy and Fuels, vol. 27, 2013, p. 4302–24. doi:10.1021/ef302003f.

[23] Niziolek AM, Onel O, Elia J a, Baliban RC, Xiao X, Floudas C a. Coal and Biomass to Liquid Transportation Fuels : Process Synthesis and Global Optimization Strategies. Ind Eng Chem Res 2014;53:17002–25. doi:10.1021/ie500505h.

[24] Becker WL, Braun RJ, Penev M, Melaina M. Production of Fischer–Tropsch liquid fuels from high temperature solid oxide co-electrolysis units. Energy 2012;47:99–115. doi:10.1016/j.energy.2012.08.047.

[25] Stempien JP, Ni M, Sun Q, Chan SH. Thermodynamic analysis of combined Solid Oxide Electrolyzer and Fischer–Tropsch processes. Energy 2015;81:682–90. doi:10.1016/j.energy.2015.01.013.

[26] Li X, Anderson P, Jhong H-RM, Paster M, Stubbins JF, Kenis PJA. Greenhouse Gas Emissions, Energy Efficiency, and Cost of Synthetic Fuel Production Using Electrochemical CO2 Conversion and the Fischer-Tropsch Process. Energy and Fuels 2016;30:5980–9. doi:10.1021/acs.energyfuels.6b00665.

[27] Chen B, Xu H, Ni M. Modelling of SOEC-FT reactor: Pressure effects on methanation process. Appl Energy 2017;185:814–24. doi:10.1016/j.apenergy.2016.10.095.

[28] Zoulias E, Varkaraki E. A review on water electrolysis. Tcjst 2004;4:41–71.

[29] FuelCellToday. Water Electrolysis & Renewable Energy Systems 2013;2:48.

[30] KREUTER W. Electrolysis: The important energy transformer in a world of sustainable energy. Int J Hydrogen Energy 1998;23:661–6. doi:10.1016/S0360-3199(97)00109-2.

[31] Carmo M, Fritz DL, Mergel J, Stolten D. A comprehensive review on PEM water electrolysis. Int J Hydrogen Energy 2013;38:4901–34. doi:10.1016/j.ijhydene.2013.01.151.

[32] Richter A, Pedersen CF, Mogensen M, Jensen SH, Sloth M, Chen M, et al. planSOEC R&D and commercialization roadmap for SOEC electrolysis R&D of SOEC stacks with improved durability. 2011.

[33] Smolinka T, Günther M, Ise F, Garche J. NOW-Studie " Stand und Entwicklungspotenzial der Wasserelektrolyse zur Herstellung von Wasserstoff aus regenerativen Energien " Kurzfassung des Abschlussberichts 2010.

[34] O'Brien JE, McKellar MG, Harvego EA, Stoots CM. High-temperature electrolysis for large-scale hydrogen and syngas production from nuclear energy – summary of system simulation and economic analyses. Int J Hydrogen Energy 2010;35:4808–19. doi:10.1016/j.ijhydene.2009.09.009.

[35] Sohal MS, Herring JS. Oxygen handling and cooling options in high temperature electrolysis plants 2008;INL/EXT-08.

[36] Miller BG. Coal Energy Systems. Elsevier; 2005. doi:10.1016/B978-012497451-7/50005-X.

[37] Basu P. Biomass Gasification Design Handbook. Elsevier; 2010. doi:10.1016/B978-0-12-374988-8.00001-5.

[38] Qin K. Entrained flow gasification of biomass. Technical University of Denmark, 2012.

[39] Higman C. State of the Gasification Industry – the Updated Worldwide Gasification Database. Gasif Technol Conf 2013:1–11.

[40] Higman C. State of the Gasification Industry – the Updated Worldwide Gasification Database. Int. Pittsburgh Coal Comference, Beijing: 2013, p. 1–11.

[41] Phillips J. Different Types of Gasifiers and Their Integration with Gas Turbines 1.2.1-1 Introduction. 2004.

[42] Qin K. Entrained flow gasification of biomass. Technical University of Denmark, 2012.

[43] de Klerk A. Fischer-Tropsch Refining. Weinheim, Germany: Wiley-VCH Verlag GmbH & Co. KGaA; 2011. doi:10.1002/9783527635603.

[44] Schulz H. Short history and present trends of Fischer–Tropsch synthesis. Appl Catal A Gen 1999;186:3–12. doi:10.1016/S0926-860X(99)00160-X.

[45] Dry ME. The Fischer–Tropsch process: 1950–2000. Catal Today 2002;71:227–41. doi:10.1016/S0920-5861(01)00453-9.

[46] van de Loosdrecht J, Botes FG, Ciobica IM, Ferreira A, Gibson P, Moodley DJ, et al. Comprehensive Inorganic Chemistry II. Elsevier; 2013. doi:10.1016/B978-0-08-097774-4.00729-4.

[47] Maitlis PM, de Klerk A. Greener Fischer-Tropsch Processes for Fuels and Feedstocks - Peter M. Maitlis, Arno de Klerk. Hoboken : Wiley; 2013.

[48] de Klerk A. Fischer–tropsch process. Kirk-Othmer Encycl Chem Technol 2013:1–20. doi:10.1002/0471238961.fiscdekl.a01.

[49] Maitlis PM, Klerk A de. Greener Fischer-Tropsch Processes for Fuels and Feedstocks - Wiley Online Library. 2013.

[50] Steynberg AP, Dry ME, Davis BH, Breman BB. Fischer-Tropsch Technology. vol. 152. Elsevier; 2004. doi:10.1016/S0167-2991(04)80459-2.

[51] Yermakova A, Anikeev VI. Thermodynamic Calculations in the Modeling of Multiphase Processes and Reactors. Ind Eng Chem Res 2000;39:1453–72. doi:10.1021/ie9905761.

[52] Aspen Technology. Aspen Plus® V8.8 2014.

[53] O'Brien JE, McKellar MG, Stoots CM, Herring JS, Hawkes GL.

Parametric study of large-scale production of syngas via high-temperature co-electrolysis. Int J Hydrogen Energy 2009;34:4216–26. doi:10.1016/j.ijhydene.2008.12.021.

[54] Bechtel Corporation. Aspen Process Flowsheet Simulation Model of a Battelle Biomass-Based Gasification, Fischer-Tropsch Liquefaction and Combined-Cycle Power Plan. Pittsburgh, Pennsylvania: 1998.

[55] Kazempoor P, Braun RJ. Model validation and performance analysis of regenerative solid oxide cells: Electrolytic operation. Int J Hydrogen Energy 2014;39:2669–84. doi:10.1016/j.ijhydene.2013.12.010.

[56] Stoots CM, O'Brien JE, Herring JS, Hartvigsen JJ. Syngas Production via High-Temperature Coelectrolysis of Steam and Carbon Dioxide. J Fuel Cell Sci Technol 2009;6:11014. doi:10.1115/1.2971061.

[57] Stempien JP, Ding OL, Sun Q, Chan SH. Energy and exergy analysis of Solid Oxide Electrolyser Cell (SOEC) working as a CO2 mitigation device. Int J Hydrogen Energy 2012;37:14518–27. doi:10.1016/j.ijhydene.2012.07.065.

[58] Stoots C, O'Brien J, Hartvigsen J. Results of recent high temperature coelectrolysis studies at the Idaho National Laboratory. Int J Hydrogen Energy 2009;34:4208–15. doi:10.1016/j.ijhydene.2008.08.029.

[59] Giglio E, Lanzini A, Santarelli M, Leone P. Synthetic natural gas via integrated high-temperature electrolysis and methanation: Part II-Economic analysis. J Energy Storage 2015;2:64–79. doi:10.1016/j.est.2015.06.004.

[60] Graves C, Ebbesen SD, Mogensen M. Co-electrolysis of CO2 and H2O in solid oxide cells: Performance and durability. Solid State Ionics 2011;192:398–403. doi:10.1016/J.SSI.2010.06.014.

[61] Ebbesen SD, Graves C, Mogensen M. Production of Synthetic Fuels by Co-Electrolysis of Steam and Carbon Dioxide. Int J Green Energy 2009;6:646–60. doi:10.1080/15435070903372577.

[62] Jensen SH, Sun X, Ebbesen SD, Knibbe R, Mogensen M. Hydrogen and synthetic fuel production using pressurized solid

oxide electrolysis cells. Int J Hydrogen Energy 2010;35:9544–9. doi:10.1016/j.ijhydene.2010.06.065.

[63] Rubin ES, Berkenpas MB, Frey HC, Chen C, McCoy S, Zaremsky CJ. Development and Application of Optimal Design Capability for Coal Gasification. 2007.

[64] Wu Y, Yang W, Blasiak W. Energy and exergy analysis of high temperature agent gasification of biomass. Energies 2014;7:2107–22. doi:10.3390/en7042107.

[65] Wu Y, Yang W, Blasiak W. Energy and Exergy Analysis of High Temperature Agent Gasification of Biomass. Energies 2014;7:2107–22. doi:10.3390/en7042107.

[66] Rauch R, Hrbek J, Hofbauer H. Biomass gasification for synthesis gas production and applications of the syngas. Wiley Interdiscip Rev Energy Environ 2014;3:343–62. doi:10.1002/wene.97.

[67] Weiland F, Hedman H, Marklund M, Wiinikka H, Öhrman O, Gebart R. Pressurized Oxygen Blown Entrained-Flow Gasification of Wood Powder. Energy & Fuels 2013;27:932–41. doi:10.1021/ef301803s.

[68] Higman C, van der Burgt M. Gasification. Elsevier; 2008. doi:10.1016/B978-0-7506-8528-3.00018-3.

[69] Smith RJB, Loganathan M, Shantha MS. A Review of the Water Gas Shift Reaction Kinetics. Int J Chem React Eng 2010;8:1–34. doi:10.1002/chin.201038231.

[70] Selexol | netl.doe.gov 2016. http://www.netl.doe.gov/research/coal/energy-systems/gasification/gasifipedia/Selexol (accessed February 1, 2016).

[71] Korens N, Simbeck DR, Wilhelm DJ. PROCESS SCREENING ANALYSIS OF ALTERNATIVE GAS TREATING AND SULFUR REMOVAL FOR GASIFICATION. California: 2002.

[72] House KZ, Baclig AC, Ranjan M, van Nierop EA, Wilcox J, Herzog HJ. Economic and energetic analysis of capturing CO2 from ambient air — Supporting Information. Proc. Natl. Acad. Sci. U. S. A., 2011, p. 13.

[73] Chen C. A Technical and Economic Assessment of CO2 Capture Technology for IGCC Power Plants. Carnegie Mellon University, 2005.

[74] Doctor RD, Molburg JC, Thimmapuram PR, Berry GF, Livengood CD. gasification combined cycle: carbon dioxide recovery, transport, and disposal. Argonne, Illinoise: 1994.

[75] Chen C. Carnegie Mellon University A Technical and Economic Assessment of CO 2 Capture Technology for IGCC Power Plants A Dissertation Submitted in Partial Fulfillment of the Requirements for the Degree of Doctor of Philosophy in Engineering and Public Policy by. Carnegie Mellon University, 2005.

[76] Todic B, Bhatelia T, Froment GF, Ma W, Jacobs G, Davis BH, et al. Kinetic Model of Fischer–Tropsch Synthesis in a Slurry Reactor on Co–Re/Al 2 O 3 Catalyst. Ind Eng Chem Res 2013;52:669–79. doi:10.1021/ie3028312.

[77] Pellegrini LA, Gamba S, Calemma V, Bonomi S. Modelling of hydrocracking with vapour–liquid equilibrium. Chem Eng Sci 2008;63:4285–91. doi:10.1016/j.ces.2008.06.002.

[78] Smith R J B, Loganathan M, Shantha MS. A Review of the Water Gas Shift Reaction Kinetics. Int J Chem React Eng 2010;8. doi:10.2202/1542-6580.2238.

[79] Mivechian A, Pakizeh M. Hydrogen recovery from Tehran refinery off-gas using pressure swing adsorption, gas absorption and membrane separation technologies: Simulation and economic evaluation. Korean J Chem Eng 2013;30:937–48. doi:10.1007/s11814-012-0221-y.

[80] You Y-W, Lee D-G, Yoon K-Y, Moon D-K, Kim SM, Lee C-H. H2 PSA purifier for CO removal from hydrogen mixtures. Int J Hydrogen Energy 2012;37:18175–86. doi:10.1016/j.ijhydene.2012.09.044.

[81] Migan G-A. Study of the operating temperature of a PV module. Lund, Sweden: 2013.

[82] European Union. PV potential estimation utility. JRC, Eur Commision 2017.

http://re.jrc.ec.europa.eu/pvgis/apps4/pvest.php# (accessed May 9, 2017).

[83] Solar Electric Supply. SOLAREX - PHOTOVOLTAIC SOLAR MODULES n.d. https://www.solarelectricsupply.com/solar-panels/solarex (accessed May 9, 2017).

[84] Guo Z. A simple method to downscale daily wind statistics to hourly wind data 2013.

[85] NASA AtSD center. NASA Surface meteorology and Solar Energy: Data Subset n.d. https://eosweb.larc.nasa.gov/cgi-bin/sse/subset.cgi?email=skip@larc.nasa.gov (accessed May 9, 2017).

[86] Mentis D, Hermann S, Howells M, Welsch M, Siyal SH. Assessing the technical wind energy potential in Africa a GIS-based approach. Renew Energy 2015;83:110–25. doi:10.1016/j.renene.2015.03.072.

[87] Burton T, Jenkins N, Sharpe D, Bossanyi E. Wind energy handbook. Wiley; 2011.

[88] Vestas. Vestas | Wind it means the world to us n.d. https://www.vestas.com/ (accessed May 9, 2017).

[89] Querol E, Gonzalez-Regueral B, Perez-Benedito JL. Practical Approach to Exergy and Thermoeconomic Analyses of Industrial Processes. London: Springer London; 2013. doi:10.1007/978-1-4471-4622-3.

[90] Lundberg WL, Holmes RA, King JE, Israelson GA, Zafred PR, Kothmann RE, et al. Pressurized Solid Oxide Fuel Cell/ Gas Turbine Power System. Pittsburgh: 2000.

[91] Newby R, Keairns D. Analysis of Natur al Gas Fuel Cell Plant Configurations. 2011. doi:DOE/NETL-2011/1486.

[92] Fu Q, Mabilat C, Zahid M, Brisse A, Gautier L, Balat M, et al. Syngas production via high-temperature steam/CO2 co-electrolysis: an economic assessment. Energy Environ Sci 2010;3:1382. doi:10.1039/c0ee00092b.

[93] Kreutz T, Williams R, Consonni S, Chiesa P. Co-production of hydrogen, electricity and CO2 from coal with commercially ready

technology. Part B: Economic analysis. Int J Hydrogen Energy 2005;30:769–84. doi:10.1016/j.ijhydene.2004.08.001.

[94] Kreutz TG, Larson ED, Liu G, Williams RH. Fischer-Tropsch Fuels from Coal and Biomass. 25th Annu. Int. Pittsburgh Coal Conf., Pittsburgh, Pennsylvania: 2008, p. 86.

[95] Gerdes KJ. Cost and Performance Baseline for Fossil Energy Plants Volume 1: Bituminous Coal and Natural Gas to Electricity. 2013. doi:DOE/NETL-2010/1397.

[96] Seider WD, Seader JD, Lewin DR, Seider WD. Product and process design principles : synthesis, analysis, and evaluation. Wiley; 2004.

[97] Davidson RL, Rearick JS, Hicks TG. STANDARD HANDBOOK OF ENGINEERING CALCULATIONS - SECTION 5:Chemical and Process Plant Engineering. 5th ed. McGraw-Hill Professional; 2004.

[98] Irena. Renewable Power Generation Costs in 2014 : An Overview. 2015.

[99] Burdick DR, Krishnamurthy R, Popa L. Water Cost Index - IBM 2014. http://researcher.watson.ibm.com/researcher/view_group.php?id=5047 (accessed October 1, 2016).

[100] Rubin ES, Davison JE, Herzog HJ. The cost of CO2 capture and storage. Int J Greenh Gas Control 2015;40:378–400. doi:10.1016/j.ijggc.2015.05.018.

[101] Grant T, Morgan D, Gerdes K. Carbon dioxide transportation and storage costs in netl studies; quality guidelines for energy systems studies. 2013.

[102] Glommers MiljöEnergi AB-GME Pellets. Glommers MiljöEnergi AB n.d. www.glommersmiljoenergi.se (accessed December 5, 2016).

[103] Eichman J, Townsend A, Melaina M. Economic Assessment of Hydrogen Technologies Participating in California Electricity Markets. 2012.

[104] YCHARTS. European Union Natural Gas Import Price n.d.

https://ycharts.com/indicators/europe_natural_gas_price (accessed June 29, 2017).

[105] Markets Insider. Naphtha price Today n.d. http://markets.businessinsider.com/commodities/naphtha (accessed June 29, 2017).

[106] ATDM. Paraffin wax price n.d. http://iranparaffinwax.com/wiki-paraffin+wax+price-337.html (accessed June 29, 2017).

[107] Chemicool. Oxygen n.d. http://www.chemicool.com/elements/oxygen.html (accessed June 29, 2017).

[108] Put J. The European District Heating Database and Mapping European District Heating Systems. Halmstad University, School of Business and Engineering, 2011.

[109] European Parliment. Directive 2009/28/EC of the European Parliament and of the Council of 23 April 2009 on the promotion of the use of energy from renewable sources and amending and subsequently repealing Directives 2001/77/EC and 2003/30/EC. Off J Eur Union 2009:16–62.

[110] Baltanas MA, Vansina H, Froment GF. Hydroisomerization and hydrocracking. 5. Kinetic analysis of rate data for n-octane. Ind Eng Chem Prod Res Dev 1983;22:531–9. doi:10.1021/i300012a004.

[111] Lox ES, Froment GF. Kinetics of the Fischer-Tropsch reaction on a precipitated promoted iron catalyst. 2. Kinetic modeling. Ind Eng Chem Res 1993;32:71–82. doi:10.1021/ie00013a011.

[112] ENTSO-E - European Network of Transmission System Operators for Electricity. Hourly Load Values for a Specific Country for a Specific Month n.d. https://www.entsoe.eu/db-query/consumption/mhlv-a-specific-country-for-a-specific-month (accessed May 26, 2017).

[113] van Vliet OPR, Faaij APC, Turkenburg WC. Fischer–Tropsch diesel production in a well-to-wheel perspective: A carbon, energy flow and cost analysis. Energy Convers Manag 2009;50:855–76. doi:10.1016/j.enconman.2009.01.008.

[114] Mathworks. Matlab V9.1 2016.

[115] Tools for biomass chains. S2Biom Proj n.d. http://www.s2biom.eu/en/ (accessed January 16, 2017).

[116] NORDPOOL. Market Data n.d. http://www.nordpoolspot.com/About-us/ (accessed May 26, 2017).

[117] Knoema.com. Free data, statistics, analysis, visualization & sharing. Knoema.com n.d. https://knoema.com/ (accessed January 7, 2017).

[118] Bottio I, Ferraresi F, Della Vedova B. Status and perspectives of the district heating and cooling infrastructures in Italy. World Geotherm Congr 2015 2015:8.

[119] Connolly D, Drysdale D, Hansen K, Novosel T. Creating Hourly Profiles to Model both Demand and Supply. Copenhagen: 2015.

[120] Pardo N, Vatopoulos K, Krook-Riekkola A, Moya JA, Perez A. Heat and cooling demand and market perspective. 2012.

[121] Connolly D, Hansen K, Drysdale D, Lund H, Mathiesen BV, Werner S, et al. Heat Roadmap Europe n.d. http://www.heatroadmap.eu/maps.php (accessed July 11, 2017).

[122] Briefing EU biofuels policy- Dealing with indirect land use change. EU Parliment 2015:10.

[123] Flach B, Lieberz S, Rondon M, Williams B, Teiken C, Stange K. Biofuels Annual-- Gain Report. 2015. doi:NL5028.

[124] Pignatelli V, Alfano V. BIOENERGY INDUSTRY AND MARKETS IN ITALY n.d.

[125] Baldi S. General Information: Policy and programs. 2011.

[126] IEA/IRENA Joint Policies and Measures database- Italy. IEA - Renew Energy n.d. http://www.iea.org/policiesandmeasures/renewableenergy/?country=Italy (accessed November 13, 2016).

[127] Dahlbacka B, Huete S. Swedish Biofuels annual report. 2009. doi:SW9008.

[128] IEA/IRENA Joint Policies and Measure database-Sweden. IEA - Renew Energy n.d.

http://www.iea.org/policiesandmeasures/renewableenergy/?country=Sweden (accessed January 8, 2017).

[129] OECD. Fossil Fuel Support and Other Analysis n.d. http://www.oecd.org/site/tadffss/data/ (accessed July 12, 2017).

[130] OECD. Fertiliser and biofuels support policies database - OECD n.d. http://www.oecd.org/tad/agricultural-policies/support-policies-fertilisers-biofuels.htm (accessed July 12, 2017).

[131] European Comission. Energy datasheets: EU-28 countries n.d. https://ec.europa.eu/energy/en/data-analysis/country (accessed July 12, 2017).

[132] Selvatico D. Low Temperature Fischer-Tropsch fuels from syngas. Polytechnic University of Turin, 2014.

[133] Kunz L, Maier L, Tischer S, Deutschmann O. Modeling and Simulation of Heterogeneous Catalytic Reactions. Weinheim, Germany: Wiley-VCH Verlag GmbH & Co. KGaA; 2011. doi:10.1002/9783527639878.

[134] Goda AM, Neurock M, Barteau MA, Chen JG. Effect of hydrocarbon chain length and cyclization on the adsorption strength of unsaturated hydrocarbons on Pt/3d bimetallic surfaces. Surf Sci 2008;602:2513–23. doi:10.1016/j.susc.2008.05.035.

[135] Evans MG, Polanyi M. Inertia and driving force of chemical reactions. Trans Faraday Soc 1938;34:11. doi:10.1039/tf9383400011.

[136] Calemma V, Gambaro C, Parker WO, Carbone R, Giardino R, Scorletti P. Middle distillates from hydrocracking of FT waxes: Composition, characteristics and emission properties. Catal Today 2010;149:40–6. doi:10.1016/j.cattod.2009.03.018.

[137] Froment GF. Kinetics of the hydroisomerization and hydrocracking of paraffins on a platinum containing bifunctional Y-zeolite. Catal Today 1987;1:455–73. doi:10.1016/0920-5861(87)80009-3.

[138] Sie ST. Acid-catalyzed cracking of paraffinic hydrocarbons. 2. Evidence for the protonated cyclopropane mechanism from catalytic cracking experiments. Ind Eng Chem Res 1993;32:397–402. doi:10.1021/ie00015a001.

[139] Day T. Degree-days : theory and application. London: The Chartered Institution of Building Services Engineers; 2006.